Assembly, Elasticity, and Structures
of Nanoparticles in Immiscible Polymer Blends

Rosaria Altobelli

PhD in *Industrial Product and Process Engineering* (XXX Cycle)

Department of Chemical, Material and Industrial Production Engineering

University of Naples Federico II

_____

PhD Supervisor: Prof Giovanni Filippone

PhD Coordinator: Prof Giuseppe Mensitieri

ABSTRACT

Assembly, Elasticity, and Structures
of Nanoparticles in Immiscible Polymer Blends

Introducing nanoscale fillers into polymer matrices can serve as a means to compatibilize polymer blends and represents a clever way to manipulate their morphology at the micro-scale. Such a novel "compatibilization" strategy represents a viable route for optimizing the performance of polymer systems, which are ubiquitous in the modern society. The effects of nanoparticles on the micrometer-sized arrangement of the polymer phases, however, are difficult to predict, and most of the recent literature on this topic lack in terms of generality.

Many issues remain unclear, and even well-established phenomena are actually far from being fully understood. Is the origin of the uneven distribution of the filler in a multiphase host matrix merely dictated by thermodynamic arguments? Is it possible to drive the systems towards desired non-equilibrium configurations? How the filler affects the blend microstructure? And how the fluids in turn affect the nanoparticle assembly? This dissertation addresses these matters from both a theoretical and a practical point of view, shedding light on the sequence of events which determine the final morphology of nanoparticle-containing polymer blends through a combination of morphological and rheological analyses. In the first experimental part of this study, the physical mechanisms that govern the melt-state microstructural evolutions of polymer blends in the presence of nanoparticles are elucidated through a combination of several analyses and measurements. Using ternary blends of polystyrene (PS), poly(methyl methacrylate) (PMMA), and clay nanoplatelets we prove the generality of the mechanism of morphology stabilization by interfacial crowding of the nanoparticles, which keeps working in spite of the high viscosity of the liquid phases and the plate-like shape of the nanoparticles. The effect of the co-continuous morphology of the host matrix is highlighted through a comparative analysis with systems based on the same polymers and nanoparticles, but in which the matrix is either a single polymer or a drop-in-matrix blend. This allows us to emphasize the role of the multiphase nature of the host medium in driving the nanoparticle assembly. In particular, the elasticity and structure of the three-dimensional filler network which forms above Φ_c were studied in detail by resorting to the percolation theory. As regards the second part of the study the attention was paid to systems in which the filler gathers inside either of the polymer phases. Nanoclays with different hydrophobicity were selected to evaluate their localizations and consequently their effect on the blend. According to the research findings, it was emerged that the refinement ability of the filler was slightly better in the case of bulk localization, but interfacial nanoplatelets were more effective in stabilizing co-continuous morphologies against phase coarsening in the melt state.

Foreground arising from the work carried out, regarding the nanoparticle-induced morphological modifications in multiphase systems, preliminary analyses were exploited for assessing the effect of nanoparticle morphology on the beginning systems.

CONTENTS

Bibliography

Bibliography

Introduction

1.1. What, how, and why?

The polymer industry traces its beginning to the early modifications of shellac, natural rubber (NR —an amorphous cis-1,4-polyisoprene), gutta-percha (GP — a semi-crystalline trans-1,4-polyisoprene), and cellulose. In 1846, Parkes patented the first polymer blend: NR with GP partially co-dissolved in CS_2. Blending these two isomers resulted in partially crosslinked (co-vulcanized) materials whose rigidity was controllable by composition [1]. Since the discovery of the first synthetic polymer Bakelite, around a century ago, a diverse range of polymeric materials with versatile properties has been synthesized and is widely being used in industrial and household applications. However, even before the possibility to synthesize new polymer materials were realized, polymer blending was already recognized as a method to generate materials with improved properties [2]. The blends had many applications ranging from picture frames, table-ware, ear-trumpets, to sheathing the first submarine cables. Polymers are classified as either *natural* that resulted from natural biosynthesis, or *synthetic*. The *natural* (polysaccharides, proteins, nucleic acids, natural rubbers, cellulose, lignin, etc.) has been used for tens of thousands of years. The term *synthetic polymer* refers equally well to linear, saturated macromolecules (e.g., thermoplastics), to unsaturated polymers (e.g., rubbers), or to any substance based on crosslinkable monomers, macromers, or pre-polymers (e.g., thermosets) [1].

As regards *synthetic polymers*, they are commonly divided into three categories:

- Commodity
- Engineering
- Specialty

The five large-volume polymeric families that belong to the commodity resins are: polyethylenes (PE), polypropylenes (PP), styrenics (PS), acrylics (PMMA), and vinyls (PVC). The five Engineering polymer families are: polyamides (PA), thermoplastic polyesters (PEST), polycarbonates (PC), polyoxymethylenes (POM), and polyphenylene ethers (PPE). The engineering and specialty polymers show high mechanical performance, and the continuous use temperature $150 \leq CUT(°C) \leq 500$ [1]. Hence, in 2012, the global engineering plastics market of around 10 million tons, consisted for around 10% of polymer alloys and blends [2]. The polymer industry increasingly favours high technology and high value-added materials. These are obtained either by means of new polymerization methods, new processing technologies, by alloying and

reinforcing and through the introduction of new types of polymers. However, the polymer technology invariably moves away from the single-phase materials to diverse combinations of polymers, additives, and reinforcements. While synergistic effects are often cited, the main reason is a need for widening the range of properties, for development of materials that would have the desired combination of properties — tailor-made polymeric systems. A significant amount of these materials is used in blends and in composites [1].

Polymer blends constitute a large percentage of the total polymer consumption, and their pertinence has increased over the decades. Polymer blending has attracted much attention thanks to their many benefits in terms of: (i) easy methods of developing polymeric materials that have versatility for commercial applications, (ii) providing materials with full set of desired properties at the lowest price, (iii) manipulating of blend properties according to their end use by correct selection of the component polymers, (iv) extending the engineering resins' performance, improving specific properties (i.e.: impact strength or solvent resistance), (v) offering the means for industrial and/or municipal plastics waste recycling [1, 3]. These systems have been intensively studied because of their theoretical and practical importance. In general, they are classified into either homogeneous (miscible on a molecular level) or heterogeneous (immiscible) blends [4]. While miscibility is limited to a specific set of conditions, the immiscibility dominates, and most polymers form immiscible blends that require compatibilization. Alloys' performance depends on the ingredients, their concentration, and morphology. The alloying process must result in stable and reproducible properties of the polymer blend. Thus, the morphology must either be stable, unchanged during the forming steps, or the changes must be well predicted [1].

Polymers immiscibility is due to their unfavourable interactions as well as to the small gain in entropy when mixing high molecular weight components [5]. As a consequence, when two polymers are blended, they usually acquire a small-scale arrangement of the phases which is referred as "microstructure". Microstructure is determined by fluid properties and flow history, and it affects the rheological, optical, and transport properties of the mixture [6]. Blending of immiscible polymers can generate materials with a wide range of mechanical and other properties that would be hard to obtain with their monophasic counterparts. In addition to desirable final properties, improved processing behaviour and cost reduction have also contributed to the success of polymeric blends as new high-performance materials. The final properties of a polymeric blend obviously depend on the properties of the components, the composition of the blend, the interfacial characteristics (e.g. interfacial adhesion) and the morphology [5].

Most immiscible polymer blends are produced by melt compounding in extruders, single or twin screw. The melting and mixing process can generate morphologies ranging from disperse drops to fibres to lamella to co-continuous structures. Controlling these morphologies is critical to performance of the final blend [7]. The mechanism of morphology development from pellet-sized or powder-sized particles in polymer blends is directly derived from the complex interplay of material parameters and processing conditions. As a result of
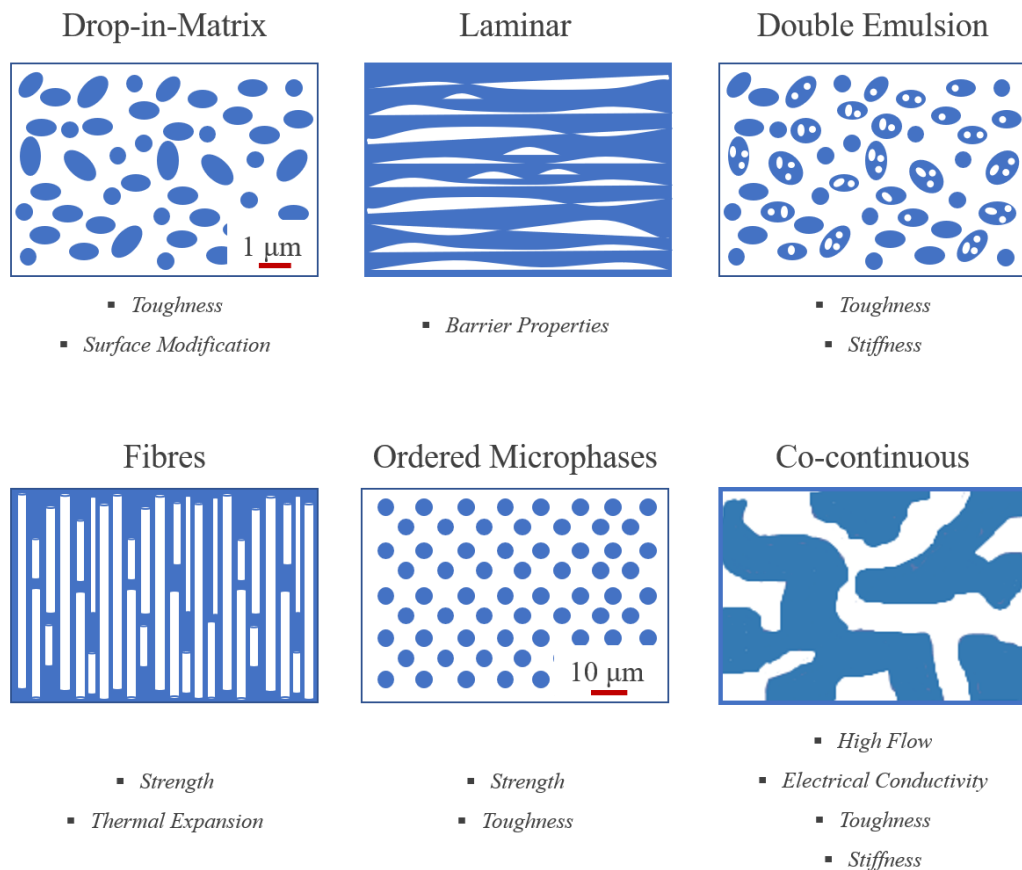
Figure 1.: Types of morphology in immiscible polymer blends [Reproduced from 7].

this, for a given blend, various types of useful morphologies (Figure 1) for different end properties such as high strength and toughness, toughness coupled with stiffness, good barrier properties, and high flow can be obtained by a judicious mixing process. However, from the point of view of a broader classification, multiphase polymer blends may be divided into two major categories:

1. Blends with a discrete phase structure (i.e., droplets in matrix)
2. Blends with a bicontinuous phase structure (i.e., co-continuous)

Other types of morphologies include fibrillar core shell and onion ring-like morphologies [8]. From a phenomenological point of view, the morphology of immiscible polymer blend is the outcome of a typical sequence of events occurring during the melt mixing step [8-11]: (i) the shear and elongational stresses peel off the softened polymer from the surface of the pellets forming ribbons and sheets; (ii) these sheets get thinner under strain until a critical thickness is reached, and then capillary wave instabilities lead to the formation of

holes; (iii) the second component coalesces through these holes; (iv) during further mixing, the pierced sheets become unstable and break into irregularly-shaped domains, whose further evolution determines the final blend morphology. Normally, after the last step of mixing process, the deformed volumes retract back to spherical shapes or break up driven by Rayleigh-type instabilities. As a result, drop-matrix morphologies commonly form [7, 12]. The type and dimensions of the morphology that is generated during processing has a significant impact on the blend properties [5]. In principle, the toughness and impact resistance of drop-matrix blends can result improved, but settling for such a result is definitely constraining. Actually, the spectrum of properties that could benefit from morphologies based on non-spherical domains is much wider. To give some examples: the barrier properties significantly improve in case of lamellar morphologies; the processability enhances in case of fiber-matrix microstructures, which also ensure low thermal expansion coefficient; the thermomechanical resistance and electrical conductivity greatly increase if the blend exhibits a co-continuous microstructure [7, 12]. Non-spherical morphologies can offer some better combinations of the component properties than are possible from dispersed-type structures. So, if the aim is a clever manipulation of the blend morphology, one of the strategies is promoting and preserving non-spherical domains in the melt state [12-13]. The formation of optimum dispersed phase particle size and the long-term stabilization of blend morphology are critical if the blend is to have optimum properties. The approaches traditionally adopted for this purpose can be divided in two categories: (i) those based on the control of the kinetics of the mixing process; (ii) those aiming at the improvement of the affinity between the polymers. The former strategy basically consists in quenching non-equilibrium morphologies, which can be promoted through the use of specific dies [14-17] or *via* chaotic mixing [18–21]. Alternatively, one can exploit the changes in the rheology of the polymer phases during processing so as to preserve the transient morphologies which form at certain stages of the melt mixing. Such an approach has been especially studied to promote co-continuous morphologies. As regards the second category, the inherent propensity of deformed domains to retract back to spherical shapes can be mitigated by adding a compatibilizing agent [12]. Compatibilization is a process of modification of the interfacial properties in immiscible polymer blend, resulting in reduction of the interfacial tension coefficient, formation and stabilization of the desired morphology. Thus, the compatibilization is an essential process that converts a mixture of polymers into an alloy that has the desired set of performance characteristics [22].

Nowadays there are many books, articles and reviews dealing with the compatibilization of polymer blends. The key routes are (i) addition of tailored block or graft copolymer, (ii) addition of reactive polymers [23], (iii) addition of multi-functional copolymer as impact modifier, (iv) addition of co-solvent [24], (v) by ionic interaction [24], and (vi) by γ-irradiation or electron beam (combined with or without a co-agent) [25]. However, most recently, a new approach has attracted interest: compatibilization by addition of targeted fillers. The adsorption of polymeric components on the solid surface was shown to change the thermodynamic state of the blends [26]. In the past ten years, the number of publications on fillers as compatibilizers for polymer blends raised dramatically. Most of them pointed out the necessary conditions on fillers to be efficient as compatibilizers. One necessary but not sufficient condition is their size: the particle radius (R_p) must be of the

same order of magnitude as the gyration radius (R_g) of the polymer. Indeed, the stabilizing energy gain is particularly efficient when the inorganic phase has a larger surface area per unit weight. Nanoparticles (NPs) have been used as modifiers to polymeric materials for many years, especially to improve elastic, barrier, thermal and fire properties [27–30]. Achieving a good NPs dispersion or exfoliation (for clays) in the polymer matrix was shown to be a key factor to obtain convenient ultimate performances. Currently, the issues of the NPs dispersion as well as the properties of the resulting composite are fairly well understood [31]. However, there is a lack of clear information on the influence of important factors, such as for instance: the nature of the NPs, the parameter of process on the effect of the NPs (structuring, compatibilizing) in polymer blends. Hence, to overcome this lack of information could be important to collect data as regards the localization and the compatibilization role of NPs and if them can be predicted by investigating different aspects (thermodynamic, wettability, dynamic processes and nature of the NPs in terms of shape, size and surface chemistry) of ternary systems.

1.2. Thesis structure

The present dissertation is divided into two main parts, which reflect the tracks on which the research activity has been carried out. Part I is provided with a wide overview of the state-of-art, embracing the skeleton of the work which also comes to light chiefly from the title: a*ssembly, elasticity, and structures* of nanoparticles in immiscible polymer blends. Part II, instead, encloses the application of the foreground arising from the first part. As a natural progression of the research activity, this part is devoted to the use of linear viscoelastic analysis as a tool for the assessment of the filler state of dispersion in polymer nanocomposites.

Part I is focused on the fundamental understanding of the phase morphology generated during blending, the mechanisms of stabilization, and rheology-morphology relationships in immiscible polymer blends. *Chapter 2* provides a background of the mechanisms of microstructural evolutions in binary and ternary polymer systems. Moreover, in this section is proposed the theory for prediction of the modes of dispersions in such systems, which is based on the interfacial and viscoelastic properties of the components. *Chapter 3* is dedicated to a wide discussion regarding the mechanisms underlying the effects of nanoparticles on the size (i.e., refinement and coarsening) and stability of the polymer domains. For correlating the linear viscoelasticity of nanocomposite polymer blends to their micro- and nanostructure an overview of this topic is provided at the end of this section.

The main results of the research activity are the subject matter of Part II. The latter rests on the competences gained and established through the research activity described in Part I. The work, depicted in *Chapter 4*, is related to a skillful use of linear viscoelastic analyses for the evaluation of the state of nanoparticles dispersion in polymer matrices, paying attention to its consequent impact on the macroscopic performances. A rheological two-phase model, recently proposed in the literature to describe the linear viscoelasticity of polymer nanocomposites, is invoked. In this chapter a further test of the robustness of the aforementioned model is given, by verifying the ability of the model to satisfactorily describe the linear viscoelasticity of other complex fluids, in which a superposition of the elasticity of the components is possible, such as nanocomposites based

on co-continuous matrices. Then is verified the effectiveness of overcoming the difficulties related to the dispersion of hydrophilic nanoparticles in hydrophobic polymer matrices. With a view to determining to what extent the nanoclay chemistry can affect the resulting morphology and because induced microstructural changes under flow sways rheological responses. The experimental results shown in *Chapter 5* are related to the same systems, but filled with different organomodified clays. Instead, the effect of the nanoparticles shape, their ease of dispersion in polymer melts and the results derived from suitable analyses are investigated in *Chapter 6*.

Finally, the *Conclusions* section is dedicated to a brief summing-up of the activities, aiming to highlight the main findings of the performed research. All the experimental details have been collected in the *Appendices* section, where necessa

BIBLIOGRAPHY

1. Utracki, L. A., & Wilkie, C. A. (Eds.). (2002). Polymer blends handbook (Vol. 1, p. 2). Dordrecht: Kluwer academic publishers.

2. Cardinaels, R. and Moldenaers, P. (2016) Morphology Development in Immiscible Polymer Blends, in Polymer Morphology: Principles, Characterization, and Processing (ed Q. Guo), John Wiley & Sons, Inc, Hoboken, NJ, USA. doi: 10.1002/9781118892756.ch19

3. Paul, D. R. (1989). Control of phase structure in polymer blends. In Functional Polymers (pp. 1-18). Springer US.

4. Visakh, P. M., Markovic, G., & Pasquini, D. (Eds.). (2016). Recent Developments in Polymer Macro, Micro and Nano Blends: Preparation and Characterisation. Woodhead Publishing.

5. Van Puyvelde, P., & Moldenaers, P. (2005). Rheology and morphology development in immiscible polymer blends. Rheology reviews, 2005, 101.

6. Tucker III, C. L., & Moldenaers, P. (2002). Microstructural evolution in polymer blends. Annual Review of Fluid Mechanics, 34(1), 177-210.

7. Macosko, C. W. (2000, January). Morphology development and control in immiscible polymer blends. In Macromolecular Symposia (Vol. 149, No. 1, pp. 171-184). WILEY-VCH Verlag.

8. Scott, C. E., & Macosko, C. W. (1991). Model experiments concerning morphology development during the initial stages of polymer blending. Polymer bulletin, 26(3), 341-348.

9. Sundararaj, U., Macosko, C. W., Rolando, R. J., & Chan, H. T. (1992). Morphology development in polymer blends. Polymer Engineering & Science, 32(24), 1814-1823.

10. Sundararaj, U., Dori, Y., & Macosko, C. W. (1995). Sheet formation in immiscible polymer blends: model experiments on initial blend morphology. Polymer, 36(10), 1957-1968.

11. Scott, C. E., & Macosko, C. W. (1995). Morphology development during the initial stages of polymer-polymer blending. Polymer, 36(3), 461-470.

12. de Luna, M. S., & Filippone, G. (2016). Effects of nanoparticles on the morphology of immiscible polymer blends–challenges and opportunities. European Polymer Journal, 79, 198-218.

13. Pötschke, P., & Paul, D. R. (2003). Formation of co-continuous structures in melt-mixed immiscible polymer blends. Journal of Macromolecular Science, Part C: Polymer Reviews, 43(1), 87-141.

14. Monticciolo, A., Cassagnau, P., & Michel, A. (1998). Fibrillar morphology development of PE/PBT blends: rheology and solvent permeability. Polymer Engineering & Science, 38(11), 1882-1889.

15. Lacroix, C., Grmela, M., & Carreau, P. J. (1999). Morphological evolution of immiscible polymer blends in simple shear and elongational flows. Journal of non-newtonian fluid mechanics, 86(1), 37-59.

16. Champagne, M. F., Dumoulin, M. M., Utracki, L. A., & Szabo, J. P. (1996). Generation of fibrillar morphology in blends of block copolyetheresteramide and liquid crystal polyester. Polymer Engineering & Science, 36(12), 1636-1646.

17. Chapleau, N., & Favis, B. D. (1995). Droplet/fibre transitions in immiscible polymer blends generated during melt processing. Journal of materials science, 30(1), 142-150.

18. Kwon, O., & Zumbrunnen, D. A. (2001). Progressive morphology development to produce multilayer films and interpenetrating blends by chaotic mixing. Journal of applied polymer science, 82(7), 1569-1579.

19. Zumbrunnen, D. A., & Inamdar, S. (2001). Novel sub-micron highly multi-layered polymer films formed by continuous flow chaotic mixing. Chemical engineering science, 56(12), 3893-3897.

20. Zumbrunnen, D. A., & Chhibber, C. (2002). Morphology development in polymer blends produced by chaotic mixing at various compositions. Polymer, 43(11), 3267-3277.

21. Zumbrunnen, D. A., Inamdar, S., Kwon, O., & Verma, P. (2002). Chaotic advection as a means to develop nanoscale structures in viscous melts. Nano Letters, 2(10), 1143-1148.

22. Utracki, L. A. (2002). Compatibilization of polymer blends. the Canadian journal of chemical Engineering, 80(6), 1008-1016.

23. Koning, C., Van Duin, M., Pagnoulle, C., & Jerome, R. (1998). Strategies for compatibilization of polymer blends. Progress in Polymer Science, 23(4), 707-757.

24. Brown, S. B. (2003). Reactive compatibilization of polymer blends. In Polymer blends handbook (pp. 339-415). Springer Netherlands.

25. Sonnier, R., Taguet, A., & Rouif, S. (2012). Modification of Polymer Blends by E-Beam and γ-Irradiation. Funct. Polym. Blends Synth. Prop. Perform, 261-304.

26. Lipatov, Y. S. (2002). Polymer blends and interpenetrating polymer networks at the interface with solids. Progress in Polymer Science, 27(9), 1721-1801.

27. Alexandre, M., & Dubois, P. (2000). Polymer-layered silicate nanocomposites: preparation, properties and uses of a new class of materials. Materials Science and Engineering: R: Reports, 28(1), 1-63.

28. Giannelis, E. P., Krishnamoorti, R., & Manias, E. (1999). Polymer-silicate nanocomposites: model systems for confined polymers and polymer brushes. In Polymers in confined environments (pp. 107-147). Springer Berlin Heidelberg.

29. Pavlidou, S., & Papaspyrides, C. D. (2008). A review on polymer–layered silicate nanocomposites. Progress in polymer science, 33(12), 1119-1198.

30. Ray, S. S., & Okamoto, M. (2003). Polymer/layered silicate nanocomposites: a review from preparation to processing. Progress in polymer science, 28(11), 1539-1641.

31. Taguet, A., Cassagnau, P., & Lopez-Cuesta, J. M. (2014). Structuration, selective dispersion and compatibilizing effect of (nano) fillers in polymer blends. Progress in Polymer Science, 39(8), 1526-1563.

Morphology of Immiscible Polymer Blends

2.1. Phase morphology

Among the crucial sides of blends development, one finds intensive research activity focusing mainly on the phase morphology generated during blending. A huge volume of literature deals exclusively with the topic. This is a clear indication that rules are hard to standardize because many processing and formulation parameters are involved in lending. Note that the development of phase morphology in polymer blends continues to be an important up-to-date research topic in many laboratories in universities or industries. Because of thermodynamic criteria, the majority of existing homopolymers form immiscible mixtures constituted of two or more phases. For a judicious control of the macroscopic properties of polymer blends, phase morphology constitutes a key parameter for many specific applications [1]. Although blending two polymers is the most common approach, also ternary blends have received a considerable amount of interest. The different morphologies occurring in ternary blends have been reviewed by Shokoohi and Arefazar [2-3]. The transition from one polymer to a binary polymer mixture provides a possibility of creating a new complex of properties. Furthermore, the transition from binary to ternary and multiphase mixtures extends the capabilities to develop a new combination of properties. Today, the use of ternary blends is not wide spread. This is due to the lack of a theory that is capable at least roughly to predict the properties of binary blends. It is clear that these difficulties are further increased in case of the ternary mixture due to an increase of the number of possible combinations of the three components. For polymer blends or composite, the term morphology describes the structures and shapes observed, often by microscopy or scattering techniques, of the different phase domains present within the mixture. Phase morphology is formed during blending of immiscible components. After mixing in a melt state, the developed phase morphology can easily be fixed by rapid cooling of the batch. Polymer blends have appeared mainly as an alternative to the synthesis of new polymers [4-5].

Similarly, there is an obvious tendency toward the increase of the number of components in polymer blends, which enhances their versatility and allows for a more flexible control over final properties of compositions [6]. A simple general principle exists according to which each component added introduces to a blend some portion of its properties or qualities. Unfortunately, this rule cannot be employed in an arbitrary way, without the knowledge of the particular phase morphology developed in a blend. The latter is the more complex the larger is the number of polymer components. The properties of any heterogeneous system are not only

determined by the properties of individual components but also depend to a considerable extent on the intensity of interaction at the interface and the phase morphology as well the latter factor characterizes the degree of dispersion, the shape, and the mutual arrangement of phases in the bulk of the blend [7].

Experience gained in the work with binary blends led to the development of practical techniques providing a variety of blends with preset phase structures. In particular, by controlling the type of flow, the ratio of blend components, and their viscoelastic and surface properties, it is possible to develop polymer compositions in which the dispersed phase domains could have the shape of discrete spheres, ellipsoids, fibres, layers of different morphology, or continuous networks. Adding the third immiscible component to a binary composition, increases the number of possible phase structures [8]. For example, should any of the three components be capable of forming a continuous phase, the two others may either form independent dispersions or encapsulate one another. If two of the three polymers form interpenetrating co-continuous phases, the third component may form domains localized predominantly in one of these phases, in both of them, or at the interface between the two continuous phases. Finally, each of the three polymers may form their own continuous structure developing the blend morphology comprising three interpenetrating continuous networks [5].

For binary immiscible polymer blends, two broad categories of morphology exist: the matrix/dispersed phase structure and the co-continuous morphology [8-9]. The dispersed phase in a binary polymer blend can take the form of fibres, lamella and A/B/A droplet-in-droplet type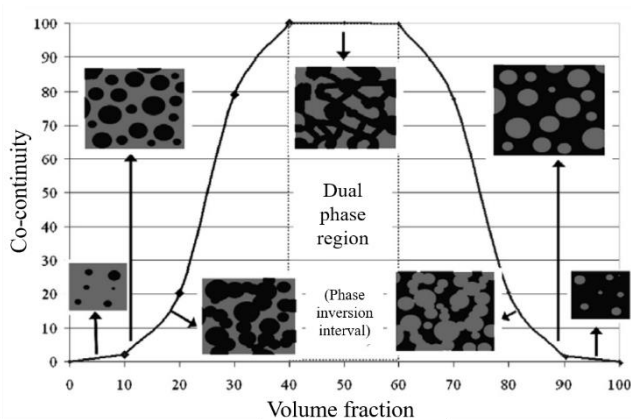 structures [10-11]. In an A/B binary blend, the dispersed phase type structure (Figure 1) is converted to a continuous type structure through an increase in the composition. By increasing the concentration of dispersed phase A, droplets coalesce resulting in a percolation threshold point being reached. This percolation threshold is the first connected pathway in the blend. Classic percolation theory defines the percolation threshold as the onset of long-range connectivity in random systems and it occurs in a range of about 15-20% concentration of minor component for a random mono-disperse

Figure 1.: Schematic representation of the morphology development in a binary blend [Reproduced from 12].

distribution of spheres [13]. Through a further increase of minor phase concentration, levels of continuity increase until a fully-interconnected co-continuous morphology is obtained (Figure 1). Co-continuity is defined as the case where each phase is fully continuous in the blend system. Since this often occurs over a concentration range for binary polymer blends, this is also known as the region of dual phase continuity. Phase inversion is defined as the concentration point where co-continuity converts into a matrix/dispersed phase morphology. It has been reported that the interfacial tension and the viscosity ratio can also influence the position of the region of dual-phase continuity [14-15.].

Much less work has been carried out on the fundamental morphological states present in ternary polymer blends comprised of significant quantities of three distinct phases. Recently, some papers have described the morphological behaviour of ternary systems with complex morphologies such as A/B/C composite-droplet structures [11, 16] and double-percolated morphology [17]. Complete wetting and partial wetting are two broad categories of morphological states possible for ternary polymer blends. In an A/B/C system, complete wetting describes the case where the most stable thermodynamic state is when one of the phases, say phase B, will always position itself to separate phases A and C. In that case phases A and B completely wet each other and phases B and C also completely wet each other (Figure 2). In the case of partial wetting, the most stable thermodynamic state is when there is three-phase contact. In that case, for example, droplets of B will situate at the A/C interface such that all three phases are in contact with each other [18- 19]. Both complete and partial wetting can be described by spreading theory as defined by Harkins equation [12].
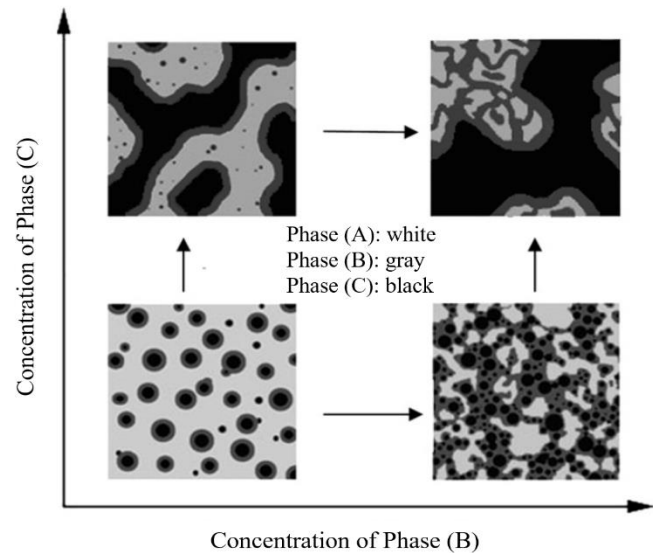

Figure 2.: Schematic representation of the morphology development in a ternary blend (complete wetting). [Reproduced from 12].

2.2. Morphology prediction

The phase structure of polymer blends, as stated above, is a function of a large number of parameters and for this reason attempts to formulate general empirical rules for its prediction have not been successful. Hence, theoretical analysis is logically inevitable if the aim is to finely control polymer blend morphology. This aim consists of an accurate prediction of the phase structure starting from a knowledge of the blend composition, properties of the components, and thermomechanical history during the blend preparation and processing. To accomplish this goal is very difficult because polymer melts are viscoelastic substances displaying elaborate rheological behavior, flow fields in mixing and processing equipment are complex, and thermomechanical history is complicated by substantial heat production [20]. It has to be said that the morphology and thermomechanical history are interdependent, since the instantaneous morphology of a polymer blend affects the flow fields during mixing and processing, the amount of dissipated energy and, consequently, temperature profile in the sample. Thus, it is not surprising that the state of the art is still far from the final desired product. Yet a number of results achieved in the theoretical description of phase structure evolution in mixtures of immiscible liquids can substantially improve the control of the phase structure in polymer blends. Most theories of the phase structure development in a mixture of immiscible liquids describe a system on a microrheological level, i.e., as domains of individual components (e.g., droplets) with characteristic

dimensions of the order of micrometers. These domains are characterized by the rheological properties of the components. An additional parameter that is used at the microrheological level is interfacial tension. Most theoretical analyses concentrate on binary blends of immiscible polymers. Less theoretical attention has been given to the phase structure development in multicomponent polymer blends. The two main characteristics of the phase structure are the *type* and *fineness*. The type of the phase structure specifies whether the structure is co-continuous or dispersed, whether the component becomes part of the matrix or the dispersed phase, and what shape is characteristic of the dispersed particles. The fineness of the phase structure describes the size of phase domains, e.g., the size of the dispersed particles. A theory to predict satisfactorily the type of the phase structure has not yet been formulated [20].

2.2.1. Binary blends

The phase structure of binary and multicomponent polymer systems has a lot in common. Therefore, it is advisable to consider features of the phase morphology and its prediction in binary mixtures the first. The phase structure of immiscible liquid binary systems (classical emulsion) is not very diverse. At rest, there are generally spherical droplets of the dispersed phase in a continuous matrix phase. Thermodynamic demand for minimization of the free surface energy initiates the droplets of the dispersed phase to coalesce so that over time the emulsion separates into two layers with a minimum interface area. Numerous papers on binary blends of immiscible polymers indicate that their phase morphology is characterized by a larger diversity. This is mainly due to the possibility of fixing the phase morphology at any stage of its formation, by, for example, fast quenching the melt. In 1972, Van Oene [21] proposed a semiquantitative theory for prediction of the modes of dispersions in polymer blends, which is based on the interfacial and viscoelastic properties of the components [5].

According to Van Oene it is shown that when a viscoelastic mixture of molten polymers is extruded, "alloy" composites are produced as a result of the formation of two distinct modes of dispersion: stratification or droplet-fibre formation. Important parameters responsible for these effects are: particle size, interfacial tension, and differences in the viscoelastic properties of the two phases. The formation of polymer spheres, ribbons, or fibres in a matrix can be predicted on the basis of his theory that provides a route to composites of controlled structure and properties [5, 21]. The essence of the theory is the assumption that during flow the differences in elasticity of the components may contribute to the value of the interfacial tension, which may be both positive and negative. Parameters responsible for the formation of a certain type of morphology are the values of the dynamic (γ'_{12}) and static (γ_{12}) interfacial tensions, the radius of the dispersed phase (*b*), and the first normal stress difference for the dispersed phase N_{1d} and the matrix N_{1m}, characterizing the viscoelastic properties of blended polymers:
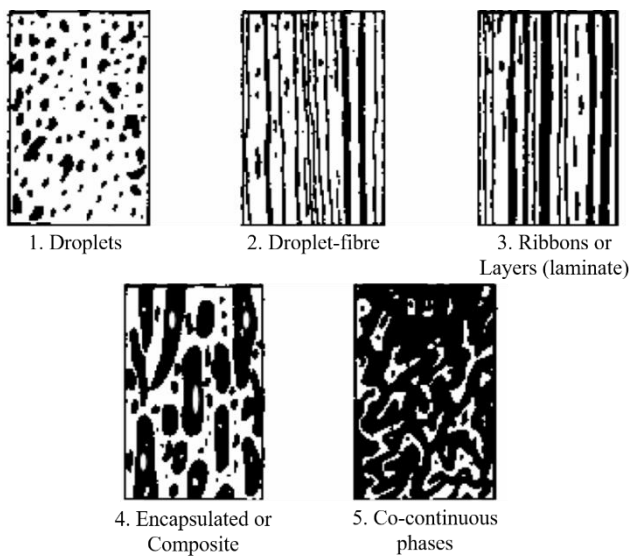
$$\gamma'_{12} = \gamma_{12} + b_1 \frac{N_{1d} - N_{1m}}{6} \qquad (2.1)$$

In the above formula, subscripts designate corresponding polymer phases. The formation of drops or fibres of phase *1* in the phase *2* takes place when $\gamma'_{12} > 0$ (provided $(N_{1d}-N_{1m}) > 0$) (Figure 3). When $\gamma'_{12} < 0$ (provided $(N_{1d}-N_{1m}) < 0$), the less elastic phase *2* is dispersed in the more elastic phase *1*, and the phase *2* stratifies. The formation of the droplet-fibre morphology of the less elastic phase will be possible if:

$$b_2^{cr} \leq 6 \frac{\gamma_{12}}{(N_{1d} - N_{1m})} \tag{2.2}$$

a quantity of the order of 1-0.1~μm for polymer melts [5, 21].

Thus, two cases can be realized when the less elastic phase is dispersed in a more elastic medium. In the initial stages of mixing when the particles of the dispersed phase are still large, that is, $b_2 = 1$ μm, $\gamma'_{12} < 0$ and phase *2*

1. Droplets   2. Droplet-fibre   3. Ribbons or Layers (laminate)

4. Encapsulated or Composite   5. Co-continuous phases

Figure 3.: Phase morphologies in polymer blends prepared by melt extrusion [Reproduced from 5].

forms layers or bands (stratified morphology). When the mixing process is effective enough and the particle size falls below the critical ($b_2 < 1$ μm), the layers split into discrete droplets and a stable droplet-fibre dispersion is developed. However, the drops of the less elastic phase *2* can capture small fragments of the matrix to form composite (encapsulated) particles (Figure 3). Differences in viscosity, shear rate, extrusion temperature, and residence time influence only the homogeneity of the dispersion and not the mode of dispersion. An important position in the hierarchy of the phase morphologies belongs to the structure of co-continuous phases shown in Figure 3 [4, 6, 8, 22-25]. Conditions favouring the formation of this morphology are sufficiently high content (above the percolation threshold) and/or a low viscosity of the dispersed phase [5, 21].

2.2.2. Ternary blends

As we have seen, VanOene's theory demonstrates the importance of the interfacial tension in the formation of the morphology of binary mixtures of polymers. This parameter is more importantly as regards his contribution in complex multiphase heterogeneous systems. Indeed, the binary systems are characterized by one interface, the interface type contacts *1–2* and the corresponding interfacial tension, while the three-phase system is characterized by three interfaces, the three corresponding types of contacts *1–2*, *1–3*, and *2–3*, and three interfacial tensions γ_{12}, γ_{13}, and γ_{23}. As mentioned above, prediction of the phase situation in a multiphase

mixture is based on the analysis of the mutual wetting (or non-wetting) of phases, which in turn is dictated by the interfacial tensions at the interfaces. The wettability represents the ability of a liquid of spreading over a solid substrate or an immiscible liquid phase. Wetting behaviour is illustrated by the fate of a liquid drop in equilibrium with a surrounding vapor, when placed onto a substrate. Either the drop forms a cap with non-vanishing contact angle θ (defined in Figure 4), and does not spread over the substrate, or the contact angle vanishes and the drop spreads to form a uniform film. Thomas Young in 1805 established the relationship between the

Figure 4.: Schematic representation of a spherical drop with the surface tension forces at equilibrium.

equilibrium contact angle θ that the drop makes with the surface and the three surface tensions γ, through a force balance in the plane of the surface at the three-phase contact line. In the case of partial wetting, Young's equation gives the contact angle:
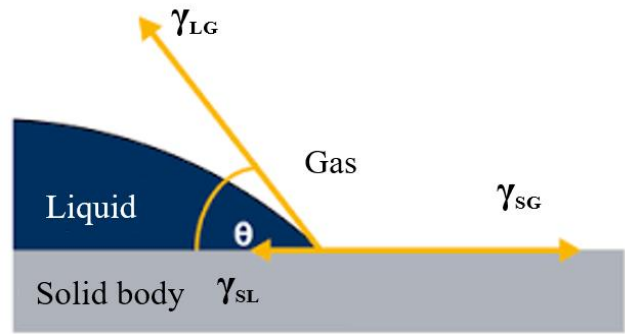
$$\gamma_{SG} = \gamma_{SL} + \gamma_{LG} cos\theta \tag{2.3}$$

where γ_s indicate various interface tensions and subscripts S, L, and G refer to substrate, liquid, and gas (or vapor, or atmosphere), respectively. If the three tensions are known, the wetting state of the fluid follows directly [37]. In the case of complete wetting:

$$\gamma_{SG} = \gamma_{SL} + \gamma_{LG} \tag{2.4}$$

because for a wet surface the solid-vapor interface is a combination of solid-liquid and liquid-vapor interfaces. In neither case does γ_{SV} exceed the sum $\gamma_{SL} + \gamma_{LV}$. In other words, in the first case, at $\theta > 90°$ and $\gamma_{SG} < \gamma_{SL}$, liquid does not wet a solid. This case is classified as non-wetting behaviour (Figure 5). If $\gamma_{SG} < \gamma_{SL} + \gamma_{LG}$ and $0 < \theta < 90°$, a droplet with a finite (equilibrium) contact angle minimizes the free energy of the system leading to partial wetting (Figure 5). If $\gamma_{SG} = \gamma_{SL} + \gamma_{LG}$, the contact angle $\theta \sim 0$. The system will consequently be in equilibrium when a macroscopic uniform [26.-
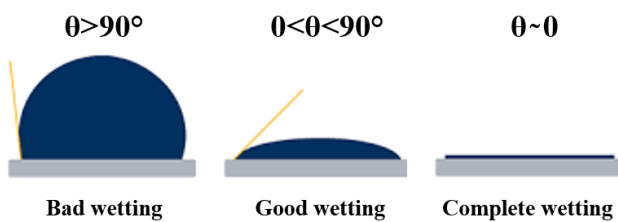
Figure 5.: Different wetting behaviours.

27, 29, 38, 29] liquid layer covers the whole solid surface corresponding to complete wetting (Figure 5). If $\theta < 90°$, the surface is said to be *hydrophilic* whereas the surface is said to be *hydrophobic* if $\theta > 90°$.

Cooper and Nuttal in 1915 [30] moved even more toward the prediction of the spreading behaviour, in this way Harkins and Feldman in 1922 [31] introduced the spreading coefficient. Harkins and Feldman defined this parameter as:

$$\lambda = W_A - W_c \tag{2.5}$$

This equation suggests that a liquid will not spread if its work of cohesion W_C is greater than the work of adhesion W_A for the interface of the liquid and another liquid or solid upon which spreading is to occur. So, the spreading behaviour and the contact angle, above mentioned, depend on a balance between adhesive and cohesive forces. Adhesive forces between a liquid and solid cause a liquid drop to spread across the substrate. Cohesive forces within the liquid cause the drop to ball up and avoid contact with the surface.

The W_A and W_C values are related to interfacial tensions by

$$W_A = \gamma_{SG} + \gamma_{LG} - \gamma_{SL} \tag{2.6}$$

$$W_C = 2\gamma_{LG} \tag{2.7}$$

So, the spreading coefficient can be defined as:

$$\lambda = \gamma_{SG} - \gamma_{LG} - \gamma_{SL} \tag{2.8}$$

It is obvious that a positive value of the spreading coefficient corresponds to spreading, a negative to non-spreading.

An up-to-date version of the spreading coefficients theory was realized by Torza and Mason [18] which were apparently the first who adapted Eq. (2.8) for the ternary mixtures of immiscible liquids.

They considered the equilibrium state established after two immiscible liquid drops of phases A and C were brought into intimate contact when they were suspended in a third immiscible liquid of the matrix phase B. As a result, the expressions for the three spreading coefficients λ_{ij} enabled to predict the morphological type of composition and wetting one phase by another were evaluated. In classic ternary emulsions depicted schematically in Figure 6, wetting or non-wetting between the inner phases A and C is considered. Therefore, phase arrangement in Figure 6b is classified as non-engulfing [18, 32] or complete non-wetting; Figures 6a and 6c refer to a complete engulfing (or complete wetting), and Figure 6d denotes the case of a partial wetting (engulfing). Unfortunately, their work was forgotten and unclaimed for almost 30 years. Meanwhile, in 1988, Hobbs et al. [33] published a work in which is adopted the Harkins equation for the case of three liquid phases and the spreading coefficient was stated as follow:

a)

$\lambda_{BAC} = \gamma_{BC} - (\gamma_{AB} + \gamma_{AC}) < 0$
$\lambda_{ABC} = \gamma_{AC} - (\gamma_{AB} + \gamma_{BC}) < 0$
$\lambda_{ACB} = \gamma_{AB} - (\gamma_{AC} + \gamma_{BC}) > 0$

b)

$\lambda_{BAC} = \gamma_{BC} - (\gamma_{AB} + \gamma_{AC}) < 0$
$\lambda_{ABC} = \gamma_{AC} - (\gamma_{AB} + \gamma_{BC}) > 0$
$\lambda_{ACB} = \gamma_{AB} - (\gamma_{AC} + \gamma_{BC}) < 0$

c)

$\lambda_{BAC} = \gamma_{BC} - (\gamma_{AB} + \gamma_{AC}) > 0$
$\lambda_{ABC} = \gamma_{AC} - (\gamma_{AB} + \gamma_{BC}) < 0$
$\lambda_{ACB} = \gamma_{AB} - (\gamma_{AC} + \gamma_{BC}) < 0$

d)

$\lambda_{BAC} = \gamma_{BC} - (\gamma_{AB} + \gamma_{AC}) < 0$
$\lambda_{ABC} = \gamma_{AC} - (\gamma_{AB} + \gamma_{BC}) < 0$
$\lambda_{ACB} = \gamma_{AB} - (\gamma_{AC} + \gamma_{BC}) < 0$

Figure 6.: Possible equilibrium morphological types in ternary polymer blends [Reproduced from 34].

$$\lambda_{31} = \gamma_{12} - \gamma_{32} - \gamma_{13} \tag{2.9}$$

Afterwards Virgilio et al. [19] focused attention on these important misconceptions, as regards the work of Hobbs et al., that still remain in the polymer blend literature concerning the use of the spreading coefficients. In particular, Hobbs et al. did not consider the third spreading coefficient λ_{21} signalling the partial wetting phenomena. A common procedure is the prediction of the morphology in ternary polymer blends based on the calculation of only one λ_{31} or two (λ_{31} and λ_{13}) spreading coefficients. This can lead to erroneous conclusions, especially when these coefficients are negative. Specifically, at both negative values λ_{31} and λ_{13}, the negative λ_{21} value predicts partial wetting (partial encapsulation Figure 6B, while a positive λ_{21} value informs about the development of the morphology of two separated dispersed phases (Figure 6C). Therefore, in ternary blends, three spreading coefficients are necessary to correctly predict the resulting morphology [5].

In the case of melt-processed ternary polymer blend with two main co-continuous phases B and C and a third dispersed phase A, a different approach based on the sign of the spreading coefficients is used [19, 34, 32]. From a thermodynamic standpoint, ternary blends of homopolymers A, B and C can typically display four types of morphologies, as predicted by the minimization of the interfacial free energy. Three are complete wetting types of structures, in which one polymer forms a layer at the interface of the other two (Figure 7a-c). The fourth microstructure corresponds to partial wetting, characterized by a line of 3-phase contact between the materials (Figure 7d) [34]. As demonstrated by Torza and Mason [18], each of these morphologies is characterized by a set of three spreading coefficients λ_{ijk} that are functions of the interfacial tensions between the materials:

Figure 7.: Morphologies in a ternary system comprised of two major phases B and C (in white and grey) and one minor phase A (black). From (a) to (c), complete wetting systems, in which phases C, B and A, respectively, wet the AB, AC and BC interfaces and in (d), partial wetting morphology showing a 3-phase line of contact [Reproduced from 19].

$$\lambda_{ABC} = \gamma_{AC} - (\gamma_{AB} + \gamma_{BC})$$
$$\lambda_{ACB} = \gamma_{AB} - (\gamma_{AC} + \gamma_{BC}) \tag{2.10}$$
$$\lambda_{BAC} = \gamma_{BC} - (\gamma_{AB} + \gamma_{AC})$$

where the γ values are the interfacial tensions between the different phases. Each spreading coefficient gives the tendency of one phase to spread and form a continuous layer at the interface of the other two.

It can be stated that the accuracy of the above analysed methods, as regards the prediction of the phase morphology of multicomponent incompatible polymers blends, can be very low due to the low reliability of
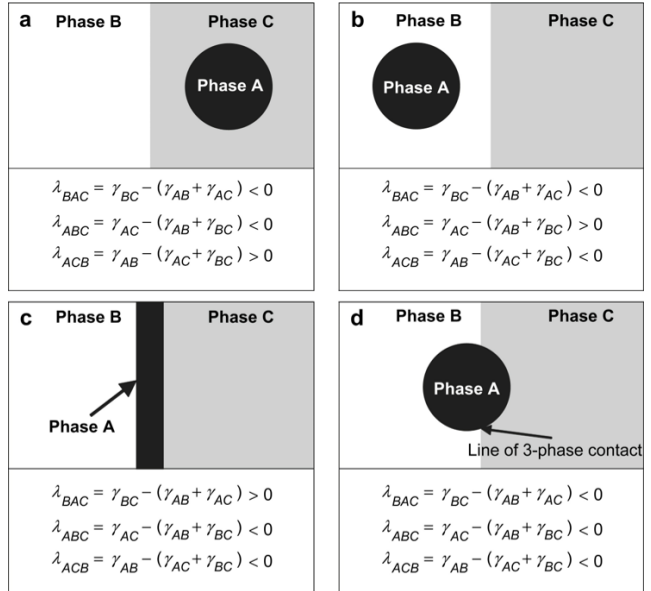
the values of interfacial tension, which may differ much from each other. This is because of the low precision and reproducibility of the existing methods of measuring γ_{ij} melts and the fact that polymers from different manufacturers may contain various impurities and additives, influencing the surface properties of materials. In this regard, the need to support the experimental data and calculations with the microscopic studies is clear [5, 35.]

2.3. Morphology development

As was widely reported, *complete wetting* and *partial wetting* are two broad categories of morphological states possible for ternary polymer blends. In this way, we pertain to two wetting behaviours: (i) complete wetting (Figures 7a–c) or (ii) partial wetting at the interface (Figure 7d). Ternary systems with the encapsulated inner phases have attracted a great deal of attention in the recent literature. As it was mentioned earlier, fully encapsulated morphologies are formed provided one of the spreading coefficients (λ_{BAC} or λ_{ACB}) is positive while $\lambda_{ABC} < 0$ (Figures 7 b and c). We want to try to summarize the influence of different factors on the formation of morphologies of such blends, including core–shell, separated disperse, and co-continuous morphologies; and also, the parameters affecting the type of morphology and its distribution state. Before we do that, we have to briefly discuss about binary polymer blends [5].

2.3.1. Binary blends

Varying the composition is one of the main methods to control the phase morphology of polymer blends. Numerous studies published since then show [4, 8-9, 38] that increasing the content of a dispersed phase A in a matrix B is accompanied by a sharp increase in the domain sizes due to increasing the frequency of collisions of drops leading to coalescence. Finally, the fusion of droplets of the dispersed phase occurs so often that they form a continuous network phase B interlaced with the continuous phase A. In this case, one can speak about the formation of the morphology of the two co-continuous phases. These blends have the potential of opening particular application fields where the presence of interconnected structures is a necessary feature (as in separation phenomena, electrical conductivity, tissue engineering scaffolds, and drug delivery devices) [5].

More to the point, in quiescent conditions, the factors that determine the morphology of a polymer blend are the *volume fraction* and *viscosity* of the different components. In a binary blend, immiscibility results in either dispersed or co-continuous morphologies. In the former, one of the phases is continuous and encompasses dispersed spheroidal inclusions of the other constituent; the latter, on the other hand, are obtained for intermediate compositions and are characterized by the mutual interpenetration of the phases. Complete co-continuity occurs around the so-called phase inversion point, where the original dispersed phase becomes continuous and, conversely, the original matrix turns itself into the dispersed phase. Concerning the effect of viscosity, Willemse and co-workers have highlighted that the volume fraction of minor component corresponding to the transition from dispersed to co-continuous morphology decreases as the ratio p between the viscosities of the minor and major phase, η_d and η_m respectively, decreases [39]. This remark is in agreement

with the predictions of the following semi-empirical rheological model developed by Jordhamo and co-workers

$$\frac{\eta_d}{\eta_m} \cong \frac{\phi_d}{\phi_m}$$

(2.11)

according to which co-continuity arises when p equals the ratio between the volume fractions of the minor and major phase, i.e. ϕ_d and ϕ_m [14]. In particular, for $p \approx 1$, phase inversion occurs when the volume fraction of both the phases is 0.5. In flow conditions, the morphological evolution of multiphase polymer systems derives from the interplay of melt-state modifications experienced by the different phases. These phenomena, basically consisting in domain breakup, coalescence and relaxation, are in turn influenced not only by the properties of the individual components, but also by their interactions and the imposed deformation rate. In dispersed morphologies, the minor phase may be present not only in the form of drops, but also of fibrils or lamellae. Concerning co-continuous morphologies, Miles and Zurek have extended the relationship between viscosity ratio and phase inversion composition expressed by Equation 2.11 to the dynamic case, implementing the model with the dependence of the viscosity of the polymers on the shear rate [40]. A significant contribution to the understanding of the mechanisms ensues from studies performed on emulsions of Newtonian fluids [41]. For polymer blends, indeed, the underlying physics is basically the same, in spite of the larger width of polymer/polymer interfaces compared with those between low molecular weight fluids [42].

In systems with dispersed morphology, the drops of the minor phase may deform, orient, and possibly break up under flow. Their response is determined by the viscosity ratio, the flow conditions (shear or elongation) and the balance between viscous stresses, which tend to deform the drops, and interfacial tension, which drives the drops to retract back to a spherical shape. The relative importance of the latter parameters is expressed by the capillary number:

$$C_a = \frac{\eta_m \dot{\gamma} R}{\alpha}$$

(2.12)

where η_m is the viscosity of the matrix, $\dot{\gamma}$ the deformation rate, R the radius of the drops of dispersed phase and α the interfacial tension. *Ca* also expresses the ratio between the interface relaxation time ($\eta_m R/\alpha$) and a characteristic time for flow induced deformation (the inverse of the shear rate). For capillary numbers lower than a critical value, the drops attain a steady shape and orientation, the deformation being exclusively induced by the flow. Conversely, above the critical capillary number the drops eventually break up due to the prevalence of viscous stresses over the interfacial tension. The critical capillary number for Newtonian droplets has been measured as a function of p by Grace in both simple shear and planar elongation, by gradually increasing the deformation rate until breakup [43]. In simple shear flow, no breakup is found when $p > 4$ due to the high viscosity of the dispersed phase; an elongational flow can instead break up droplets of any viscosity ratio. Data for intermediate flows have been provided by Bentley and Leal [Bentley and Leal, 1986]. Briefly

commenting on the droplet breakup mechanisms, for $Ca<<1$, the steady drop shape is slightly ellipsoidal, its long axis being oriented at 45° to the flow; with increasing Ca, the viscous effect also increases, and the drop axis shifts toward the flow direction. When Ca is slightly greater than the critical value, the breakup mode depends on p: small droplets can be released from the end of a sigmoidal drop, or alternatively the central part of the drop can gradually neck up, giving rise to the breakup into two "daughter" drops and smaller satellite droplets. When Ca is well above the critical value, the drop stretches into a slender fibril, which subsequently breaks up by a capillary-wave Rayleigh instability. For a gradual increase of the shear rate, a series of breakup steps takes place, bringing about the formation of smaller and smaller droplets. On the other hand, breakup for a sudden shear rate increase is a single event that causes the formation of daughter drops characterized by low values of Ca, hence remaining nearly spherical. The capillary number being equal, a viscoelastic drop can stretch more than a Newtonian one, hence the timescales for its breakup are much longer; for small deformations, however, the treatise described so far can be reasonably extended to non-Newtonian fluids.

When a multiphase fluid system with drop-matrix morphology is sheared at a low capillary number, the characteristic size of dispersed phase may increase due to coalescence phenomena that follow the collision of drops coming into contact. Differently from breakup, coalescence may also take place after flow cessation, due to the approaching of deformed drops that are recovering their spherical shape. After colliding, the drops develop a flat or dimpled interface over which they are separated by a thin film of matrix fluid. Hydrodynamic forces push the drops together during some finite interaction time, and the film thins due to the drainage of matrix fluid. If the film thickness falls below a critical value, estimated to be approximately 10 nm for polymer blends, then van der Waals forces become relevant, the film ruptures, and the droplets coalesce [44]. Alternately, the hydrodynamic forces may reverse before the film ruptures, so that the droplets separate without coalescing. The efficiency with which the collisions result in coalescence depends on how effectively the matrix layer is drained from between the droplets. Film drainage has been modelled through various assumptions: (i) a partially mobile interface, appropriate if p is close to 1 and the main resistance to film drainage comes from viscous stresses within the droplet; (ii) a fully mobile interface, if $p << 1$ and the dispersed fluid phase provides no resistance to drainage; (iii) an immobile interface, suitable in the case of $p >> 1$ and absence of interfacial deformation in response to shear stresses in the film. Each drainage model gives a different dependence of the coalescence-limited drop size on shear rate. In any case, the growth of drop size due to coalescence (estimable through scaling relationships not discussed here) is determined by factors such as the frequency of collisions, the interaction time, and the hydrodynamic forces, which in turn depend on the volume fraction of the dispersed phase, the flow rate and the rheological and interfacial properties of the constituents. Larger drops are less likely to coalesce than smaller ones because they flatten more easily, and it is more difficult to drain the matrix fluid from the film. The dynamic interplay of breakup and coalescence phenomena is mainly governed by phase concentrations, interfacial tension and shear rate, and determines the so-called morphological hysteresis. The minimum drop size for breakup and the maximum drop size for coalescence coincide at a critical shear rate. Above this value, the steady-state drop size is determined by a competition between breakup and coalescence and is a unique function of shear rate. Below the critical

shear rate, instead, there exists a range of drop diameters that are too small to break up but are also too large to coalesce in a reasonable time. After the cessation of the flow, further morphological evolutions ensue from the competition of two processes driven by interfacial tension: the relaxation of the deformed drops, which are not stable and tend to retract back to a spherical shape, and the formation of capillary waves that cause the breakup of large drops. The two phenomena prevail at low and high values of the drop aspect ratio, respectively. This means that slightly deformed droplets will retract back to a spherical shape, very elongated droplets will relax into a string of droplets via capillary wave instabilities, whereas droplets with intermediate aspect ratio will undergo end pinching: the drop forms bulbous ends which pinch off into separate drops. If the drop is long enough, bulbs form again on the new ends, and the process is repeated until the remaining portion of the drop is small enough to retract back to a sphere. The morphology of multiphase polymer materials directly reflects itself on the linear viscoelastic response of the systems, characterized by the combination of the inherent viscoelasticity of the polymeric constituents and the features of the polymer/polymer interfaces. The tendency of the latter to relax under the interfacial tension, bringing the drops back to their spherical shape, determines an excess elasticity evidenced by an increase of the elastic shear modulus G' at low frequencies; conversely, the viscous modulus G" is not show significantly affected by the presence of the drops. If the characteristic relaxation times of the drops (typically, on the order of seconds) is longer than the relaxation time of the polymers, the contribution of the drops is revealed by a "shoulder" in the curve of G' versus ω, which shifts to higher frequencies with decreasing the drop size. The excess elasticity is less evident for co-continuous morphologies, G' exhibiting a power law behaviour at low frequencies; this is ascribed to the high interconnection between the phases of the systems and the consequent resistance to flow [45]. The linear viscoelastic moduli of a polymer blend with drop-matrix morphology can be predicted by the Palierne model (which is an extension of the theory by Oldroyd on Newtonian multiphase systems) once the interfacial tension and the drop size distribution are known [46-48]. If the polydispersity (ratio between volume-average and number-average drop radii) is lower than 2, the volume average drop radius can be reasonably used in place of the drop size distribution. Although the amounts and properties of the constituent play an important role in its determination, morphology is controlled by the deformation history and is not an intrinsic property of a blend. When a third phase is incorporated, further complications emerge due to the varied interphase interactions.

2.3.2. Ternary blends

In ternary blends, the main attention is also paid to co-continuous morphologies. Here, the results of research are expected to be even more interesting, since the continuous phases can be developed by two or all three phases. Also, the influence of the *component ratios* in the composite domains on the phase sizes is of interest and importance [5]. For example, Tchomakov et al. [49] observed that under all the processing conditions they experimented, the most stable morphology was obtained with the dispersed phase composition of 50/50 for HDPE/PS/PMMA blends. This composition was also stable over a wide range of polymer feeding sequence, minor component viscosity and minor phase concentration. Luzinov and his co-workers [50] changed the

weight ratio of PE and PS in ternary PS/SBR/PE blends at constant SBR content (25 wt %). Different morphologies are observed depending on this ratio. At low PE (or PS) content, PE (or PS) is encapsulated by an SBR shell and dispersed in the PS (or PE) matrix. When the PE (or PS) content is increased the particles formed by this component are much larger and much irregularly shaped but still coated by an SBR layer. At PE/PS weight ratios of 40/60, 50/50 and 60/40, three co-continuous phases are formed. In addition to co-continuous phases, PE and PS particles enveloped by SBR also coexist. Core–shell morphology for the minor phase is observed at quite different PE/PS weight ratios, independent of the thermoplastic that forms the matrix, either with the more viscous and elastic PE or with the less viscous and elastic PS. Observation of co-continuity (triple-phase continuity) complies with the minimization of the total interfacial free energy for the system [3].
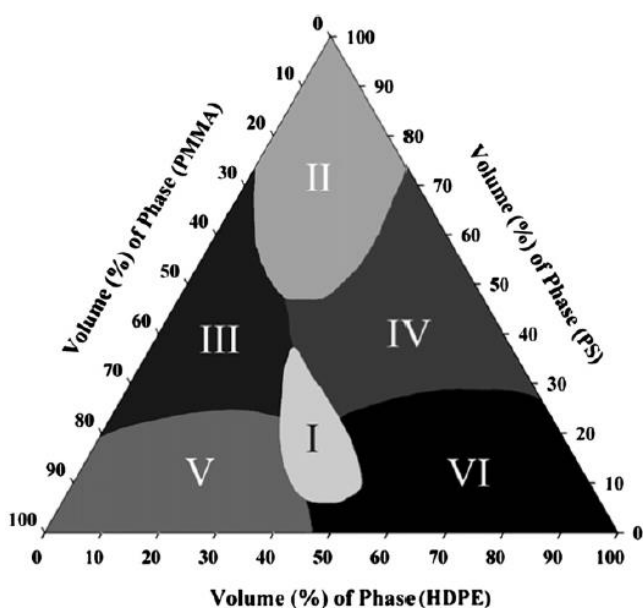

Figure 8.: Triangular concentration diagram showing the various regions of the morphological states for ternary HDPE/PS/PMMA [Reproduced from 12].

Ravati and Favis [12] and Ravati [51] examined the complete range of morphological types in ternary blends of high-density polyethylene (HDPE), polystyrene (PS), and poly (methyl metacrilate) (PMMA) prepared by melt mixing over the entire composition variation. HDPE, PS, and PMMA are selected as a model system showing a positive spreading coefficient of PS over PMMA. Thus, in all cases the PS phase separates HDPE and PMMA. Four subcategories of morphologies were identified, depending on the composition of phases (Figure 8), including: (a) matrix/core–shell dispersed phase (V, VI); (b) tri-continuous (I); (c) bi-continuous/dispersed phase (II, IV); and (d) matrix/two separate dispersed phases (II) morphologies. The phases in these sub-morphologies are identified and illustrated qualitatively by electron microscopy as well as a technique based on the combination of focused ion beam irradiation and atomic force microscopy [5]. Letuchii et al. [51, 53] also studied the effect of composition on the formation of different types of morphology in the PMMA/PS/PBT blends. Different structures formed by the core and shell phases placed into a matrix phase define a variety of morphologies in these systems. They have been classified in five types of morphologies and characterized as follows (Figure 9): I - separated dispersed phases; II - single core–shell; III - multiple cores–shell; IV-dispersion of the separate domains in one of the bicontinuous phases; V - all three phases are co-continuous (partial encapsulation/partial wetting is not considered) [5].
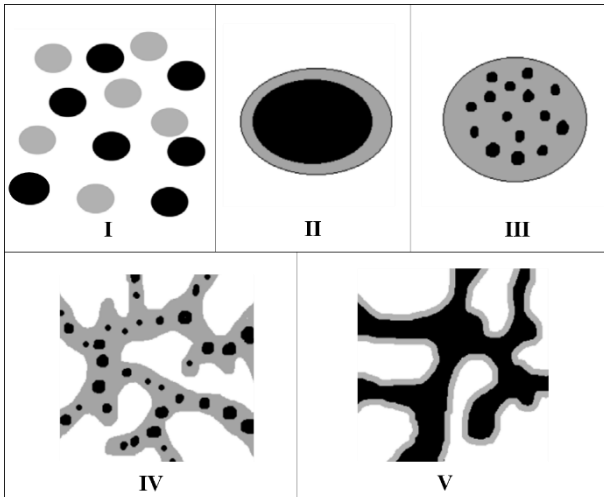
Figure 9.: Morphological types in ternary polymer blends with phase encapsulation Reproduced from 5].

As we have seen, the composition has a strong impact on the phase morphologies of immiscible ternary blends with encapsulated inner phases. By appropriate choice of the content of constituent polymers, polymer blends with two or three co-continuous phases can be prepared. Increase of concentration of one of or both dispersed phases result in increasing total sizes of the composite domains. Mutual disposition of the core and shell phases in the composite domains is developed in agreement with thermodynamic demand of minimization of surface free energy. Therefore, increasing the concentration of the core phase will never result in phase inversion phenomena. Instead, at high core phase content, the single core composite droplets are formed while at low content –the multiple cores are developed [5].

Studies on the encapsulated morphologies in multiphase, mainly ternary, immiscible polymer blends have become very popular in the recent years. Expressing a consolidated opinion about the validity of the spreading coefficient theory and the key role of interfacial forces in development of the encapsulated morphologies, most of the authors also reported on the importance of *kinetic factors*. Indeed, although the encapsulation itself is a thermodynamically driven phenomenon, the rate of approach to the equilibrium morphology is a time-dependent process controlled by phase viscosity (and elasticity) ratios, the type of flow in a mixer, the intensity and sequence of mixing, and so on [5]

The effect of the viscosity ratio is still controversial and a critical topic among the authors. In the case of ternary blends with core–shell morphologies of the dispersed phase, it might be assumed that the size of the core is influenced by the viscosity ratio of the core forming polymer to the shell precursor. Luzinov et al. [54] claimed that the core diameter is determined by the viscosity ratio of core to shell and also the composite droplet size is affected by the viscosity ratio of the shell to matrix. Hemmati et al. [55] modified this theory and claimed that in ternary polymer systems, the average viscosity ratio of minor phases (have) to the matrix determines the droplet size, which is easily calculated by the mixture law:

$$\eta_{ave} = \eta_1 \phi_1 + \eta_2 \phi_2 \tag{2.13}$$

where ϕ_1 and ϕ_2 are volume fractions, and η_1 and η_2 are viscosities of the dispersed phases. Their investigations showed that the torque ratios affected only the size of the dispersed phases and have no influence on the type of morphology. Hemmati et al. [55] used the steady state torque (from Brabender torque versus time plots) as a measure of viscosity, to study the effect of viscosity ratio on morphology and particle size of the dispersed phase [54-59]. For core–shell morphology, they used the ratio of average steady-state torque of two minor phases to the matrix, to predict the dispersed phase size as a whole, [55] and torque ratio of the core to shell

for prediction of core size [59]. Considering all of the results reported above, it can be declared that the effect of viscosity ratio in controlling the morphology of ternary blends compared to interfacial tension, is of a smaller importance [3].

As far as the dependence of the blend morphology on the mixing sequence is concerned there is no common point of view among the authors. Huang et al. [60] studied PP/EOR/EOR-g-MAH and claimed that the order of mixing, simultaneous mixing, master batch preparation or premixed method, does not affect the particle size. They reported that the order of mixing of the components seems to cause a negligible difference in the average size of the particles or their poly-dispersity for the blends with a uni-modal particle size distribution regardless of the matrix; however, for the blends having a bimodal particle size distribution, the order of mixing seems to affect the dispersed rubber particle size a little more but still not significantly [3, 61] working with multiphase polymer blends have indicated that the mixing sequence had a strong impact on the final morphology [5]. Huang et al. [60, 62] found that the intensity of mixing or extruder type affects the average particle size as might be expected; however, the choice of extruder does not seem to affect whether there is a bimodal particle size distribution or not. Macosko et al. [63] studied the evolution of the average diameter of (PMMA/PS/poly(S-b-MMA) diblock copolymer) blends as a function of the mixing residence time; 3 min. of mixing (at a maximum shear rate of about 50 s-1) was adequate to reach the final particle size [3].

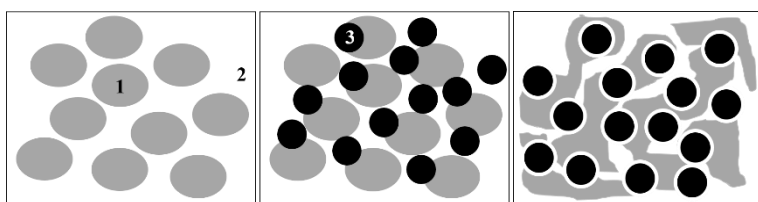## 2.4. Ternary Systems with One Solid Phase

Figure 10.: Double action of solid particles added to dispersed phases.

There are not so few publications devoted to morphology and properties of immiscible binary blends containing dispersed solid particles as the third phase. From a phenomenological perspective, the mechanism is based on an idea of free space of matrix (FSM) [52-53]. Adopting the simpler case that assumes a polymer matrix *2* filled with a large enough portion of liquid primary dispersed phase *1*. The latter, nevertheless, still does not form a co-continuous structure and consists of nearly spherical droplets, as sketched in Figure 10. On subsequent addition of the solid dispersion of phase 3 (black spheres), the overall concentration of both inner phases becomes higher. If it is supposed that the values of both spreading coefficients λ_{31} and λ_{13} are negative, the contacts between domains 1 and 3 are unfavourable and their encapsulation is prohibited. Since there is not enough room in the matrix for arranging spherical particles 3 and 1, the latter are forced to deform during blending and to occupy the vacant volumes between solid spheres 3 [5].

Spatial deformation of adjacent liquid drops results in collision and fusion of its tentacle-like ends followed by formation of co-continuous phase, on the one hand, and increase of the specific interface area, that is, the degree of dispersion of this phase, on the other hand. It is clear that when both inner phases are liquid, they accommodate their shapes simultaneously and stimulate each other to develop their own continuous phases at proper concentrations. Huitric et al. [64] reported on the effect of organically modified layered silicate on the

rheological, morphological, and structural properties of immiscible polyethylene/polyamide (PE/PA) blends. It was observed that the dispersed phase sizes decreased with increasing clay content up to 2% and tended to stabilize at higher clay fractions. In blends with PE matrix, clay particles were located predominantly at the PE/PA interface with its thickness increasing with clay content. For PA matrix blends with 2% of clay, the interphase thickness was stabilized at 11 nm while further addition of clay resulted in its dispersion in the PA phase. Fisher et al. [65] studied ternary system composed of PP, ethylene-vinyl alcohol copolymer (EVON) and glass beads (GB). They found that in the PP matrix GBs were encapsulated by EVON with some of the minor EVON component separately dispersed in the matrix. Modification of the interfaces resulted in complete encapsulation of GBs. Wu et al. [66] observed a significant change of the phase morphology of PBT/PE blends in the presence of clay. When PE was the matrix (PBT/PE 40/60), the addition of more than 2% of clay changed the morphology to co-continuous. In contrast, the addition of clay in PBT/PE 60/40 with PBT as the matrix, significantly reduced the PE domain sizes. In this case, clay was concentrated in the PBT phase [5].

Morphology refinement is probably the most renowned consequence of adding particles to immiscible polymer blends. In recent years the literature on this topic has significantly increased, but most of the times the conclusions which have been drawn were ambiguous and/or system-specific. When morphology refinement is the goal, many questions must be addressed: which kind of particles is the most effective? Is interfacial-localization to be preferred, or should one aim at promoting nanoparticle assembly inside either of the phases? And, in the latter case, is it better that the filler resides in the matrix or in the droplets?

Appendix A

A.1. Measurement and estimation methods for interfacial tensions

Liquid–liquid interfacial tensions can be measured by some of the same methods as for liquids. However, for other interfaces (solid–liquid, solid–solid) of importance in wetting and adhesion studies as well as for surface modification such direct measurements are not possible. Nonetheless, interfacial tension values for all interfaces are important in practical applications and thus development of estimation methods for interfacial tensions has become a very active research field. There are many theories for estimating interfacial tensions. They roughly belong to two families: "surface component theories" and "direct theories", with the former being the most widely used. In the "surface component theories", the link between surface tensions and intermolecular forces is exploited. The surface tension is divided into different "components" (contributions) due to the various intermolecular forces. Among the various intermolecular forces, the dispersion forces are universal (and the only ones present in alkanes), while all the other forces are "specific", i.e. they only exist for specific molecules. Examples of "specific" contributions are those due to polar and hydrogen bonding forces [1].

In "direct theories", the interfacial tension is expressed directly as a function of the surface tensions in some universal way, although some adjustable parameters are often needed. In the early method of Girifalco and Good [2, 3], the interfacial tension is given as:

$$\gamma_{ij} = \gamma_i + \gamma_j - 2\varphi\sqrt{\gamma_i\gamma_j} \tag{A.1}$$

In the more modern and widely used theory of Neumann and co-workers [4-6], the interfacial tension is expressed as:

$$\gamma_{ij} = \gamma_i + \gamma_j - 2\varphi\sqrt{\gamma_i\gamma_j}\,e^{-\beta(\gamma_i-\gamma_j)^2} \tag{A.2}$$

The major characteristic of the Neumann equation is that the solid–liquid interfacial tension depends, in a universal way, on the solid and liquid surface tensions only (and not on their force-components, as in the "surface component" theories). The equation-of-state theory of Neumann has been criticized for not accounting for strong chemical effects, e.g. hydrogen bonding [1].

Early theories of interfacial tensions are based on the extension of the Fowkes equation [7]. These theories are those often cited in classical colloid and surface chemistry textbook literature. In the Fowkes theory, the surface tension is divided into dispersion (d) and specific (spec) components:

$$\gamma = \gamma_i^{\,d} + \gamma_j^{\,spec} \tag{A.3}$$

The interfacial tension is given as:

$$\gamma_{ij} = \gamma_i + \gamma_j - 2\sqrt{\gamma_i^{\,d}\gamma_j^{\,d}} \tag{A.4}$$

Notice that, unlike the Girifalco–Good equation, the cross term includes a contribution only from the dispersion forces. Thus, the Fowkes equation is based on the fundamental assumption that the cross-interaction term across the interface (work of adhesion) is due to dispersion forces alone. Extensions of the Fowkes equation have been proposed, which account explicitly for polar and hydrogen bonding effects in the expression for the interfacial tension using geometric-mean rules for all terms. Two such well-known theories are the Owens–Wendt theory [8], which is often used for polymer surfaces, and the Hansen/Skaarup model [9]. It can be seen that these theories resemble the Fowkes equation, but one or two additional cross terms are added to account for the "specific" interactions (a combined "specific" terms are used for Owens–Wendt while both polar and hydrogen bonding terms are used in the Hansen equation). The relevant equations for the surface and interfacial tensions for these two theories are given in following expressions:

Owens-Wendt

$$\gamma = \gamma_i^{\ d} + \gamma_j^{\ spec}$$
$$\gamma_{ij} = \gamma_i + \gamma_j - 2\sqrt{\gamma_i^{\ d}\gamma_j^{\ d}} - 2\sqrt{\gamma_i^{\ spec}\gamma_j^{\ spec}}$$

(A.5)

Hansen/Beerbower (or Hansen/Skaarup)

$$\gamma_{ij} = \gamma_i + \gamma_j - 2\sqrt{\gamma_i^{\ d}\gamma_j^{\ d}} - 2\sqrt{\gamma_i^{\ p}\gamma_j^{\ p}} - 2\sqrt{\gamma_i^{\ h}\gamma_j^{\ h}}$$

(A.6)

Notice that in the Hansen/Beerbower theory we have a separate treatment of polar (p) and hydrogen bonding (h) effects [1].

Wu [10, 11] accepted the idea of Owen and Wendt, proposing the harmonic mean to combine the polar and dispersion components of the solid and liquid surface energies. Instead of using the geometric mean as in equation (A.5), proposed the following expression, in order to obtain the solid-liquid interfacial energy:

$$\gamma_{ij} = \gamma_i + \gamma_j - 4\frac{\gamma_i^{\ d}\gamma_j^{\ d}}{\gamma_i^{\ d} + \gamma_j^{\ d}} - 4\frac{\gamma_i^{\ spec}\gamma_j^{\ spec}}{\gamma_i^{\ spec} + \gamma_j^{\ spec}}$$

(A.7)

The empirical basis for this is provided by interfacial tension measurements between polymer melts, i.e., materials with a predominantly low surface tension for the individual phases. Accordingly, the Wu method is mostly used for surface free energies calculation for polymers with low surface free energies (up to 30-40 mJ/m^2). Dalal [12] performed a comparative study of the two approaches, Geometric mean and Harmonic mean, on 12 common polymers using the published data with six liquids. It is found that the total surface energy of the solid obtained by the two methods are generally quite close, and neither of the two conceptually different equations is clearly incompatible with the available experimental data. However, the more widely used Geometric mean approach is preferable because it consistently fits the data better [13].

Despite the success of the classical "surface components theories", described above, in many practical situations such as for polymer surfaces, they are gradually being abandoned. This may be attributed to the doubtful use of the geometric-mean rule for the polar and especially for the hydrogen bonding interactions.

One of the most successful and widely used recent methods is the van Oss et al. [14] theory or acid– base theory, hereafter called van Oss–Good. In this theory, the hydrogen bonding (in general "Lewis acid–Lewis base" interactions) are expressed via asymmetric combining. More specifically, according to this theory, the surface tension is given as the sum of the van der Waals forces (LW) and an asymmetric acid–base term, which accounts for hydrogen bonding and other Lewis acid (electron acceptor +)/Lewis base (electron donor –) interactions. A Fowkes-type geometric-mean term is used for the LW forces. The equations for the surface and interfacial tensions are:

$$\gamma = \gamma^{LW} + \gamma^{AB} = \gamma^{LW} + 2\sqrt{\gamma^+ \gamma^-}$$
$$\gamma_{ij} = (\sqrt{\gamma_i^{LW}} - \sqrt{\gamma_j^{LW}})^2 + 2(\sqrt{\gamma_i^+} - \sqrt{\gamma_j^+})(\sqrt{\gamma_i^-} - \sqrt{\gamma_j^-})$$

(A.8)

where LW are the London/van der Waals forces (dispersion, induction and polar) and AB are the acid(+)/base(–) forces. Liquids or solids containing only LW terms are characterized as "apolar", those containing only an acid or base component "monopolar" and those having both are "bipolar". The theories discussed above have been applied extensively and it is now clear that all of them have strengths and weaknesses [1].

BIBLIOGRAPHY

1. Harrats, C., Coltelli, M.-B. and Groeninckx, G. (2016) Features on the Development and Stability of Phase Morphology in Complex Multicomponent Polymeric Systems: Main Focus on Processing Aspects, in Polymer Morphology: Principles, Characterization, and Processing (ed Q. Guo), John Wiley & Sons, Inc, Hoboken, NJ, USA. doi: 10.1002/9781118892756.ch22

2. Cardinaels, R. and Moldenaers, P. (2016) Morphology Development in Immiscible Polymer Blends, in Polymer Morphology: Principles, Characterization, and Processing (ed Q. Guo), John Wiley & Sons, Inc, Hoboken, NJ, USA. doi: 10.1002/9781118892756.ch19

3. Shokoohi, S., & Arefazar, A. (2009). A review on ternary immiscible polymer blends: morphology and effective parameters. Polymers for Advanced Technologies, 20(5), 433-447.

4. Utracki, L. A., & Favis, B. D. (1989). Polymer alloys and blends (Vol. 4, pp. 121-185). Marcel Dekker: New York.

5. Kuleznev, V. N., & Miroshnikov, Y. P. (2016). Phase Morphology and Properties of Ternary Polymer Blends. Encyclopedia of Polymer Blends, Volume 3: Structure, 3.

6. Boudenne, A., Ibos, L., Candau, Y., & Thomas, S. (Eds.). (2011). Handbook of multiphase polymer systems. John Wiley & Sons.

7. Paul, D. R. (2012). Polymer blends (Vol. 1). Elsevier.

8. Favis, B.D. (2000) Factors influencing the morphology of immiscible polymer blends in melt processing, in Polymer Blends, vol. 1, Formulations (eds D.R. Paul and C.B. Bucknall), John Wiley & Sons Inc., New York, Chapter 16.

9. Pötschke, P., & Paul, D. R. (2003). Formation of co-continuous structures in melt-mixed immiscible polymer blends. Journal of Macromolecular Science, Part C: Polymer Reviews, 43(1), 87-141.

10. Molau, G. E., & Keskkula, H. (1966). Heterogeneous polymer systems. IV. Mechanism of rubber particle formation in rubber-modified vinyl polymers. Journal of Polymer Science Part A: Polymer Chemistry, 4(6), 1595-1607.

11. Reignier, J., & Favis, B. D. (2000). Control of the subinclusion microstructure in HDPE/PS/PMMA ternary blends. Macromolecules, 33(19), 6998-7008.

12. Ravati, S., & Favis, B. D. (2010). Morphological states for a ternary polymer blend demonstrating complete wetting. Polymer, 51(20), 4547-4561.

13. Scher, H., & Zallen, R. (1970). Critical density in percolation processes. The Journal of Chemical Physics, 53(9), 3759-3761.

14. Jordhamo, G. M., Manson, J. A., & Sperling, L. H. (1986). Phase continuity and inversion in polymer blends and simultaneous interpenetrating networks. Polymer Engineering & Science, 26(8), 517-524.

15. Mekhilef, N., & Verhoogt, H. (1996). Phase inversion and dual-phase continuity in polymer blends: theoretical predictions and experimental results. Polymer, 37(18), 4069-4077.

16. Reignier, J., Favis, B.D., and Heuzey, M. C. (2003) Factors influencing behavior in composite droplet-type polymer blends. Polymer, 44,49–59.

17. Zhang, J., Ravati, S., Virgilio, N., & Favis, B. D. (2007). Ultralow percolation thresholds in ternary cocontinuous polymer blends. Macromolecules, 40(25), 8817-8820.

18. Torza, S., & Mason, S. G. (1970). Three-phase interactions in shear and electrical fields. Journal of Colloid and Interface Science, 33(1), 67-83.

19. Virgilio, N., Marc-Aurèle, C., & Favis, B. D. (2009). Novel self-assembling close-packed droplet array at the interface in ternary polymer blends. Macromolecules, 42(9), 3405-3416.

20. Harrats, C., Thomas, S., & Groeninckx, G. (Eds.). (2005). Micro-and nanostructured multiphase polymer blend systems: phase morphology and interfaces. CRC Press.

21. Vanoene, H. (1972). Modes of dispersion of viscoelastic fluids in flow. Journal of Colloid and Interface Science, 40(3), 448-467.

22. Utracki, L. A., & Wilkie, C. A. (Eds.). (2002). Polymer blends handbook (Vol. 1, p. 2). Dordrecht: Kluwer academic publishers.

23. Paul, D. R., & Barlow, J. W. (1980). Polymer blends. Journal of Macromolecular Science—Reviews in Macromolecular Chemistry, 18(1), 109-168.

24. Willemse, R. C., De Boer, A. P., Van Dam, J., & Gotsis, A. D. (1998). Co-continuous morphologies in polymer blends: a new model. Polymer, 39(24), 5879-5887.

25. Lyngaae-Jørgensen, J. (1993). Rheology of polymer blends. In Polymer Blends and Alloys (pp. 75-102). Springer Netherlands.

26. De Gennes, P. G. (1985). Wetting: statics and dynamics. Reviews of modern physics, 57(3), 827.

27. Dobbs, H., & Bonn, D. (2001). Predicting wetting behavior from initial spreading coefficients. Langmuir, 17(15), 4674-4676.

28. Erbil, H. Y. (2006). Surface chemistry of solid and liquid interfaces (pp. 309-310). Blackwell Pub..

29. Geoghegan, M., & Krausch, G. (2003). Wetting at polymer surfaces and interfaces. Progress in Polymer Science, 28(2), 261-302.

30. Cooper, W. F., & Nuttall, W. H. (1915). Insecticides from a chemical standpoint. Annals of Applied Biology, 1(3-4), 273-279.

31. Harkins, W. D., & Feldman, A. (1922). Films. The spreading of liquids and the spreading coefficient. Journal of the American Chemical Society, 44(12), 2665-2685.

32. Virgilio, N., Desjardins, P., L'Espérance, G., & Favis, B. D. (2009). In situ measure of interfacial tensions in ternary and quaternary immiscible polymer blends demonstrating partial wetting. Macromolecules, 42(19), 7518-7529.

33. Hobbs, S. Y., Dekkers, M. E. J., & Watkins, V. H. (1988). Effect of interfacial forces on polymer blend morphologies. Polymer, 29(9), 1598-1602.

34. Virgilio, N., Sarazin, P., & Favis, B. D. (2010). Towards ultraporous poly (l-lactide) scaffolds from quaternary immiscible polymer blends. Biomaterials, 31(22), 5719-5728.

35. Cayla, A., & Salaün, F. (2012). Microscopy as a tool to control predicted morphology and/or dispersion of a binary and ternary compounds in polymeric particles and fibre.

36. Kontogeorgis, G. M., & Kiil, S. Surface and Interfacial Tensions–Principles and Estimation Methods. Introduction to Applied Colloid and Surface Chemistry, 34-73.

37. Sharma, P. K., & Rao, K. H. (2002). Analysis of different approaches for evaluation of surface energy of microbial cells by contact angle goniometry. Advances in Colloid and Interface Science, 98(3), 341-463.

38. Van Krevelen, D. W., & Te Nijenhuis, K. (2009). Properties of polymers: their correlation with chemical structure; their numerical estimation and prediction from additive group contributions. Elsevier.

39. Willemse, R. C., De Boer, A. P., Van Dam, J., & Gotsis, A. D. (1999). Co-continuous morphologies in polymer blends: the influence of the interfacial tension. Polymer, 40(4), 827-834.

40. Miles, I. S., & Zurek, A. (1988). Preparation, structure, and properties of two-phase co-continuous polymer blends. Polymer Engineering & Science, 28(12), 796-805.

41. Taylor, G. I. (1932). The viscosity of a fluid containing small drops of another fluid. Proceedings of the Royal Society of London. Series A, Containing Papers of a Mathematical and Physical Character, 138(834), 41-48.

42. Ajji, A., & Utracki, L. A. (1996). Interphase and compatibilization of polymer blends. Polymer Engineering & Science, 36(12), 1574-1585.

43. Grace, H. P. (1982). Dispersion phenomena in high viscosity immiscible fluid systems and application of static mixers as dispersion devices in such systems. Chemical Engineering Communications, 14(3-6), 225-277.

44. Chesters, A. (1991). The modelling of coalescence processes in fluid-liquid dispersions: a review of current understanding. Chemical engineering research & design, 69(A4), 259-270.

45. Steinmann, S., Gronski, W., & Friedrich, C. (2002). Influence of selective filling on rheological properties and phase inversion of two-phase polymer blends. Polymer, 43(16), 4467-4477.

46. Oldroyd, J. G. (1953, June). The elastic and viscous properties of emulsions and suspensions. In Proceedings of the Royal Society of London A: Mathematical, Physical and Engineering Sciences (Vol. 218, No. 1132, pp. 122-132). The Royal Society.

47. Palierne, J. F. (1990). Linear rheology of viscoelastic emulsions with interfacial tension. Rheologica acta, 29(3), 204-214.

48. Graebling, D., & Muller, R. (1990). Rheological behavior of polydimethylsiloxane/polyoxyethylene blends in the melt. Emulsion model of two viscoelastic liquids. Journal of Rheology, 34(2), 193-205.

49. Tchomakov, K. P., Favis, B. D., Huneault, M. A., Champagne, M. F., & Tofan, F. (2004). Composite droplets with core/shell morphologies prepared from HDPE/PS/PMMA ternary blends by twin-screw extrusion. Polymer Engineering & Science, 44(4), 749-759.

50. Luzinov, I., Pagnoulle, C., & Jérôme, R. (2000). Ternary polymer blend with core–shell dispersed phases: effect of the core-forming polymer on phase morphology and mechanical properties. Polymer, 41(19), 7099-7109.

51. Ravati, S. (2010) Novel conductive polymer blends. PhD Thesis. Ecole Polytechnique de Montreal. Montreal, Canada, 262 p.

52. Letuchii, M. A., & Miroshnikov, Y. P. (2015). Interaction of domains in ternary polymer melt blends with separate dispersions of the inner phases. Journal of Macromolecular Science, Part B, 54(4), 433-449.

53. Letuchii, M. A., Klepper, L. Y., & Miroshnikov, Y. P. (2015). Percolation thresholds in ternary polymer melt blends with separate dispersions of the inner phases: mathematical model. Journal of Macromolecular Science, Part B, 54(4), 393-400.

54. Luzinov, I., Xi, K., Pagnoulle, C., Huynh-Ba, G., & Jérôme, R. (1999). Composition effect on the core–shell morphology and mechanical properties of ternary polystyrene/styrene–butadiene rubber/polyethylene blends. Polymer, 40(10), 2511-2520.

55. Hemmati, M., Nazokdast, H., & Shariat Panahi, H. (2001). Study on morphology of ternary polymer blends. I. Effects of melt viscosity and interfacial interaction. Journal of applied polymer science, 82(5), 1129-1137.

56. Gupta, A. K., & Srinivasan, K. R. (1993). Melt rheology and morphology of PP/SEBS/PC ternary blend. Journal of applied polymer science, 47(1), 167-184.

57. Stehling, F. C., Huff, T., Speed, C. S., & Wissler, G. (1981). Structure and properties of rubber-modified polypropylene impact blends. Journal of applied polymer science, 26(8), 2693-2711.

58. Kojima, T., Kikuchi, Y., & Inoue, T. (1992). Morphology-Properties relationship of a ternary polymer alloy. Polymer Engineering & Science, 32(24), 1863-1869.W. Zheng, Y. Leng, X. Zhu, Plast. Rubber Compos. Process. App. 1996, 25, 490.

59. Hemmati, M., Nazokdast, H., & Shariat Panahi, H. (2001). Study on morphology of ternary polymer blends. II. Effect of composition. Journal of applied polymer science, 82(5), 1138-1146.

60. Huang, J. J., Keskkula, H., & Paul, D. R. (2006). Elastomer particle morphology in ternary blends of maleated and non-maleated ethylene-based elastomers with polyamides: Role of elastomer phase miscibility. Polymer, 47(2), 624-638.

61. Shokoohi, S., Arefazar, A., & Naderi, G. (2011). Compatibilized Polypropylene/Ethylene–Propylene–Diene-Monomer/Polyamide6 ternary blends: Effect of twin screw extruder processing parameters. Materials & Design, 32(3), 1697-1703.

62. Huang, J. J., Keskkula, H., & Paul, D. R. (2004). Rubber toughening of an amorphous polyamide by functionalized SEBS copolymers: morphology and Izod impact behavior. Polymer, 45(12), 4203-4215.

63. Macosko, C. W., Guegan, P., Khandpur, A. K., Nakayama, A., Marechal, P., & Inoue, T. (1996). Compatibilizers for melt blending: Premade block copolymers. Macromolecules, 29(17), 5590-5598.

64. Huitric, J., Ville, J., Médéric, P., Moan, M., & Aubry, T. (2009). Rheological, morphological and structural properties of PE/PA/nanoclay ternary blends: Effect of clay weight fraction. Journal of rheology, 53(5), 1101-1119.

65. Fisher, I., Siegmann, A., & Narkis, M. (2002). The effect of interface characteristics on the morphology, rheology and thermal behavior of three-component polymer alloys. Polymer composites, 23(1), 34-48.

66. Wu, D., Zhou, C., & Zhang, M. (2006). Effect of clay on immiscible morphology of poly (butylene terephthalate)/polyethylene blend nanocomposites. Journal of applied polymer science, 102(4), 3628-3633.

BIBLIOGRAPHY Appendix A

1. Kontogeorgis, G. M., & Kiil, S (2016). Surface and Interfacial Tensions–Principles and Estimation Methods. Introduction to Applied Colloid and Surface Chemistry, 34-73.

2. Girifalco, L. A., & Good, R. J. (1957). A theory for the estimation of surface and interfacial energies. I. Derivation and application to interfacial tension. The Journal of Physical Chemistry, 61(7), 904-909.

3. Good, R. J., & Girifalco, L. A. (1960). A theory for estimation of surface and interfacial energies. III. Estimation of surface energies of solids from contact angle data. The Journal of Physical Chemistry, 64(5), 561-565.

4. Amirfazli, A., Kwok, D. Y., Gaydos, J., & Neumann, A. W. (1998). Line tension measurements through drop size dependence of contact angle. Journal of colloid and interface science, 205(1), 1-11.

5. Kwok, D. Y., & Neumann, A. W. (1999). Contact angle measurement and contact angle interpretation. Advances in colloid and interface science, 81(3), 167-249.

6. Kwok, D. Y., & Neumann, A. W. (2000). Contact angle interpretation in terms of solid surface tension. Colloids and Surfaces A: Physicochemical and Engineering Aspects, 161(1), 31-48.

7. Fowkes, F. M. (1964). Attractive forces at interfaces. Industrial & Engineering Chemistry, 56(12), 40-52.

8. Owens, D. K., & Wendt, R. C. (1969). Estimation of the surface free energy of polymers. Journal of applied polymer science, 13(8), 1741-1747.Hansen/Skaarup (van Krevelen and Hoftyzer, 1972; Hansen, 2000.

9. Van Krevelen, D. W. (1972). with the collaboration of Hoftyzer PJ, Properties of Polymers, Correlations with Chemical Structure.

10. Wu, S. (1971, January). Calculation of interfacial tension in polymer systems. In Journal of Polymer Science: Polymer Symposia (Vol. 34, No. 1, pp. 19-30). Wiley Subscription Services, Inc., A Wiley Company.

11. Wu, S. (1982). Polymer interface and adhesion. M. Dekker.

12. Dalal, E. N. (1987). Calculation of solid surface tensions. Langmuir, 3(6), 1009-1015.

13. Sharma, P. K., & Rao, K. H. (2002). Analysis of different approaches for evaluation of surface energy of microbial cells by contact angle goniometry. Advances in Colloid and Interface Science, 98(3), 341-463.

14. Van Oss, C. J., Chaudhury, M. K., & Good, R. J. (1987). Monopolar surfaces. Advances in colloid and interface science, 28, 35-64.

Polymer Nanocomposites

3.1. Preliminary considerations

Recent technological breakthroughs and the desire for new functions generate an enormous demand for novel materials. Many of the well-established materials, such as metals, ceramics or plastics cannot fulfill all technological desires for the various new applications. Scientists and engineers realized early on that mixtures of materials can show superior properties compared with their pure counterparts. One of the most successful examples is the group of composites which are formed by the incorporation of a basic structural material into a second substance, the *matrix*. Usually the systems incorporated are in the form of particles, whiskers, fibers, lamellae, or a mesh. Most of the resulting materials show improved mechanical properties and a well-known example is inorganic fiber-reinforced polymers. Nowadays they are regularly used for lightweight materials with advanced mechanical properties, for example in the construction of vehicles of all types or sports equipment. The structural building blocks in these materials which are incorporated into the matrix are predominantly inorganic in nature and show a size range from the lower micrometer to the millimeter range and therefore their heterogeneous composition is quite often visible to the eye. Soon it became evident that decreasing the size of the inorganic units to the same level as the organic building blocks could lead to more homogeneous materials that allow a further fine tuning of materials' properties on the molecular and nanoscale level, generating novel materials that either show characteristics in between the two original phases or even new properties [1]. Although we do not know the original birth of hybrid materials exactly it is clear that the mixing of organic and inorganic components was carried out in ancient world. At that time, the production of bright and colorful paints was the driving force to consistently try novel mixtures of dyes or inorganic pigments and other inorganic and organic components to form paints that were used thousands of years ago. Therefore, hybrid materials or even nanotechnology is not an invention of the last decade but was developed a long time ago. However, it was only at the end of the 20th and the beginning of the 21st century that it was realized by scientists, in particular because of the availability of novel physicochemical characterization methods, the field of nanoscience opened many perspectives for approaches to new materials. The combination of different analytical techniques gives rise to novel insights into hybrid materials and makes it clear that bottom-up strategies from the molecular level towards materials' design will lead to novel properties in this class of materials. Apart from the use of inorganic materials as fillers for organic polymers,

such as rubber, it was a long time before much scientific activity was devoted to mixtures of inorganic and organic materials. Inorganic–organic hybrids can be applied in many branches of materials chemistry because they are simple to process and are amenable to design on the molecular scale. Currently there are four major topics in the synthesis of inorganic–organic materials: (a) their molecular engineering, (b) their nanometer and micrometer-sized organization, (c) the transition from functional to multifunctional hybrids, and (d) their combination with bioactive components [1].

Due to the type of matrix, one can distinguish following composites: metal matrix composites (MMCs), ceramic matrix composites (CMC) or polymer matrix composites (PMCs) [2]. The latter type of composite materials dominates over other in terms of technical applications. PMCs are comprised of a broad variety of reinforcements bound together by an organic polymer matrix. These materials are designed so that the mechanical loads to which the structure is subjected in service are supported by the reinforcement. PMCs are often divided into two categories: reinforced plastics, and "advanced composites". The distinction is based on the level of mechanical properties (usually strength and stiffness); however, there is no unambiguous line separating the two. The matrix properties determine the resistance of the PMC to most of the degradative processes that eventually cause failure of the structure. These processes include impact damage, delamination, water absorption, chemical attack, and high-temperature creep. Thus, the matrix is typically the weak link in the PMC structure. Instead, additives are responsible for their high strength and stiffness [3]. To attain superior mechanical properties the interfacial adhesion, between the matrix and the reinforcing, should be strong. Matrix molecules can be anchored to the reinforcing surface by chemical reaction or adsorption, which determine the extent of interfacial adhesion. The shape of the reinforcing particles can be spherical, cubic, platelet, regular or irregular geometry. On the other hand, the chief advantages of polymers as matrix are low cost, easy processability, good chemical resistance, and low specific gravity. Regarding dispersed phase composite materials might be distinguished into:

1. particle reinforced composites; dispersed phase includes particles of greater rigidity and hardness than matrix; external loads are transferred both by matrix and filler, while the effective reinforcement is observed when filler content exceeds 20%

2. dispersion reinforced composites; the strengthening occurs at microscopic level; external loads are transferred by matrix, while reinforcement is effective when filler content does not exceed 15%

3. fibre reinforced composites; filler involve fibres (glass, graphite, carbon or organic fibres) of varying degree of order and different parameters

4. structural composites, composed of continuous structures of construction components (e.g. plywood, rods, etc.) [2].

Reinforced polymer composites are used in almost every type of advanced engineering structure, with their usage ranging from aircraft, helicopters, and spacecraft through to boats, ships, and offshore platforms and to automobiles, sports goods, chemical processing equipment, and civil infrastructure such as bridges and buildings. The usage of reinforced polymer composites continues to grow at an impressive rate as these

materials are used more in their existing markets and become established in relatively new markets such as biomedical devices and civil structures. A key factor driving the increased applications of composites over the recent years is the development of new advanced forms of materials. This includes developments in high performance resin systems and new styles of reinforcement, such as carbon nanotubes and nanoparticles [4-5].

The manufacturing of polymer composites is a rather difficult task, since there are several requirements regarding the technology, design, function, and cost-effectiveness. The applicable manufacturing technique is determined by the balance of these requirements and strongly influenced by the chosen matrix material, reinforcement, reinforcing content, reinforcing size, architecture, and so on. Matrix materials can be different thermoplastic and thermosetting polymers, and their viscosity varies in a very broad range. On the other hand, reinforcements with different type, geometry (continuous or discontinuous), and structure (random or oriented) require different composite processing technologies. Moreover, they can be arranged to one-dimensional (roving, yarn), two-dimensional (mat, woven and knitted fabric), or three-dimensional (braid, fabric) systems. Geometry, holes, inserts, undercuts, and surface quality mean further constraints, similar to curing time, pressure, and temperature demands of the matrix. Nowadays the amount of thermoplastic matrix composites produced approaches to that of composites with thermosetting matrix. The most important character of thermoplastic composites – and their most important difference from thermosetting ones – is the fact that no chemical reaction occurs during processing. The thermoplastic offers smaller health hazard, cleaner (and more environment-friendly) technologies, and short cycle times and techniques capable of producing large series with constant quality. However, the higher viscosity of thermoplastic melts impedes the impregnation, compaction, and consolidation of composites in many cases. The main goal of reinforcing thermoplastics – besides enhancing mechanical properties – is the increasing of heat deflection temperature, stiffness, creep resistance, wear resistance, and toughness, tailoring the electric properties and decreasing the thermal expansion coefficient. Injection moulding, extrusion, and compression moulding are typical technologies that can produce large quantities of thermoplastic composite parts with good dimensional accuracy and complex geometry [5].

Among various possible types of polymer composite materials, the most important ones are nano- and biocomposites that are recently of great interest due to their unique properties [2, 6]. An important aspect is that if the reinforcements are in the nanoscale range, they have an exceptional potential to generate new phenomena, which leads to special properties in the final composite. It may be pointed out that the reinforcing efficiency of these composites, even at low volume fractions, is comparable to 40-50% for fibres in microcomposites. Addition of nanoreinforcements to a wide variety of polymer resins produces a dramatic improvement in their biodegradability. This underlines a good example of polymer matrix nanocomposites as promising systems for ecofriendly applications [7].

3.2. Polymer nanocomposites: generalities

Since the first reports in the early 1990s the term "polymer nanocomposite" has evolved to refer to a multicomponent system, where the major constituent is a polymer or blend thereof and the minor constituent exhibits a length scale below 100 nm. As such, the term is sometimes used as a synonym for inorganic-organic hybrids, molecular composites, or to encompass mature commercial products, such as filled polymers with carbon black or fumed silica. The numerous reports of large property changes with very small (<5 vol %) addition of nanoparticles have fuelled the view that nanoparticle addition to polymers delivers huge dividends [8]. These new kinds of materials have attracted steadily growing interest in numerous industrial applications, mainly in the transportation sector, building/construction industries and food packaging plastics [9]. They often exhibit remarkable properties, including unique mechanical and electrical conductivity, high gas and liquid barrier, flame retardant and thermal properties as compared to the neat polymers [10]. The development and progression of environmentally friendly/green nanocomposites materials, will not only benefit on the plastic industry, but would lead to reduce the percentage of the expensive polymer used in the manufacture of materials, such as polypropylene, polyacrylic, polyester and epoxies etc. [11]. They are hazardous to the environment, non-degradable and take a long time to decompose, which generates huge many environmental problems associated with their disposal, including damage to the environment eco-system, water supplies, and sewer systems as well as to the lakes, rivers and streams. Furthermore, they are non-renewable; and their high price and unstable with impending depletion of petroleum resources [12]. The incorporation of nano-sized particles in the polymer nanocomposites can reduce their production cost, through the substitution of small amount of polymer by a cheap and abundant organic or inorganic resource [13]. Given the extensive variety of nanoparticles now commercially accessible (clays, carbon nanotubes, quantum dots, metals, silica, titania, zirconia, and various oxides, etc.), the potential combinations of polymers and nanoparticles, and thus the tailorability of the property suite, is essentially endless. The diversity in scientific investigation, technology advancement, processing innovations, and product development is staggering. A significant number of excellent review papers (e.g., clays14-21 and carbon nanotubes20-24) and books 25-28 are available that chronicle and summarize the status of various nanoparticle-polymer combinations and the broad scientific and technological challenges still to be overcome. Arguably, the goal for the vast majority of these investigations is to achieve increased thermomechanical performance through dispersion at the single-particle level. The resulting polymer nanocomposites (PNCs) are treated much as an isotropic, filled polymer. Thus, from the historic perspective, nanocomposites today are really nanoparticle-filled plastics [8].

3.2.1. Fillers

Traditionally, fillers were considered as additives, which, due to their unfavourable geometrical features, surface area or surface chemical composition, could only moderately increase the modulus of the polymer, while strength (tensile, flexural) remained unchanged or even decreased. Their major contribution was in lowering the cost of materials by replacing the more expensive polymer; other possible economic advantages were faster moulding cycles as a result of increased thermal conductivity and fewer rejected parts due to

warpage. Depending on the type of filler, other polymer properties could be affected; for example, melt viscosity could be significantly increased through the incorporation of fibrous materials. On the other hand, mould shrinkage and thermal expansion would be reduced, a common effect of most inorganic fillers. The term reinforcing filler has been coined to describe discontinuous additives, the form, shape, and/or surface chemistry of which have been suitably modified with the objective of improving the mechanical properties of the polymer, particularly strength. Inorganic reinforcing fillers are stiffer than the matrix and deform less, causing an overall reduction in the matrix strain, especially in the vicinity of the particle as a result of the particle/matrix interface. The additive materials employed in the production of polymer composites can be classified according to their several properties. In this way, they may be *continuous*, for example, long fibres or ribbons; these are embedded in the polymer in regular geometric arrangements that extend throughout the dimensions of the product. On the other hand, additives may be *discontinuous* (short), for example, short fibres (say, <3 cm in length), flakes, platelets, spheres, or irregulars (millimetre to micrometre size); fibres and flakes are usually dispersed in different orientations and multiple geometric patterns throughout the continuous matrix [29]. These nanoscale particles can further be classified upon their *origin* in three types as natural, incidental, and engineered nanoparticles depending on their pathway. Natural nanoparticles, which are formed through natural processes, occur in the environment (example: volcanic dust, lunar dust, magneto-tactic bacteria, minerals, etc.). Incidental nanoparticles occur as the result of manmade industrial processes (diesel exhaust, coal combustion, welding fumes, etc.). Sometimes, they are also called as waste or anthropogenic particles. Mostly, both natural and incidental nanoparticles may have irregular or regular shapes. Engineered nanoparticles most often have regular shapes, such as tubes, spheres, rings, etc. Engineered nanomaterials can be produced either by milling or lithographic etching of a large sample to obtained nanosized particles ("top-down" approach), or by assembling smaller subunits through crystal growth or chemical synthesis to grow nanoparticles of the desired size and configuration ("bottom-up" approach). Depending on *practical applications*, nanoscale particles regardless of engineered or natural ones, so far seem to fall into four basic categories. The group currently with the largest number of commercial nanomaterials is the metal oxides, such as zinc or titanium oxides, which are used in ceramics, chemical polishing agents, scratch-resistant coatings, cosmetics, and sunscreens. A second significant group is nanoclays, naturally occurring plate-like clay particles that strengthen or harden the materials or make them flame-retardant. A third group is nanotubes, which are used in coatings to dissipate or minimize static electricity (e.g. in fuel lines, in hard disk handling trays, or in automobile bodies to be painted electrostatically). The last group is quantum dots, used in exploratory medicine or in the self-assembly of nanoelectronic structures. As it is not easy for every official source to find the same categorization useful, the U.S. Environmental Protection Agency also divides engineered nanoparticles into four types. They are carbon-based materials (nanotubes, fullerenes), metal-based materials (including both metal oxides and quantum dots), dendrimers (nanosized polymers built from branched units of unspecified chemistry), and composites (including nanoclays) [30].

Over the conventional micro-composites, the nanoscopic *dimensions* and inherent extreme *aspect ratios* of the nanofillers result in several interrelated characteristics, which distinguish the obtained nanocomposites. To convey the origin and interrelation of these distinguishing characteristics, Figure 1 compares the dominant morphological scale of a microfiber (1μm×25μm) filled polymer matrix to that of a nanofiber (1nm×25 nm) filled system at the same volume fraction of filler. There are three main material constituents in any composite: the matrix, the reinforcement (fibre), and the so-called interfacial region. The interfacial region is responsible for 'communication' between the matrix and filler and is conventionally ascribed properties different from the bulk matrix because of its proximity to the surface of the filler. It is explained in terms of the radius of gyration of the matrix (R_g), which is key spatial parameter to which the majority of the polymer's static and dynamic properties can be ultimately related and has a value in a few tens of
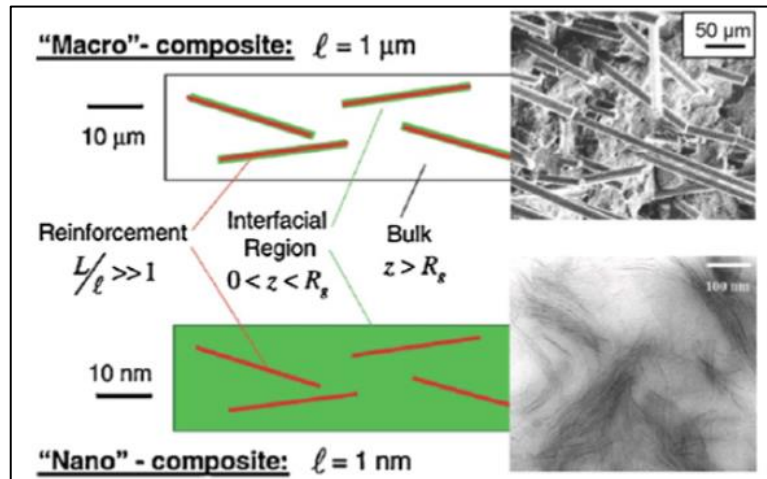

Figure 1.: Comparison of conventional fibre composite and nanocomposites [Reproduced from 30].

nanometers. As shown in Figure 1, contrast to conventional fillers, in the nanoparticles filled system, the distance between particles comparable to the size of the interfacial region (10 nm) because of the increased number density of particles. Thus, the relative volume fraction of interfacial material to bulk is drastically increased as the size becomes smaller [30].

Nanosized particles can be mainly classified into three categories upon their *dimensionality* of the [31]:

i. Plate-like nanofillers (1D) are layered materials typically with a thickness on the order of 1 nm, but with an aspect ratio following their two remaining dimensions of at least 25. The most popular 1D fillers are layered silicates including smectic clays, layered double hydroxides as well as graphene sheets.

ii. Nanofibers or whiskers (2D) have a diameter below 100 nm and characterized with an aspect ratio of at least 100. Carbon nanotubes, nanocellulose substrates, and so on all fall under this category.

iii. Nanoparticles (3D) exhibit 3D dimensions below 100 nm. The most well-known 3D nanofillers are silica particles, polyhedral oligomeric silsesquioxane and metal oxides.

In the case of particles and fibres, the surface area per unit volume is inversely proportional to the filler's diameter: the smaller the diameter, the greater the surface area per unit volume. For fibre and layered nanosized filler, the surface area/volume is dominated by the first term in the equation. The second term (2/l and 4/l) has a very small influence and generally omitted, compared to the first one. Therefore, a change in particle diameter, layer thickness, or fibre diameter from the micrometer to nanometer range will affect the surface area-to-volume ratio by three orders of magnitude [31]. Common particle geometries and their respective surface area-to-volume ratios are shown in Figure 2. In general, nanomaterials provide reinforcing efficiency because of their high aspect ratios. The properties of a nanocomposite are greatly influenced by the size scale
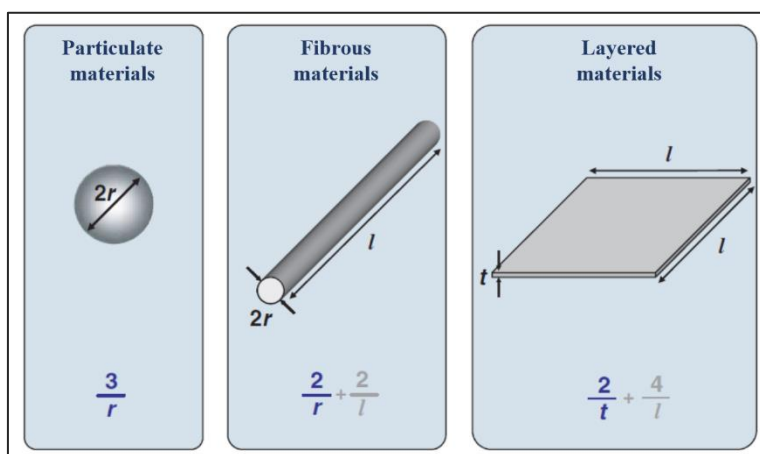
Figure 2.: Common particle reinforcements/geometries and their respective surface area-to-volume ratios [Reproduced from 21].

of its component phases and the degree of mixing between the two phases. Depending on the nature of the components used (layered silicate or nanofiber, cation exchange capacity, and polymer matrix) and the method of preparation, significant differences in composite properties may be obtained [21]. Regarding the preparation of polymeric nanocomposites, there are four main routes [30]: (i) solution method starting from the dissolution of polymers in adequate solvent with nanoscale particles together with evaporation of solvent or precipitation; (ii) melt-mixing involving the direct melt-mixing of polymers with nanofillers; (iii) in situ polymerization where the nanofillers are first dispersed in liquid monomer or monomer solution, followed by polymerization in presence of nanoscale particles; and (iv) template synthesis where the nanofillers are synthesized from precursor solution using polymers as template. Depending on the association between polymers and nanofillers and the preparation method thereof, the interface between nanofillers and polymers, chain-mobility, chain conformation, and degree of chain ordering or crystallinity can all vary continuously from the filler/matrix interface, to some extent in the polymer bulk itself. It has indeed reported that this polymer/nanofiller interphase represents a significant volume fraction generated even at low filler concentrations [31].

The greatest stumbling block to the large-scale production and commercialization of nanocomposites is the dearth of cost-effective methods for controlling the dispersion of the nanoparticles in polymeric hosts [32]. Dispersion of the nanoparticle and adhesion at the particle–matrix interface play crucial roles in determining the mechanical properties of the nanocomposite [21]. The nanoscale particles typically aggregate, which negates any benefits associated with the nanoscopic dimension. There is a critical need for establishing processing techniques that are effective on the nanoscale yet are applicable to macroscopic processing. Another hurdle to the broader use of nanocomposites is the absence of structure-property relationships. Because

increased research activity in this area has only spanned the past decade, there are limited property databases for these materials [33]. Thus, greater efforts are needed to correlate the morphology of the mixtures with the macroscopic performance of the materials. Establishing these relationships requires a better understanding of how cooperative interactions between flexible chains and nanoscopic solids can lead to unexpected behaviour. The interactions of nanoparticles with polymers are mediated by the ligands attached to the nanoparticles; thus, the ligands markedly influence particle behaviour and spatial distribution [32]. With this in mind, the *surface chemistry* of nanoparticles is very relevant. First and foremost is its effect on the strength of interaction between the particles and the polymer matrix. This interaction is critical and can vary from strong to weak. The surface chemistry of nanoparticle functionalization evolved in part from studies on functionalized planar surfaces, including self-assembled monolayers [34] and polymer brushes [35] on substrates ranging from gold to metal oxides. As with planar substrates, functional small molecules and polymers can be attached to nanoparticles by physical adsorption or covalent attachment. Synthetic strategies that give polymer-functionalized nanoparticles include performing the particle synthesis directly in the polymer matrix, replacing small-molecule ligands inherent to a nanoparticle synthesis with functional polymers in a "grafting-to" process, and growth of polymers from functionalized nanoparticles in a "grafting-from" process. It is imperative, though, that the conditions used retain the specific characteristics of the nanoparticles [32].

Recent investigations of nanoparticles in immiscible mixtures have focused on using the particles to stabilize evolving morphologies and/or arrest domain coarsening. For example, Lin et al. demonstrated that nanoparticles can behave like surfactants, localizing at the interfaces in oil/water mixtures [36]. More specifically, the particles formed a monolayer around the dispersed droplets, allowing the fabrication of novel nanoparticle capsules. Such interfacial activity can also be exploited in polymer blends. Rafailovich and co-workers [37]. observed a significant reduction in the domain size in phase-separating binary blends using clays modified with organic ligands as a result of the localization of the clay sheets at the interface between the immiscible components. Controlling the domain size in this manner improves the overall mechanical integrity of the material. Nanoparticles have also been shown to influence the phase-separation kinetics in polymer mixtures. Tanaka et al. showed that nanoparticles can significantly alter the coarsening dynamics of mixtures [32, 38]. Theoretical studies of nanoparticle-filled mixtures suggest the existence of distinct pattern formation at early stages of phase separation (50, 51) and a subsequent slowing of domain growth at later times [39]. Experiments of Composto et al. [40] and Krishnamoorti et al. [41] confirmed a substantial slowing of phase separation with the addition of nanoparticles to a polymer mixture. There have been relatively few systematic experimental or theoretical studies of the thermodynamic properties of mixtures of nanoparticles and binary polymer blends. Consequently, there is little quantification of the influence of nanoparticle size, volume fraction, or chemical nature on the phase behaviour of the system. Ginzburg [42] and He et al. [43] recently carried out thermodynamic calculations to determine the influence of nanoparticles on the miscibility of blends of A and B homopolymers. By decreasing the size of the nanoparticles, a phase separating system can be driven into a thermodynamically miscible, one-phase region. Thus, by tailoring the particle size, desired phase behaviour can be controlled [43]. As in the case of nanoparticle-filled diblocks, a critical challenge lies in

predicting how the morphology of the filled blends affects the macroscopic properties of the composite. To date, there have only been a few theoretical studies in this area. Buxton et al. [44] integrated different computational approaches to relate the morphology of a particle-filled mixture to mechanical behaviour and electrical conductance. In these rod-filled binary blends, the reinforcement efficiency of the nanorods and the electrical conductivity of the materials were significantly higher than the respective behaviour for homopolymer composites [32]. Central to discussions of nanoparticle-polymer composites is a consideration of enthalpic and entropic interactions when functionalized nanoparticles are introduced into polymers. Although nanoparticle-filled polymers will continue to evolve toward improved properties for materials applications, it is exciting to consider the extent to which synthetic nanoparticle-filled polymer materials can be directed to assemble into hierarchically ordered nanocomposites, as found in nature in the abalone nacre or mother of pearl, a naturally occurring organic/inorganic composite. The construction of such complex structures remains a challenge but will lead to materials with new functionalities. Essential to meeting this challenge is establishing guidelines for process optimization, discovering assembly methods that yield a desired structure, and understanding structure-property relationships to predict the performance of a given architecture [32].

3.2.2. Effect of nanoparticles on the morphology of polymer blends

A clever use of nanoparticles offers an elegant way to manipulate the space arrangement of the polymer phase at the micron-scale without the need for substantial modifications of the mixing processes and/or investments in new chemistry. Such an approach has received a great deal of interest in recent years.

Morphology refinement has been observed either when the filler locates in the <u>continuous or in the dispersed phase</u> or when it locates at <u>polymer-polymer interface</u>. In the former case, the refinement can be explained by invoking rheological arguments: changes in the viscosity ratio can alter the breakup/coalescence equilibrium in favour of the former. More precisely, since coalescence involves flows in both the drops and the matrix, an increased viscosity of either of the phases delays the merging process necessary for coalescence. The situation is particularly critical when the particles assemble in three-dimensional filler networks, as such structures drastically slow down the relaxation processes of the host phase. Nevertheless, many authors neglect the role of bulk rheology in the process of morphology refinement, proposing alternative physical
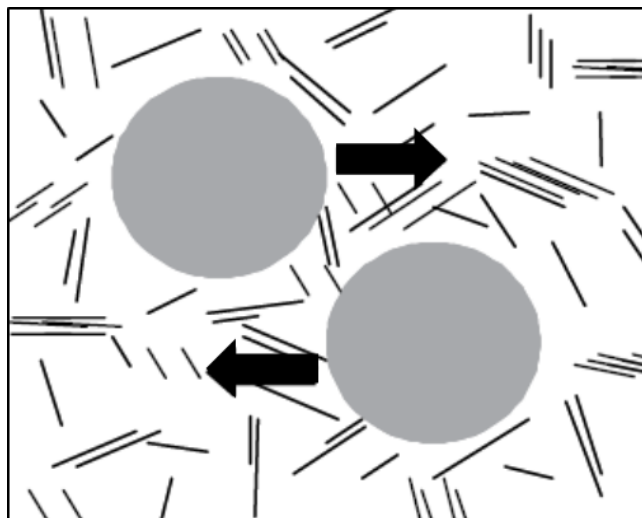

Figure 3.: One of possible mechanisms explaining coalescence inhibition in polymer blends containing nanofillers (layered silicate type in the illustration): particles confined in the matrix acting as obstacles to coalescence [Reproduced from 56].

mechanisms. Among others, the most common one is coalescence suppression: the nanoparticles dispersed in

the matrix interpose themselves between colliding droplets preventing them from coalescing (Figure 3). Although invoked also in case of spherical fillers [45], simple geometrical arguments suggest that such a shielding mechanism could be particularly effective when plate-like nanoparticles are considered [46-49]. The effect can result accentuated if the filler is assembled in three-dimensional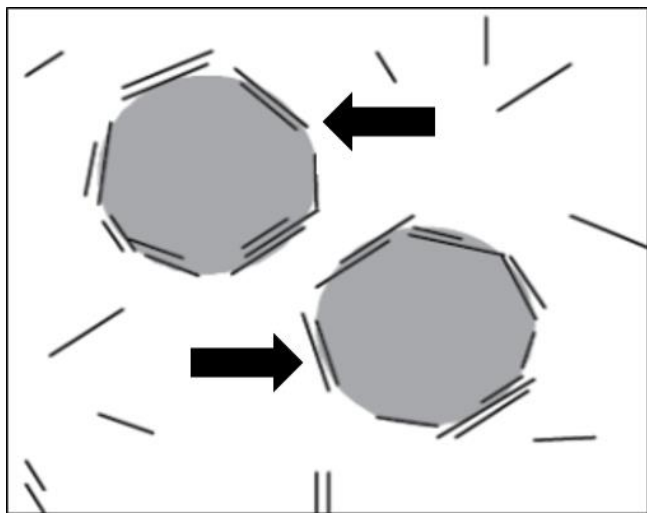 networks that trap the droplets of the minor phase [50]. It is important to observe that the effect of the filler embedded in either of bulk phase may be difficult to distinguish from that of particles gathered in the proximity of the drop-matrix interface [51]. Nanoparticles accumulated at the polymer-polymer interface are particularly effective in refining the microstructure of immiscible polymer blends. The underlying mechanisms are still controversial, but two main arguments are most commonly invoked: compatibilizing action and effects on the interfacial rheology [51]. Undoubtedly, numerous experimental works evidence the compatibilizing effect of nanofillers on binary polymer blends nevertheless several interpretations are proposed.

Figure 4.: One of possible mechanisms explaining coalescence inhibition in polymer blends containing nanofillers (layered silicate type in the illustration): barrier of particles concentrated at the interface [Reproduced from 56].

Actually, several phenomena can lead to morphology changes:

i. The *reduction of the interfacial energy* due to the distribution of the filler at the polymer/polymer interface is often cited as a potential explanation for the compatibilization [45, 53-54]. The interfacial tension change is sometimes calculated with the help of rheology and the reader can refer to the section dedicated to viscoelastic properties. Actually, the interface between the two polymers can be seen as a more complicated interfacial zone with filler/polymer1, filler/polymer2 and polymer1/polymer2 interfaces. Thus, the definition of an apparent or an effective interfacial tension is more appropriate [55]. The modification of the interfacial tension affects the breakup/colascence equilibrium in favour of the breakup and should lead to smaller drops. In addition, the filler can form a rigid shell around the polymer drop, modifying strongly its deformation ability. This is observed in low viscosity emulsions when the total coverage of the interface by interacting solid particles is achieved [56].

ii. The *inhibition of coalescence* by the presence of a solid barrier around the minor polymer drops. As regards this mechanism, many authors agree to assert that the definitive or temporary localization of the nanofiller at the interface of a blend is one of the requisite mechanisms to ensure a reduction of the size of the minor polymer phase. The similarity with liquid emulsions is again highlighted as the particles accumulated at the interface build a solid barrier preventing the fusion of the drops. In situations where a polar polymer is employed for the matrix, the filler distributes in that phase due to favourable polymer–particle interaction. An important reduction of the drop size is nevertheless sometimes reported. If the filler has a high aspect

ratio (clay for instance) it may be trapped in the matrix film between two colliding drops and slow down coalescence (Figure 4) [56].

iii. The *improving of the interfacial adhesion*. Excluding the case in which the filler catalyses interfacial chemical reactions, stronger interfacial interactions establish in case of simultaneous adsorption of the two polymers on the nanoparticles surface. The inherently amphiphilic feature of graphene oxide or properly functionalized multiwalled carbon nanotubes (CNTs) promote polymer adsorption [57-58]. However, simultaneous chemical adsorption seems not strictly necessary in the case of organo-clays, which may exhibit coupling ability even if one or both of the polymers exhibit scarce affinity with the particles [59]. The idea is that intercalation of the polymer(s) in the inter-layer galleries of interfacially-located clay stacks plays the same role as a strong adsorption on the platelet surface. The non-specificity of such a coupling mechanism was emphasized by Rafailovich and co-workers, who proposed the employ of organo-clays for compatibilizing recycled blends with uncertain composition [37, 51, 60].

It is interesting to observe that the phenomenon takes place also in blends with co-continuous morphology. Unless rare exceptions [55,56], the refinement of co-continuous morphology is often merely noticed, the attention being focused on other effects related to the presence of nanoparticles. To give some examples, clear morphology refinements can be noticed in [57,58], but the authors address the possibility of reducing the percolation threshold of conductive fillers via selective interfacial localization; a drastic refinement was shown also in [59], but in this case the focus is on the shift in the onset of phase co-continuity. Actually, the refinement of co-continuous morphologies can have a relevant impact on the mechanical and transport properties of the blends, and the potential offered by a focused employ of nanoparticles should deserve greater attention.

The *stability of the morphology* is another important aspect in the development of new materials [56]. The morphology of immiscible polymer blends produced through melt mixing is usually in a non-equilibrium state. As a consequence, the frozen-in phase morphology quickly evolves when the blend is melted again. This happens quite frequently in industrial contexts, in which the materials can experience multiple melt processing steps. Since the microstructural changes proceed in an uncontrolled way, they are generally unwanted. Again, nanoparticles represent a feasible solution for stabilizing the blend morphology either during flow or in quiescent conditions [51]. Small amounts of nanoparticles are known to substantially reduce the sensitivity of the blend microstructure to shear flows [61-63]. Such stabilizing action depends on the localization of the filler, which is particularly effective in case of interfacial positioning [62]. Essentially the same mechanism was invoked by Tong et al., who additionally identified a second stabilizing phenomenon when low amounts of particles reside inside the matrix phase: non-coalescing clusters of droplets form during shear flows as a consequence of nanoparticle-induced drop bridging [50]. It is important to observe that nanoparticles can also have the opposite effect of reducing the blend stability, promoting morphological changes under flow (e.g.: drop coalescence, drop clustering) [64] [65]. When a blend is subjected to quiescent post-treatments at temperatures above the softening/melting point of the polymeric constituents, its morphology evolves over time towards phase coarsening [66-67]. The phenomenon is especially evident in case of co-continuous blends, which are particularly unstable because of their high specific interface. Such a propensity to coarsening of co-

continuous blends can be ingeniously exploited to obtain porous and/or gradient microstructures [68-69]. However, generally the goal is preserving fine morphologies. Gubbels et al. first reported that co-continuity in a blend of polyethylene (PE) and polystyrene (PS) is stabilized during thermal annealing by carbon black selectively distributed in the PE phase [70]. Since an interface-active filler is expected to accumulate at the interface, the authors excluded that stabilization was due to a reduction of the interfacial tension. They instead ascribed coarsening inhibition to the increased viscosity of the host phase, which slows down the coalescence step. Macosko and co-workers focused on the stabilizing effect of interfacially-adsorbed clay nanoparticles on the morphology of co-continuous blends [71]. The authors found that coarsening takes place until the entire interface is covered by the filler. This suggests that interfacial jamming is the main mechanism responsible for the arrest of coarsening. Morphology stabilization is much less pronounced when the plate-like nanoparticles enrich the bulk phases. In this case the effect simply reflects the increased viscosity of the host phase, which slows down the coarsening rate. Although less studied, coarsening during quiescent thermal annealing takes place also in case of distributed morphologies. Parpaite et al. investigated the stability of a drop-matrix blend filled with different kinds of silica nanoparticles [72]. Irrespective of its localization within the blend, the filler was found to inhibit coalescence during quiescent thermal annealing. Differently, the stabilizing efficacy of plate-like nanoparticles seems to be strongly dependent on their localization. Noticeable stabilization effects were observed when the filler enriches the continuous phase [46, 73]. The effect was mainly ascribed to the barrier effect against coalescence provided by the lamellae. On the other hand, the stabilizing action was not confirmed when the filler accumulates in the dispersed phase [72-74].

3.2.3. Effect of nanoparticles on the rheology of polymer blends[*]

Polymer nanocomposites exhibit an intriguing rheological behavior that has been the subject of intensive studies in the last decade. The multiphase nature of the host medium affects the dynamics and structures of the nanoparticles, which in turn influence the morphology of the blend. As a result of such complex and mutual interactions, the rheological behaviour of nanocomposite polymer blends is generally more complex than that of their homopolymer-based counterparts.

Power of LVA for the study of immiscible blends and polymer nanocomposites
Linear viscoelastic analysis (LVA) is a very simple and yet powerful tool widely employed in rheology to interrogate the internal structure of multiphase liquids. LVA is typically carried out by subjecting the sample to small amplitude oscillatory shear (SAOS) experiments. The sample is subjected to a sinusoidal shear deformation, $\gamma(t) = \gamma_0 \sin \omega t$, where γ_0 and ω are the oscillation amplitude and frequency, respectively. The output stress signal is out of phase of an angle δ, $\sigma(t) = \sigma_0 \sin(\omega t + \delta)$. Provided the γ_0 is small enough not to alter the material morphology while testing, the relationship between stress and strain is linear, and the elastic

---

[*] The results presented in this section have still not been published.

(G′) and viscous (G″) shear moduli can be easily computed. At fixed temperature and pressure, such material properties depend on the oscillation frequency, ω. The simplest test is the *frequency scan*, which consists in subjecting the sample to oscillation at fixed amplitude, recording the moduli as a function of ω. For homogeneous polymer melts, Maxwell-type dependence is observed:

$$G'(\omega) = \sum_{i=1}^{N} G_i \frac{\omega^2 \tau_i^2}{1 + \omega^2 \tau_i^2} \tag{3.1}$$

$$G''(\omega) = \sum_{i=1}^{N} G_i \frac{\omega \tau_i}{1 + \omega^2 \tau_i^2} \tag{3.2}$$

where G_i and τ_i are the modulus and relaxation time of the i-th spring-dashpot (Maxwell) element of the generalized Maxwell [75]. Typical curves of $G'(\omega)$ and $G''(\omega)$ of polymer melts in the frequency range usually accessed with common rotational rheometers are shown in Figure 5. From a practical point of view, proceeding from high to low ω provides information about the relaxation modes of increasingly large (hence slow) "items". In case of homogeneous polymer melts, LVA sheds light on the dynamics of more and more long chain subunits; when the macromolecule is fully relaxed, we talk about "terminal behavior" and the moduli scale as $G'\sim\omega^2$ and $G''\sim\omega^1$ (see cartoons in Figure 5). When

Figure 5.: Typical log-log plots showing the frequency-dependence of polymer melts. The cartoon shows the chain and chain subunits able to relax at each frequency.

the material is heterogeneous, additional dynamical families emerge, and their relaxation processes can be effectively studied by means of LVA. The peculiar linear viscoelastic behavior of immiscible polymer blends and polymer nanocomposites (PNCs) is outlined below.
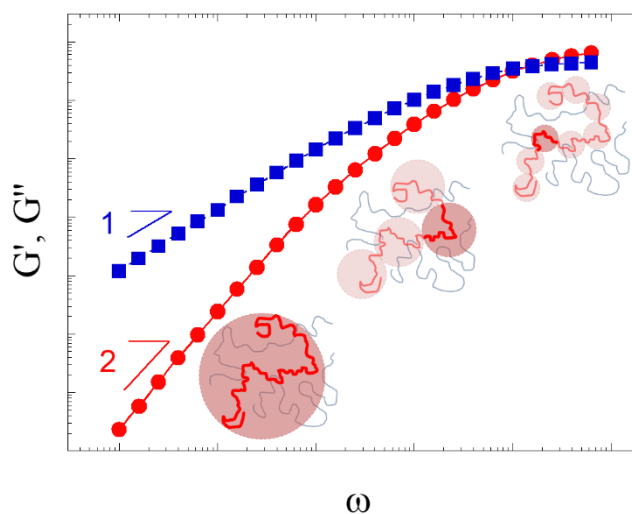
Immiscible polymer bends

Due to a negligible melt mixing entropy, polymers are usually immiscible. As a result, polymer blends exhibit a micro-scale arrangement of the phases that is the result of breakup, coalescence and relaxation phenomena [76]. Among the various morphologies resulting from melt mixing of immiscible polymers with conventional processing apparatus, the two most common ones are drop-in-matrix and co-continuous. The former is much easier to obtain, while co-continuity is much less stable and it can only form in a restricted range of composition essentially defined by the ratio of the viscosities of the constituents [77]. Whatever their morphology, polymer blends exhibit complex relaxation spectra, in which relaxation processes related to the shape of the phases add up to those of the polymer chains of the constituents. Consider first the case of drop-in matrix morphology. When the blend is subjected to an oscillatory flow, each droplet of the dispersed phase deforms, cyclically

assuming an ellipsoidal shape. This brings about an increase of interfacial area, and the interfacial tension, Γ, drives the drop to relax back to a spherical shape. The Palierne'model [78], which is widely employed to describe the linear viscoelasticity of immiscible polymer blends, predicts that the time of such shape relaxation process is [79]:

$$t_d = \frac{(19p + 16)(2p + 3 - 2f(p-1))}{10(p+1) - 2f(5p+2)} \frac{Rh_m}{4G} \tag{3.3}$$

where Φ is the volume fraction of drops, p is the ratio between the viscosity of the drop phase (η_d) over that of matrix (η_m), and R is the drop radius. For blends with sufficiently narrow drop size distribution (ratio between volume and number average drop radius, R_v/R_n, lower than 2), R_v can be used instead of R. For typical polymer blends τ_d is of order of seconds, which is a timescale commonly accessed during LVAs. Therefore, for oscillation frequencies $\omega > \tau_d^{-1}$ the shape relaxation process is frozen, and the viscoelastic moduli reflect the average of those of the blend constituents, while at $\omega < \tau_d^{-1}$ the droplets' contribution emerges as an extra-elasticity G_d given by [79]:

$$G_d = \frac{20f}{(2p + 3 - 2f(p-1))^2} \frac{G}{R} \tag{3.4}$$

Provided that the interfacial elasticity is at least comparable to the G' of the matrix, a peculiar shoulder in the curve of G' vs. ω appears at $\omega_d \sim \tau_d^{-1}$ (Figure 6a). Note that the effect of the droplets on G'' is negligible and will be neglected hereinafter. Now consider a blend with co-continuous morphology.

Respect to the case of drop-in-matrix blends, in which R_v can be set as the unique characteristic size of the
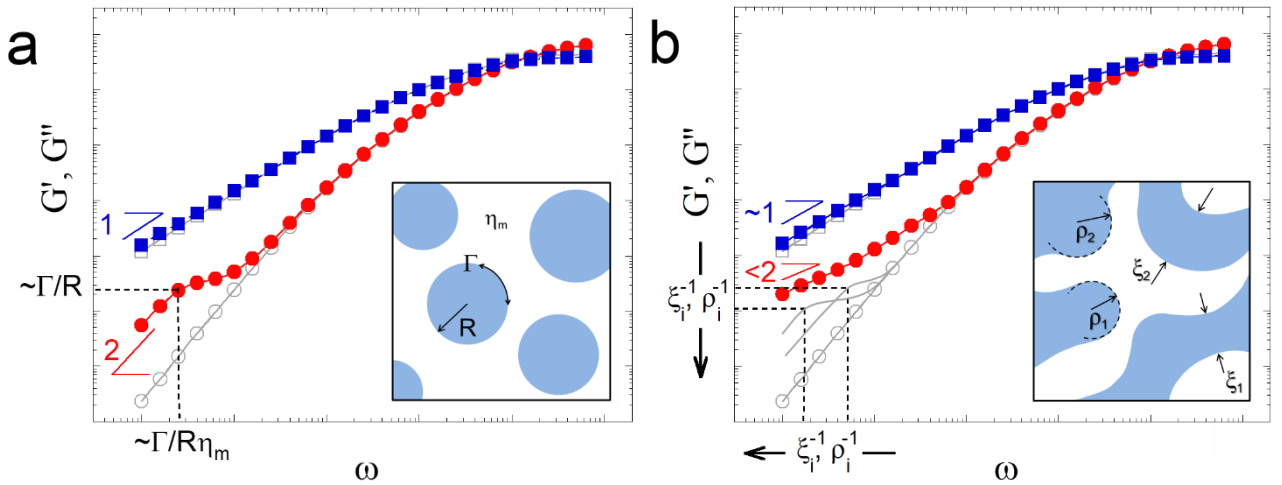

Figure 6.: Typical log-log plots showing the frequency-dependence of the linear viscoelastic moduli of immiscible polymer blends with drop-in-matrix (a) and cocontinuous (b) morphology. Empty gray symbols are the average moduli of the blend constituents.

dispersed phase, in co-continuous blends there is a broad distribution of domains with different sizes, ξ_i, and radii of curvature, ρ_j. Each one of such items relaxes driven by the interfacial tension following essentially the same mechanism as an isolated droplet. The envelope of the distinct relaxation modes of the various domains

results in power-law formats for $G'(\omega)$, the power-law exponent being predicted to be lower than 1 [80] or, in any case, significantly lower than 2 [67] (Figure 6b). As for blends with drop-in-matrix microstructure, the interface has no appreciable effect on G''.

Polymer nanocomposites

The polymer domains of immiscible blends behave like springs when deformed, their elastic constant being dictated by the interfacial tension. Similarly, structures based on fine particulate solids provide additional elasticity to a host polymer matrix. This is the case of PNCs, whose peculiar relaxation spectrum can be profitably studied with LVA. Unless adopting targeted expedients, nanoparticles added to a polymer matrix tend to form agglomerates (flocs), which further assemble into a space whole space spanning network when the filler volume fraction, Φ, exceeds the percolation threshold, Φ_c. Such flocs/network can be modeled as deformable, fractal structures with a predominant elastic feature [81-82]. Therefore, nanoparticle flocs and networks play a similar role as drops and interpenetrated phases in immiscible polymer blends, respectively, providing the PNC with an extra-elastic contribution that alters its relaxation spectrum. Unlike polymer blends, the modeling of the linear viscoelasticity of PNCs is still far from reaching a unifying description. This is mainly due to the wide variety of the possible particle-polymer and particle-particle interactions, which results in a broad spectrum of viscoelastic responses. Despite

Figure 7.: Typical log-log plots showing the frequency-dependence of the linear viscoelastic moduli of polymer nanocomposites at filler content below (a) and above (b) the percolation threshold φ_c. The moduli of the unfilled matrix are shown as empty grey symbols.

the impossibility of defining a "universal" viscoelastic behavior for PNCs, recurring patterns can be identified. Typical frequency-dependences of the linear viscoelastic moduli of PNCs are outlined in Figure 7 for filler contents below (7a) and above (7b) Φ_c. In both cases, a simple vertical shift of the moduli is observed at high frequency. Gleissle and Hochstein showed that hydrodynamic arguments can be invoked to account for such a behavior in concentrated suspensions of microparticles [83]; later, Filippone and coworkers proved that the same concept can be extended to PNCs [84]. In brief, because of the confinement between contiguous flocs, the polymer matrix locally experiences oscillatory deformations larger than what externally imposed,
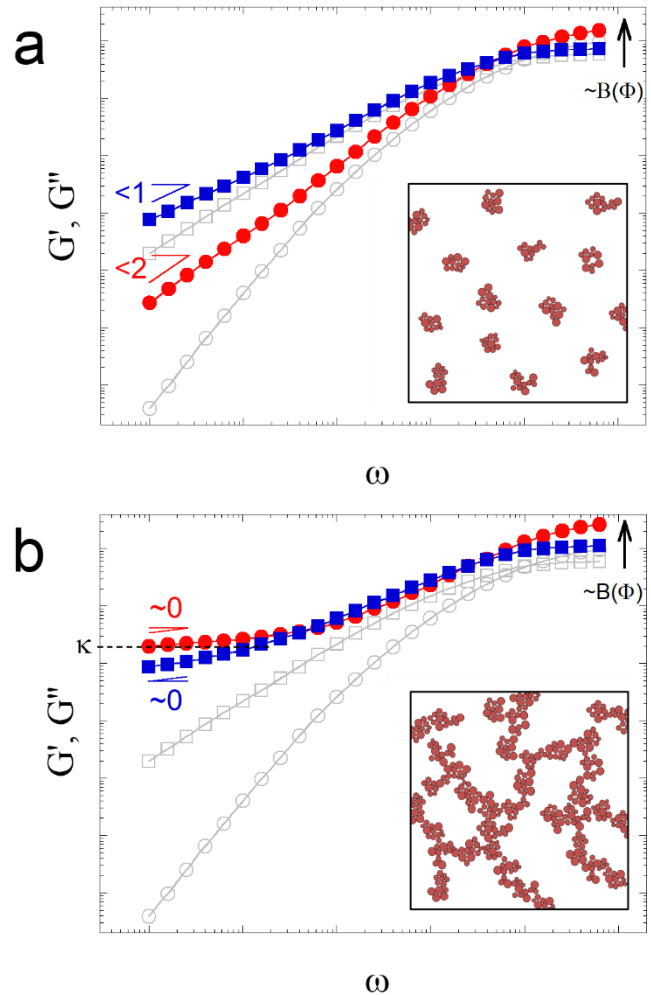
$\gamma_{floc} = B(\Phi)\gamma_0$, with $B(\Phi) > 1$. As a result, the complex modulus ($G^* = \sqrt{G'^2 + G''^2}$) of a PNC at high frequency is simply amplified by the factor $B(\Phi)$ respect to that of the pure polymer, and essentially the same can be said for G' and G''. Now consider the low-frequency behavior. At $\Phi < \Phi_c$ the moduli of PNCs typically exhibit power-law scaling with frequency, the exponents being lower than those of terminal Maxwellian behavior. This reveals the presence of a wide population of dynamical species, each relaxing with its own characteristic timescale. The most convincing interpretation relies on the concept of a "glassy layer" of polymer adsorbed on/confined by the nanoparticles, whose relaxation dynamics are slower than those of the non-interacting chains [85-87]. This picture has been recently reconsidered in terms of a long-ranged gradient of chain mobility, which accounts for the broadness of the relaxation spectrum [88-89]. Increasing the filler content below Φ_c implies the involvement of larger portions of polymer, but at $\Phi < \Phi_c$ the behavior essentially remains "liquid-like" ($G'' > G'$). Things change when the filler content is raised above Φ_c. In these conditions, the filler network provides the material with "solid-like" features, viz. predominant elastic connotation ($G' > G''$) and weak frequency-dependence of both moduli. The strength of the filler network and its permanent or transient character determine relative magnitude of the low-frequency plateaus, slope of the $G'(\omega)$ and $G''(\omega)$ curves, and presence of specific relaxation phenomena. If G' approaches a frequency-independent value, the latter can be taken as the network elasticity, κ. Despite the broad spectrum of possible viscoelastic responses, a two-phase model recently proposed by our group is able to describe the behavior of PNCs at $\Phi > \Phi_c$ as the superposition of two main populations of dynamical species: the filler network, possibly involving a fraction of adsorbed polymer and responsible for the material's elasticity, and the host (non-interacting) polymer, responsible for the viscous connotation [90]. The simple additivity of the contributions of the polymer and filler phase greatly simplifies the LVA of PNCs above Φ_c.

LVA of immiscible blends and PNCs: issues related to the time stability of the sample

LVA is an easy-to-use and yet powerful experimental technique that sheds light of the wide variety of relaxation phenomena occurring in multiphase materials, such as blends and PNCs. On the other hand, the correct assignment of a specific process to a certain relaxation event strictly requires the stability over time of morphological features and chemo-physical properties of each member of the dynamical family. If changes occur in the material while testing, the shape of the curves varies and the outcome of LVA becomes difficult to be interpreted. Here we restrict our attention on the alteration of the rheological response induced by changes in the blend microstructure and/or variations in the space arrangement of the nanoparticles. The requirement of time stability is typically not crucial in case of drop-in-matrix blends, while it may represent a severe limitation in case of PNCs and co-continuous blends, which experience significant changes in their inner structure over the typical timescales of LVA. In particular, co-continuous morphologies are inherently unstable, and quickly evolve towards coarser configurations characterized by lower interfacial area during rheological analysis driven by interfacial tension [91]. Regarding PNCs, the non-negligible mobility of nanoparticles even in highly viscous polymer matrices results in space rearrangements of the filler, such as flocculation [92], loss of orientation [93], or changes in the state of dispersion [94]. Reliable information is

collected only if the duration of the test is negligible respect to the characteristic time of the variation of the rheological properties. Alternatively, even the direction of frequency sweeping (i.e. from low to high or from high to low frequencies) affects the relaxation spectrum collectable through SAOS experiments. Employing time-resolved rheological approaches repres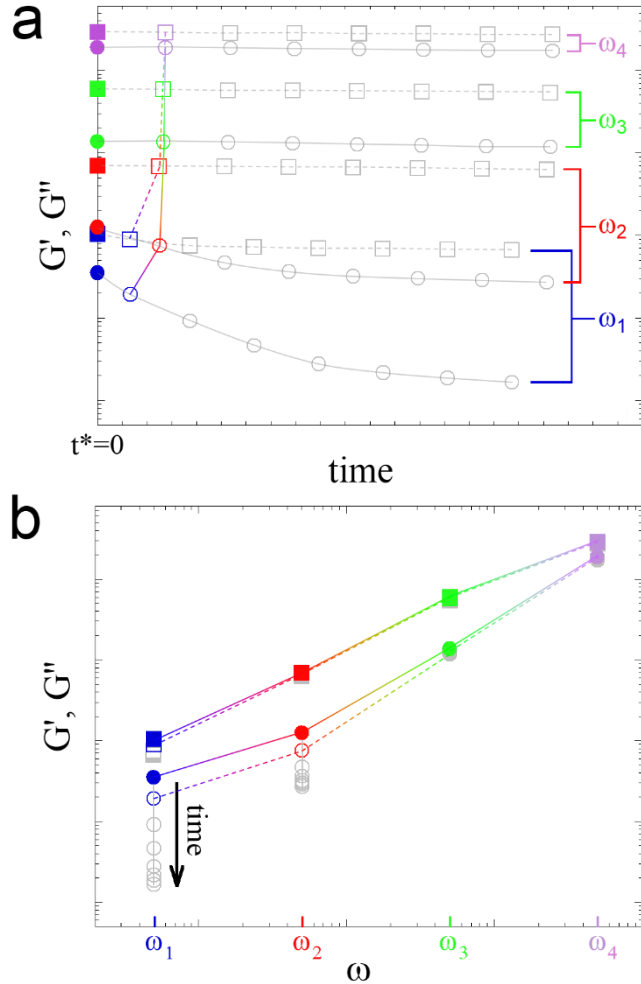ents a simple and yet highly effective way to elude the time evolutions of the moduli and capture the mere frequency-dependent behavior [95]. The two kinds of test that can be performed for this purpose are (i) Fourier-transformed mechanical spectroscopy [96] and (ii) cyclic frequency sweeps [97]. The former type of test consists in subjecting the sample to a strain waveform constituted by the sum of N independent sinusoidal signals, $\gamma(t) = \sum_{i=1}^{N} \gamma_{oi} \sin \omega_i t$; a discrete Fourier transform is performed on the resulting stress data to obtain the individual stress values for each frequency component, from which $G'(\omega)$ and $G''(\omega)$ are finally computed [98]. This minimizes the duration of the test, allowing for neglecting the effects related to the evolutions of the material. At best, one can collect reliable $G'(\omega)$ and $G''(\omega)$ curves in a time interval equal that needed to complete one cycle at the lowest frequency ("fundamental frequency"). The second approach consists in performing a simple sequence of independent frequency scans. Plotting the results as a function of time and interpolating the G' and G'' data, purely isochronal viscoelastic curves can be easily obtained at any instant of time t^* by crossing with a vertical line even in case of materials that experience very rapid evolutions [99-100]. In particular, the behavior of the "as-prepared sample",

Figure 8.: a) Typical outcome of a sequence of SAOS experiment carried out on a sample that experiences time evolution (decrease) of the linear viscoelastic moduli (G' as circles, G'' as squares). Each SAOS is performed from low to high frequency ($\omega_1 < \omega_2 < \omega_3 < \omega_4$). Full symbols are the isochronal moduli at $t^*=0$ («as-prepared sample»); the outcome of the first SAOS is highlighted using colored symbols. b) Same data and symbols as in (a) plotted as a function of frequency.

i.e. before the occurrence of any change in the morphology resulted from processing, can be obtained by extrapolating the moduli at $t^*=0$ (Figure 8a). It is important to notice that the relaxation spectrum of such a virgin sample can substantially differ from the outcome of the first SAOS (Figure 8b). The main source of inaccuracy of the previous approach stems from the interpolation procedure. The accuracy diminishes by reducing the frequencies to be probed, since the points to be interpolated distance themselves. In any case, time-resolved rheometry is strongly recommended if one aims at collecting reliable data on the relaxation

dynamics of complex systems such those addressed in this paper, for which a simple frequency scan likely leads to inaccurate conclusions.

LVA of nanoparticle-containing immiscible polymer blends

The complexity of the relaxation spectrum of immiscible polymer blends filled with nanoparticles derives from the combination of the responses of numerous dynamical families. This can generate uncertainty in the assignment of the various relaxation processes, and the outcomes of LVA are difficult to be interpreted. Another critical issue stems from the radical impact that nanoparticles have on the blend morphology [51]; the subsequent alterations in the relaxation spectrum must be taken into account when interpreting the results of LVA. Moreover, the response of one or more species can prevail over the other(s), concealing the response of the latter. As a result, the viscoelastic behavior of nanocomposite polymer blends results similar to that of either one-polymer nanocomposites or unfilled polymer blends. Despite the complexity of the subject, the existence of repetitive patterns in the literature suggests that LVA can be used as an indirect probe of the material's microstructure able to provide evidence of the space arrangement of polymers and nanoparticles.

Drop-in-matrix blends – Nanoparticles in either of the bulk phases
When nanoparticles are added to a blend with drop-in-matrix morphology, the first aspect to be addressed is the localization of the filler. Thermodynamics and kinetics effects drive the system towards a uneven distribution of the particles, which can gather inside the drops, enrich the matrix, or assemble at the polymer-polymer interface [52]. Actually, unless using very low amounts of filler, most of the time a combination of two or even all the three situations is observed, and the interpretation of the outcome of LVA becomes tricky. We start our analysis by considering the cases of *exclusive* positioning of the filler inside either of the bulk phases. In this case, the interfacial tension can be reasonably assumed not to change, and only two main effects have to be considered, namely the alteration in the rheological properties of the host polymer and the changes in the average size of the drops, which typically become smaller in the presence of nanoparticles. We perform our analysis in the framework of the Palierne's model, which does not fix particular limitations about the viscoelastic nature of the blend constituents [79]. The moduli of a nanoparticle-containing blend were hence derived by introducing in the model the moduli of a PNC for either of the phases. The results of the modeling are summarized in Figure 9. Two cases were examined, namely low ($\Phi<\Phi_c$) and high ($\Phi>\Phi_c$) amount of nanoparticles. In addition, each curve was derived for two different values of drop radius to account for the changes in the size of the drops typically induced by the nanoparticles.

The effect of nanoparticles embedded in the drops is negligible irrespective of their content. In particular, the moduli of the sample at low Φ are almost perfectly superimposed to those of the unfilled blend. Some difference emerges due to the morphology refinement induced by the filler, which causes the shoulder of G' to move towards higher frequency while becoming less defined (see Figure 9a). Regarding the sample at high Φ, a slight increase of G' is noticed at low frequency, i.e. where the filler network in the drops causes their rheological transition from liquid- to solid-like (see Figure 7b). Some increase of G' can also be observed at high frequency. In this regime the moduli of the blend are a weighted average of those of the
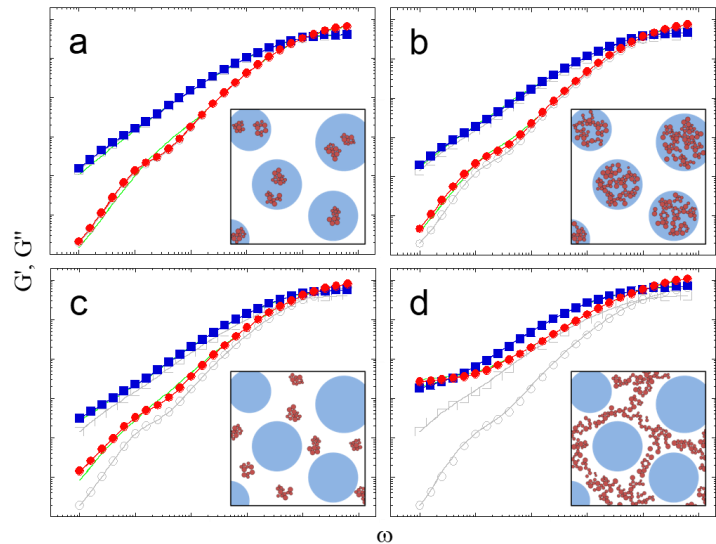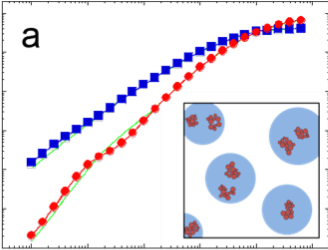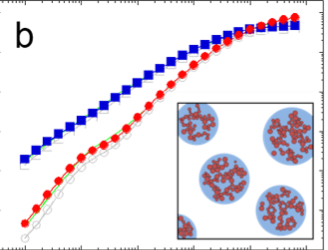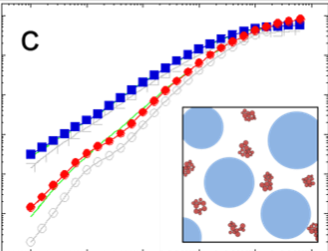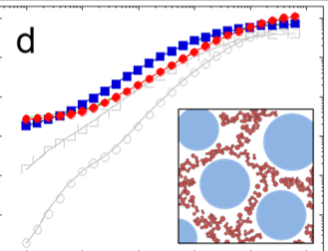
Figure 9.: Elastic (full circles) and viscous (full squares) moduli of drop-in-matrix blends with nanopaticles embedded in either of the bulk phases according to the expectations of the Palierne's model. Empty symbols are the moduli of the unfilled blend with the same average radius and interfacial tension. The expectations of the Palierne's model in case of drops with half radius are reported as green lines.

unfilled matrix and filled drops, and the latter increase due to hydrodynamic effects (see Figure 7). In general, however, only a moderate effect on the blend relaxation spectrum is observed in spite of the divergence of the relaxation time of the drops [101]. This reflects the fact that LVA is particularly sensitive to percolating structures that span large portion of sample. As a consequence, confining the filler inside well defined and separated domains has a minor effect, the rheological response being essentially dominated by the unfilled continuous phase. Things indeed change when the nanoparticles locate inside the matrix. In this case, the contributions of filler and continuous polymer phase combine as they were in parallel. Therefore, the drops contribution only emerges if the amount of nanoparticles is small enough not to hide it (Figure 9c). In this case, the shape of the curves is reminiscent of unfilled blends except for the higher value of the moduli at low frequency, i.e. where the filler causes positive deviation from the behavior of the host polymer (see Figure 7a). If the amount of particles exceeds a certain threshold, the effect of the filler dominates over that of the drops: the shoulder of G' disappears and the behavior approaches that of single-polymer nanocomposites. For $\Phi > \Phi_c$ the drops are entrapped in the nanoparticle network and do not give any appreciable contribution, even if drastic refinement takes place (Figure 9d). A collection of papers reporting falling into one or more of the four categories of Figure 9 is reported in Table 1.

Table 1.: Collection of papers illustrating examples discussed above.

	Ref.: 102, 103, 104, 105, 61	Ref.: 102, 106, 107, 108, 103, 105, 61	
	Ref.: 109, 110, 103, 111, 105	Ref.: 109, 103, 110, 106, 107, 112, 111, 61	

The better way to conclude this chapter and, in particular, this section is to let know in advance that all the remaining cases (i.e.: drop-in-matrix and co-continuous systems with particles located at the polymer-polymer interface, and co-continuous systems with particles in the bulk phases) will be discussed extensively and item by item in the next sections. We will provide to explain and discuss each case with the experimental data, supported by a lot of deep analyses. A wider framework will be offered carrying out even an analysis of the literature looking for repeated patterns. This could let the identification of some main types of viscoelastic behaviour and a phenomenology that could be clearly recognized.

BIBLIOGRAPHY

1. Kickelbick, G. (2006). 1 Introduction to Hybrid Materials.

2. Barton, J., Niemczyk, A., Czaja, K., Korach, L., & Sachermajewska, B. (2014). Polymer composites, biocomposites and nanocomposites. Production, composition, properties and application fields. Chemik, 68(4), 280-287.

3. U.S. Congress: Office of Technology Assessment, Advanced Materials by Design. U.S. Government Printing Office 1988.

4. Shokrieh, M. M., & Rafiee, R. (2010). Stochastic multi-scale modeling of CNT/polymer composites. Computational Materials Science, 50(2), 437-446.

5. Thomas, S., Kuruvilla, J., Malhotra, S. K., Goda, K., Sreekala M. S. (2012). Polymer Composites: Volume 1. Wiley-VCH Verlag GmbH & Co. KGaA, Weinheim, Germany.

6. Nwabunma, D., & Kyu, T. (Eds.). (2008). Polyolefin composites. John Wiley & Sons.

7. Barnes, H. A. (2003). A review of the rheology of filled viscoelastic systems. Rheology reviews, 1-36.

8. Vaia, R. A., & Maguire, J. F. (2007). Polymer nanocomposites with prescribed morphology: going beyond nanoparticle-filled polymers. Chemistry of Materials, 19(11), 2736-2751.

9. Galpaya, D., Wang, M., Liu, M., Motta, N., Waclawik, E. R., & Yan, C. (2012). Recent advances in fabrication and characterization of graphene-polymer nanocomposites. Graphene, 1(2), 30-49.

10. Yeh, M. H., & Hwang, W. S. (2006). High mechanical properties of polychloroprene/montmorillonite nanocomposites. Materials transactions, 47(11), 2753-2758.

11. Alonso, A., Bastos-Arrieta, J., Davies, G. L., Gun'ko, Y. K., Vigués, N., Muñoz-Berbel, X., ... & Muraviev, D. N. (2012). Ecologically friendly polymer-metal and polymer-metal oxide nanocomposites for complex water treatment. In Nanocomposites-New Trends and Developments. InTech.

12. Majeed, K., Jawaid, M., Hassan, A., Bakar, A. A., Khalil, H. A., Salema, A. A., & Inuwa, I. (2013). Potential materials for food packaging from nanoclay/natural fibres filled hybrid composites. Materials & Design, 46, 391-410.

13. Šupová, M., Martynková, G. S., & Barabaszová, K. (2011). Effect of nanofillers dispersion in polymer matrices: a review. Science of Advanced Materials, 3(1), 1-25.

14. Giannelis, E. P. (1996). Polymer layered silicate nanocomposites. Advanced materials, 8(1), 29-35.

15. Alexandre, M., & Dubois, P. (2000). Polymer-layered silicate nanocomposites: preparation, properties and uses of a new class of materials. Materials Science and Engineering: R: Reports, 28(1), 1-63.

16. Ray, S. S., & Okamoto, M. (2003). Polymer/layered silicate nanocomposites: a review from preparation to processing. Progress in polymer science, 28(11), 1539-1641.

17. Okamoto, M. Polymer/Clay Nanocomposites (2004). In Encyclopedia of Nanoscience and Nanotechnology; Nalwa, H. S., Ed.; American Scientific: Stevenson Ranch, CA; Vol. 8, p 1.

18. Thostenson, E. T., Li, C., & Chou, T. W. (2005). Nanocomposites in context. Composites Science and Technology, 65(3), 491-516.

19. Drummy, L. F., Koerner, H., Farmer, B. L., & Vaia, R. A. (2006). Advanced Morphology Characterization of Clay-Based Polymer Nanocomposites: CMS Workshop Lecture Series. Clay Minerals Society, Chantilly, VA.

20. Tjong, S. C. (2006). Structural and mechanical properties of polymer nanocomposites. Materials Science and Engineering: R: Reports, 53(3), 73-197.

21. Hussain, F., Hojjati, M., Okamoto, M., & Gorga, R. E. (2006). Polymer-matrix nanocomposites, processing, manufacturing, and application: an overview. Journal of composite materials, 40(17), 1511-1575.

22. Xie, X. L., Mai, Y. W., & Zhou, X. P. (2005). Dispersion and alignment of carbon nanotubes in polymer matrix: a review. Materials Science and Engineering: R: Reports, 49(4), 89-112.

23. Moniruzzaman, M., & Winey, K. I. (2006). Polymer nanocomposites containing carbon nanotubes. Macromolecules, 39(16), 5194-5205.

24. Pinnavaia, T. J., & Beall, G. W. (Eds.). (2000). Polymer-clay nanocomposites. John Wiley.

25. Krishnamoorti, R., & Vaia, R. A. (Eds.). (2001). Polymer nanocomposites: synthesis, characterization, and modeling. American Chemical Society. (23) Ray, S. S.; Bousmina, M. Polymer Nanocomposites and Their Applications;

26. Ray, S. S., & Bousmina, M. (2006). Polymer nanocomposites and their applications. American Scientific.

27. Mai, Y. W., & Yu, Z. Z. (2006). Polymer nanocomposites. Woodhead publishing.

28. Nanocomposites, F. R. P. (2007). Morgan, AB, Wilkie, CA, Eds.

29. Xanthos, M. (Ed.). (2010). Functional fillers for plastics. John Wiley & Sons.

30. Kumar, A. P., Depan, D., Tomer, N. S., & Singh, R. P. (2009). Nanoscale particles for polymer degradation and stabilization—trends and future perspectives. Progress in polymer science, 34(6), 479-515.

31. Raquez, J. M., Habibi, Y., Murariu, M., & Dubois, P. (2013). Polylactide (PLA)-based nanocomposites. Progress in Polymer Science, 38(10), 1504-1542.

32. Balazs, A. C., Emrick, T., & Russell, T. P. (2006). Nanoparticle polymer composites: where two small worlds meet. Science, 314(5802), 1107-1110.

33. Ajayan, P. M., Schadler, L. S., & Braun, P. V. (2006). Nanocomposite science and technology. John Wiley & Sons.

34. Bain, C. D., & Whitesides, G. M. (1988). Molecular-level control over surface order in self-assembled monolayer films of thiols on gold. Science, 240(4848), 62-64.

35. Husseman, M., Malmström, E. E., McNamara, M., Mate, M., Mecerreyes, D., Benoit, D. G., ... & Hawker, C. J. (1999). Controlled synthesis of polymer brushes by "living" free radical polymerization techniques. Macromolecules, 32(5), 1424-1431.

36. Lin, Y., Skaff, H., Emrick, T., Dinsmore, A. D., & Russell, T. P. (2003). Nanoparticle assembly and transport at liquid-liquid interfaces. Science, 299(5604), 226-229.

37. Si, M., Araki, T., Ade, H., Kilcoyne, A. L. D., Fisher, R., Sokolov, J. C., & Rafailovich, M. H. (2006). Compatibilizing bulk polymer blends by using organoclays. Macromolecules, 39(14), 4793-4801.

38. Tanaka, H., Lovinger, A. J., & Davis, D. D. (1994). Pattern evolution caused by dynamic coupling between wetting and phase separation in binary liquid mixture containing glass particles. Physical review letters, 72(16), 2581.

39. Lee, B. P., Douglas, J. F., & Glotzer, S. C. (1999). Filler-induced composition waves in phase-separating polymer blends. Physical Review E, 60(5), 5812.

40. Chung, H. J., Taubert, A., Deshmukh, R. D., & Composto, R. J. (2004). Mobile nanoparticles and their effect on phase separation dynamics in thin-film polymer blends. EPL (Europhysics Letters), 68(2), 219.

41. Yurekli, K., Karim, A., Amis, E. J., & Krishnamoorti, R. (2003). Influence of layered silicates on the phase-separated morphology of PS− PVME blends. Macromolecules, 36(19), 7256-7267.

42. Ginzburg, V. V. (2005). Influence of nanoparticles on miscibility of polymer blends. A simple theory. Macromolecules, 38(6), 2362-2367.

43. He, G., Ginzburg, V. V., & Balazs, A. C. (2006). Determining the phase behavior of nanoparticle-filled binary blends. Journal of Polymer Science Part B: Polymer Physics, 44(17), 2389-2403.

44. Buxton, G. A., & Balazs, A. C. (2004). Predicting the mechanical and electrical properties of nanocomposites formed from polymer blends and nanorods. Molecular Simulation, 30(4), 249-257.

45. Elias, L., Fenouillot, F., Majesté, J. C., & Cassagnau, P. (2007). Morphology and rheology of immiscible polymer blends filled with silica nanoparticles. Polymer, 48(20), 6029-6040.

46. Khatua, B. B., Lee, D. J., Kim, H. Y., & Kim, J. K. (2004). Effect of organoclay platelets on morphology of nylon-6 and poly (ethylene-r an-propylene) rubber blends. Macromolecules, 37(7), 2454-2459.

47. Lee, H. S., Fasulo, P. D., Rodgers, W. R., & Paul, D. R. (2005). TPO based nanocomposites. Part 1. Morphology and mechanical properties. Polymer, 46(25), 11673-11689.

48. Vo, L. T., & Giannelis, E. P. (2007). Compatibilizing poly (vinylidene fluoride)/nylon-6 blends with nanoclay. Macromolecules, 40(23), 8271-8276.

49. Mallick, S., Kar, P., & Khatua, B. B. (2012). Morphology and properties of nylon 6 and high density polyethylene blends in presence of nanoclay and PE-g-MA. Journal of Applied Polymer Science, 123(3), 1801-1811.

50. Filippone, G., Dintcheva, N. T., La Mantia, F. P., & Acierno, D. (2010). Using organoclay to promote morphology refinement and co-continuity in high-density polyethylene/polyamide 6 blends–Effect of filler content and polymer matrix composition. Polymer, 51(17), 3956-3965.

51. de Luna, M. S., & Filippone, G. (2016). Effects of nanoparticles on the morphology of immiscible polymer blends–challenges and opportunities. European Polymer Journal, 79, 198-218.

52. Elias, L., Fenouillot, F., Majesté, J. C., Alcouffe, P., & Cassagnau, P. (2008). Immiscible polymer blends stabilized with nano-silica particles: Rheology and effective interfacial tension. Polymer, 49(20), 4378-4385.

53. Ray, S. S., Pouliot, S., Bousmina, M., & Utracki, L. A. (2004). Role of organically modified layered silicate as an active interfacial modifier in immiscible polystyrene/polypropylene blends. Polymer, 45(25), 8403-8413.

54. Hong, J. S., Kim, Y. K., Ahn, K. H., Lee, S. J., & Kim, C. (2007). Interfacial tension reduction in PBT/PE/clay nanocomposite. Rheologica Acta, 46(4), 469-478.

55. Levine, S., & Bowen, B. D. (1993). Capillary interaction of spherical particles adsorbed on the surface of an oil/water droplet stabilized by the particles: 3. Effective interfacial tension. Colloids and Surfaces A: Physicochemical and Engineering Aspects, 70(1), 33-45.

56. Fenouillot, F., Cassagnau, P., & Majesté, J. C. (2009). Uneven distribution of nanoparticles in immiscible fluids: morphology development in polymer blends. Polymer, 50(6), 1333-1350.

57. Cao, Y., Zhang, J., Feng, J., & Wu, P. (2011). Compatibilization of immiscible polymer blends using graphene oxide sheets. Acs Nano, 5(7), 5920-5927.

58. Wu, D., Zhang, Y., Zhang, M., & Yu, W. (2009). Selective localization of multiwalled carbon nanotubes in poly (ε-caprolactone)/polylactide blend. Biomacromolecules, 10(2), 417-424.

59. Fang, Z., Xu, Y., & Tong, L. (2007). Effect of clay on the morphology of binary blends of polyamide 6 with high density polyethylene and HDPE-graft-acrylic acid. Polymer Engineering & Science, 47(5), 551-559.

60. Zhang, W., Lin, M., Winesett, A., Dhez, O., Kilcoyne, A., Ade, H., ... & Tenne, R. (2011). The use of functionalized nanoparticles as non-specific compatibilizers for polymer blends. Polymers for Advanced Technologies, 22(1), 65-71.

61. Bose, S., Özdilek, C., Leys, J., Seo, J. W., Wübbenhorst, M., Vermant, J., & Moldenaers, P. (2010). Phase separation as a tool to control dispersion of multiwall carbon nanotubes in polymeric blends. ACS applied materials & interfaces, 2(3), 800-807.

62. Vermant, J., Cioccolo, G., Nair, K. G., & Moldenaers, P. (2004). Coalescence suppression in model immiscible polymer blends by nano-sized colloidal particles. Rheologica acta, 43(5), 529-538.

63. Huang, J., Zhu, Y., Jiang, W., Cardinaels, R., Moldenaers, P., & Shi, D. (2014). Morphology control and stabilization in immiscible polypropylene and polyamide 6 blends with organoclay. International Polymer Processing, 29(4), 522-534.

64. Kong, M., Huang, Y., Lv, Y., Wang, S., Yang, Q., & Li, G. (2014). Flow-induced morphological instability in nanosilica-filled polyamide 6/polystyrene blends. Polymer, 55(16), 4348-4357.

65. Filippone, G., & Acierno, D. (2012). Clustering of coated droplets in clay-filled polymer blends. Macromolecular Materials and Engineering, 297(9), 923-928.

66. Willemse, R. C., Ramaker, E. J. J., Van Dam, J., & De Boer, A. P. (1999). Coarsening in molten quiescent polymer blends: The role of the initial morphology. Polymer Engineering & Science, 39(9), 1717-1725.

67. López-Barrón, C. R., & Macosko, C. W. (2012). Rheological and morphological study of cocontinuous polymer blends during coarsening. Journal of Rheology, 56(6), 1315-1334.

68. Yao, D., Zhang, W., & Zhou, J. G. (2009). Controllable growth of gradient porous structures. Biomacromolecules, 10(5), 1282-1286.

69. Sarazin, P., Roy, X., & Favis, B. D. (2004). Controlled preparation and properties of porous poly (L-lactide) obtained from a co-continuous blend of two biodegradable polymers. Biomaterials, 25(28), 5965-5978.

70. Gubbels, F., Blacher, S., Vanlathem, E., Jérôme, R., Deltour, R., Brouers, F., & Teyssie, P. (1995). Design of electrical composites: determining the role of the morphology on the electrical properties of carbon black filled polymer blends. Macromolecules, 28(5), 1559-1566.

71. Trifkovic, M., Hedegaard, A. T., Sheikhzadeh, M., Huang, S., & Macosko, C. W. (2015). Stabilization of PE/PEO cocontinuous blends by interfacial nanoclays. Macromolecules, 48(13), 4631-4644

72. Parpaite, T., Otazaghine, B., Taguet, A., Sonnier, R., Caro, A. S., & Lopez-Cuesta, J. M. (2014). Incorporation of modified Stöber silica nanoparticles in polystyrene/polyamide-6 blends: Coalescence inhibition and modification of the thermal degradation via controlled dispersion at the interface. Polymer, 55(11), 2704-2715.

73. Tiwari, R. R., & Paul, D. R. (2011). Effect of organoclay on the morphology, phase stability and mechanical properties of polypropylene/polystyrene blends. Polymer, 52(4), 1141-1154.

74. Moghbelli, E., Sue, H. J., & Jain, S. (2010). Stabilization and control of phase morphology of PA/SAN blends via incorporation of exfoliated clay. Polymer, 51(18), 4231-4237.

75. Ferry, J. D. (1980). Viscoelastic properties of polymers. John Wiley & Sons.

76. Tucker III, C. L., & Moldenaers, P. (2002). Microstructural evolution in polymer blends. Annual Review of Fluid Mechanics, 34(1), 177-210.

77. Pötschke, P., & Paul, D. R. (2003). Formation of co-continuous structures in melt-mixed immiscible polymer blends. Journal of Macromolecular Science, Part C: Polymer Reviews, 43(1), 87-141.

78. Palierne, J. F. (1990). Linear rheology of viscoelastic emulsions with interfacial tension. Rheologica acta, 29(3), 204-214.

79. Graebling, D., Muller, R., & Palierne, J. F. (1993). Linear viscoelastic behavior of some incompatible polymer blends in the melt. Interpretation of data with a model of emulsion of viscoelastic liquids. Macromolecules, 26(2), 320-329.

80. Weis, C., Leukel, J., Borkenstein, K., Maier, D., Gronski, W., Friedrich, C., & Honerkamp, J. (1998). Morphological and rheological detection of the phase inversion of PMMA/PS polymer blends. Polymer Bulletin, 40(2), 235-241.

81. Shih, W. H., Shih, W. Y., Kim, S. I., Liu, J., & Aksay, I. A. (1990). Scaling behavior of the elastic properties of colloidal gels. Physical review A, 42(8), 4772.

82. Wu, H., & Morbidelli, M. (2001). A model relating structure of colloidal gels to their elastic properties. Langmuir, 17(4), 1030-1036.

83. Gleissle, W., & Hochstein, B. (2003). Validity of the Cox–Merz rule for concentrated suspensions. Journal of rheology, 47(4), 897-910.

84. Filippone, G., Romeo, G., & Acierno, D. (2009). Viscoelasticity and structure of polystyrene/fumed silica nanocomposites: filler network and hydrodynamic contributions. Langmuir, 26(4), 2714-2720.

85. Kaufman, S., Slichter, W. P., & Davis, D. D. (1971). Nuclear magnetic resonance study of rubber–carbon black interactions. Journal of Polymer Science Part B: Polymer Physics, 9(5), 829-839.

86. O'Brien, J., Cashell, E., Wardell, G. E., & McBrierty, V. J. (1977). An NMR investigation of the interaction between carbon black and cis-polybutadiene. Rubber Chemistry and Technology, 50(4), 747-764.

87. Dutta, N. K., Choudhury, N. R., Haidar, B., Vidal, A., Donnet, J. B., Delmotte, L., & Chezeau, J. M. (1994). High resolution solid-state nmr investigation of the filler-rubber interaction: 1. High speed 1H magic-angle spinning nmr spectroscopy in carbon black filled styrene-butadiene rubber. Polymer, 35(20), 4293-4299.

88. Berriot, J., Montes, H., Lequeux, F., Long, D., & Sotta, P. (2003). Gradient of glass transition temperature in filled elastomers. EPL (Europhysics Letters), 64(1), 50.

89. Jouault, N., Vallat, P., Dalmas, F., Said, S., Jestin, J., & Boué, F. (2009). Well-dispersed fractal aggregates as filler in polymer− silica nanocomposites: long-range effects in rheology. Macromolecules, 42(6), 2031-2040.

90. Filippone, G., & Salzano de Luna, M. (2012). A unifying approach for the linear viscoelasticity of polymer nanocomposites. Macromolecules, 45(21), 8853-8860.

91. Yuan, Z., & Favis, B. D. (2005). Coarsening of immiscible co-continuous blends during quiescent annealing. AIChE journal, 51(1), 271-280.

92. Romeo, G., Filippone, G., Russo, P., & Acierno, D. (2009). Effects of particle dimension and matrix viscosity on the colloidal aggregation in weakly interacting polymer-nanoparticle composites: a linear viscoelastic analysis. Polymer bulletin, 63(6), 883.

93. Kim, H., & Macosko, C. W. (2009). Processing-property relationships of polycarbonate/graphene composites. Polymer, 50(15), 3797-3809.

94. Wang, X., Sun, P., Xue, G., & Winter, H. H. (2010). Late-state ripening dynamics of a polymer/clay nanocomposite. Macromolecules, 43(4), 1901-1906.

95. Mours, M., & Winter, H. H. (1994). Time-resolved rheometry. Rheologica acta, 33(5), 385-397.

96. Holly, E. E., Venkataraman, S. K., Chambon, F., & Winter, H. H. (1988). Fourier transform mechanical spectroscopy of viscoelastic materials with transient structure. Journal of non-newtonian fluid mechanics, 27(1), 17-26.

97. Scanlan, J. C., & Winter, H. H. (1991). Composition dependence of the viscoelasticity of end-linked poly (dimethylsiloxane) at the gel point. Macromolecules, 24(1), 47-54.

98. Filippone, G., Dintcheva, N. T., Acierno, D., & La Mantia, F. P. (2008). The role of organoclay in promoting co-continuous morphology in high-density poly (ethylene)/poly (amide) 6 blends. Polymer, 49(5), 1312-1322.

99. Filippone, G., Carroccio, S. C., Mendichi, R., Gioiella, L., Dintcheva, N. T., & Gambarotti, C. (2015). Time-resolved rheology as a tool to monitor the progress of polymer degradation in the melt state–Part I: Thermal and thermo-oxidative degradation of polyamide 11. Polymer, 72, 134-141.

100. Filippone, G., Carroccio, S. C., Curcuruto, G., Passaglia, E., Gambarotti, C., & Dintcheva, N. T. (2015). Time-resolved rheology as a tool to monitor the progress of polymer degradation in the melt state–Part II: Thermal and thermo-oxidative degradation of polyamide 11/organo-clay nanocomposites. Polymer, 73, 102-110.

101. Liu, X. Q., Sun, Z. Y., Bao, R. Y., Yang, W., Xie, B. H., & Yang, M. B. (2014). Nanoparticle retarded shape relaxation of dispersed droplets in polymer blends: an understanding from the viewpoint of molecular movement. Rsc Advances, 4(77), 41059-41068.

102. Salehiyan, R., Song, H. Y., Kim, M., Choi, W. J., & Hyun, K. (2016). Morphological Evaluation of PP/PS Blends Filled with Different Types of Clays by Nonlinear Rheological Analysis. Macromolecules, 49(8), 3148-3160.

103. Özdilek, C., Bose, S., Leys, J., Seo, J. W., Wübbenhorst, M., & Moldenaers, P. (2011). Thermally induced phase separation in PαMSAN/PMMA blends in presence of functionalized multiwall carbon nanotubes: Rheology, morphology and electrical conductivity. Polymer, 52(20), 4480-4489.

104. Vermant, J., Vandebril, S., Dewitte, C., & Moldenaers, P. (2008). Particle-stabilized polymer blends. Rheologica acta, 47(7), 835-839.

105. Salehiyan, R., Song, H. Y., Choi, W. J., & Hyun, K. (2015). Characterization of effects of silica nanoparticles on (80/20) PP/PS blends via nonlinear rheological properties from Fourier transform rheology. Macromolecules, 48(13), 4669-4679.

106. Du, B., Handge, U. A., Majeed, S., & Abetz, V. (2012). Localization of functionalized MWCNT in SAN/PPE blends and their influence on rheological properties. Polymer, 53(24), 5491-5501.

107. Huang, C., Gao, J., Yu, W., & Zhou, C. (2012). Phase separation of poly (methyl methacrylate)/poly (styrene-co-acrylonitrile) blends with controlled distribution of silica nanoparticles. Macromolecules, 45(20), 8420-8429.

108. Hwang, T. Y., Yoo, Y., & Lee, J. W. (2012). Electrical conductivity, phase behavior, and rheology of polypropylene/polystyrene blends with multi-walled carbon nanotube. Rheologica acta, 51(7), 623-636.

109. Huitric, J., Ville, J., Médéric, P., Moan, M., & Aubry, T. (2009). Rheological, morphological and structural properties of PE/PA/nanoclay ternary blends: Effect of clay weight fraction. Journal of rheology, 53(5), 1101-1119.

110. Bitinis, N., Verdejo, R., Maya, E. M., Espuche, E., Cassagnau, P., & Lopez-Manchado, M. A. (2012). Physicochemical properties of organoclay filled polylactic acid/natural rubber blend bionanocomposites. Composites Science and Technology, 72(2), 305-313.

111. Liu, Y., & Kontopoulou, M. (2006). The structure and physical properties of polypropylene and thermoplastic olefin nanocomposites containing nanosilica. Polymer, 47(22), 7731-7739.

112. Kontopoulou, M., Liu, Y., Austin, J. R., & Parent, J. S. (2007). The dynamics of montmorillonite clay dispersion and morphology development in immiscible ethylene–propylene rubber/polypropylene blends. Polymer, 48(15), 4520-4528.

Assembly, elasticity and structures of clay nanoparticles trapped at the polymer-polymer interface*

4.1. Introduction

The ability of fine particles to stabilize fluid–fluid interfaces has attracted considerable attention since its discovery [1, 2]. Since then, the interfacial adsorption of micro- or nanoparticles has been widely exploited to control the phase morphology of low-viscosity emulsions, while less attention has been devoted to their high-viscosity counterparts, viz. immiscible polymer blends. Actually, the underlying physics does not depend on the nature of the fluids, which mostly dictate the timescales of the phenomena [3]. Nowadays, the ability of nano-sized particles in gluing polymer drops to form clusters, preserving non-spherical domains and promoting stable co-continuous morphologies in polymer blends is widely recognized [4]. As a result, the interest is now mainly directed towards the use of the filler as a clever tool for manipulating the blend morphology at the micron scale [5]. Governing the microstructure of polymers blends is highly attractive from a technological point of view. The reason is that the macroscopic properties of this class of materials are strictly related to the small-scale arrangement of the polymer phases [6]. The possibility of a fine tuning of the blend morphology is particularly intriguing in case of co-continuous polymer blends, in which the mutual interpenetration of the phases can result in a synergistic combination of the properties of the constituents. The addition of nanoparticles to co-continuous blends is known to be effective in suppressing phase coarsening [7-9], but the spectrum of possibilities offered by a clever use of the filler is actually much wider. Recently, the addition of nanoparticles to co-continuous blends has been ingeniously exploited to promote hierarchical structures [10], to enhance the heat deflection temperature of bio-based polymers [11], to improve the mechanical properties of engineering plastics [12], or to refine the dispersion of nanoparticles in polymer matrices [13]. Besides exploiting the ability of nanoparticles to alter the blend morphology, one can refer to the other side of the coin by profiting from the phase-separated morphology of the matrix to control the space arrangement of the filler. In principle, the continuous liquid-liquid interface can be used as a template for a controlled three-dimensional assembly of nanoparticles, opening new routes for a bottom-up material design. Some notable results have

---

* Part of the results presented in this chapter has been published in:
  - Filippone, G., Causa, A., de Luna, M. S., Sanguigno, L., & Acierno, D. (2014). Assembly of plate-like nanoparticles in immiscible polymer blends–effect of the presence of a preferred liquid–liquid interface. Soft Matter, 10(18), 3183-3191.
  - Altobelli, R., de Luna, M. S., & Filippone, G. (2017). Interfacial crowding of nanoplatelets in co-continuous polymer blends: assembly, elasticity and structure of the interfacial nanoparticle network. Soft matter, 13(37), 6465-6473.

been obtained in systems based on low-viscosity fluids [14-15], but a full understanding of the complex interplay between fluid evolution and nanoparticles self-assembly is still far from being reached, especially in the case of high viscosity polymer blends. An important step in this direction is due to Macosko and co-workers, who monitored in real time the interface dynamics in bicontinuous, interfacially jammed, emulsion gels (bijels) to access the changes in the interfacial particle coverage [16]. The authors shed light on the sequence of events that lead to the formation of the bijel, which results from the shrinking of the liquid-liquid interface until interfacial particle jamming. However, extending their conclusions to inherently immiscible blends of highly viscous polymers is not straightforward. Different scenarios are also expected when non-spherical particles are considered. Plate-like fillers, indeed, better adapt to the polymer–polymer interface and, if provided with sufficient bending stiffness, they can constrain the evolution of the fluid phases without the need of interfacial jamming, which is instead required for spheres. Moreover, the strength of the interfacial network of nanoparticles, ultimately responsible for the mechanical stability of the material in the melt state, has not been studied in detail.

In this work we address these issues, investigating the dynamics of assembly, the elasticity and the structure of interfacial networks of clay nanoplatelets in drop-in-matrix and in co-continuous blends of polystyrene (PS) and poly (methyl methacrylate) (PMMA). We use a combination of morphological and rheological analyses to investigate the assembly of particles using a reference system based on a pure PS matrix, to study altered dynamics of the interface, as a result of the organically-modified clay adsorption on the surface of the PMMA, trough the drop-matrix blend, to prove the generality of the mechanism of morphology stabilization by interfacial crowding of nanoparticles in the case of co-continuous systems, which keeps working in spite of the high viscosity of the liquid phases and the plate-like shape of the nanoparticles. The structure and stress-bearing ability of the resulting interfacial network of nanoparticles are investigated through a descriptive viscoelastic model that enables to isolate the elastic contribution of the nanoparticle network from that of the host matrix, both in the case of mono- and in the case of biphasic polymer matrix. Moreover, the effect of the co-continuous morphology of the host matrix is highlighted through a comparative analysis with systems in which the matrix is either a single polymer or a drop-in-matrix blend. This allows to emphasize the role of the multiphase nature of the host medium in driving the nanoparticle assembly. To sum up, we sought to assess how nanoparticles govern the blend morphology and how the structural evolutions of the fluids in turn dictate the space arrangement of the filler.
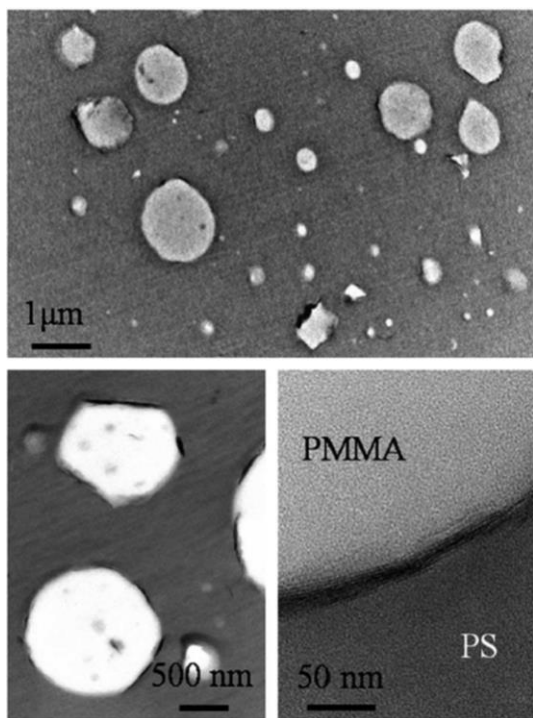
4.2. Experimental section

The polystyrene (PS, trade name Edistir® 2982, by Polimeri Europa) has glass transition temperature Tg=100°C, density ρ=1.04 g cm-3. The poly (methyl methacrylate) (PMMA, trade name Optix® CA-51, by Plaskolite, Inc.) has Tg=110°C, ρ=1.18 g cm-3. The filler is a montmorillonite modified with dimethyl dihydrogenated tallow quaternary ammonium salt (Cloisite® 15A by Southern Clay Products, Inc.), having organic content ~43 wt% and ρ=1.66 g cm-3. Previous studies showed that Cloisite® 15A accumulates at the polymer-polymer interface when dispersed in PS-PMMA blends [16].

Unfilled and filled PS/PMMA blends at 85/15 (*drop-in-matrix systems*) and 55/45 (*co-continuous systems*) weight ratio were prepared by melt compounding the constituents using a recirculating, conical twin screw micro-compounder (Xplore MC 15 by DSM). The polymers and the filler, dried overnight under vacuum at T=90°C, were loaded simultaneously in the mixing apparatus. The extrusions were performed at T=190°C in nitrogen atmosphere at a screw speed of 150 rpm. The residence time was about 5 minutes. The extrudate was granulated, dried again, and finally compression-moulded in the form of disks (diameter 40 mm, thickness ~1.5 mm) for the subsequent rheological and morphological analyses. The unfilled PS and PS/PMMA blend used as reference materials were processed in the same conditions. The particle loading was accurately estimated for each sample by means of thermogravimetric analyses (TGA, Q5000 by TA Instruments). Tests were carried out small pieces cut from the disks recovered at the end of rheological analyses. The samples were heated at 10°C min^{-1} in nitrogen atmosphere from room temperature up to T=700°C, and the residuals were recorded at T=600°C. The reported values of filler content, expressed in terms of percentage volume fraction of the inorganic fraction, Φ, are averages computed from three independent measurements. The morphology of the samples was investigated by means of electron microscopy. TEM analyses (Tecnai G2 Spirit Twin T-12 by FEI) were carried out to identify the space arrangement of the nanoplatelets. The samples were ~100 nm-thick slices randomly cut at room temperature from the disks used for rheological analyses by using a Leica EM UC7 ultra-microtome equipped with a diamond knife. SEM analyses (Quanta 200 FEG-SEM by FEI) were performed to study the morphology of the polymer phases. Before observations, the surface of the cryo-fractured samples was etched with formic acid to selectively remove the PMMA phase, and then coated with a 15-nm thick Au/Pd layer using a sputter coating system. The SEM micrographs were, in the case of co-continuous systems, analysed to get an estimate of the characteristic size of the PMMA phase, ξ, which was defined as 1/Q, where Q is the interfacial length per unit area. For each sample, several images at different magnifications were analysed by manually detecting the interfacial perimeter. Rheological tests were performed at T=215°C in dry nitrogen atmosphere using a stress-controlled rotational rheometer (ARG2 by TA Instruments) in parallel-plate configuration. The elastic (G') and viscous (G") shear moduli were collected by means of time and frequency scans. All the tests were performed at strain amplitudes low enough to be in the linear regime. The latter was evaluated for each sample through preliminary strain amplitude tests.

4.3. Effects of the nanoparticles on the blend microstructure

4.3.1. Drop-in-matrix systems

Wettability calculations (for details see Appendix B) and morphological analyses revealed the propensity of the clay to gather at the polymer–polymer interface. TEM micrographs of a representative as-extruded PS/PMMA/clay systems at filler volume fraction $\Phi=0.32\%$ are shown in Figure 1. Micrometric PMMA drops are suspended in the PS matrix. The clay is in the form of stacks of several silicate layers lying on the surface of the droplets. It is worth noting that the tactoids, which at this composition do not saturate the available polymer–polymer interface, do not bend to trace out the contours of the drops, being instead the latter, which adapt to the clay. In other words, the bending stiffness of the particles prevails over the interfacial tension and stabilizes non-spherical drops (Figure1). Similar localized variations in the mean curvature would require a surface completely covered with a jammed or crystalline layer of spherical particles [3]. Nano-sized particles are inclined to rearrange towards more stable configurations once the temperature is raised up above the melting/softening point of the host polymer matrix. The kinetics of such a process have been monitored looking at the time evolution of the linear

Figure 1.: TEM micrographs of the as-extruded PS/PMMA/clay sample at $\Phi=0.32\%$.

elastic modulus G′ at a frequency low enough to neglect the elastic contribution of the polymer matrix. The results of time scans at 190 °C and $\omega=0.1$ rad s^{-1} are shown in Figure 2 for PS/clay and PS/PMMA/clay samples at different filler content. The moduli have been divided by their initial value, G′(0). The viscous moduli, not shown, remain essentially stable over time. The elasticity of the PS/clay samples grows during time at any Φ. The growth rate is faster in the earlier stages, then the elasticity approaches a time-independent value, G′(∞). The normalized equilibrium moduli, G′(∞)/G′(0), gradually scale with Φ at low filler contents, then a kind of saturation is achieved (see inset of Figure 2a). Differently, the behaviour of the PS/PMMA/clay samples at Φ < 0.93% exactly retraces that of the unfilled blend. Only above this threshold the elasticity starts to grow over time. The sudden transition around $\Phi=1\%$ can be clearly appreciated in the inset of Figure 2b. The growth of elasticity at rest is a rheological fingerprint of nano-filled polymers. In the specific case of plane fillers, the

growth of G′ at very low Φ reflects the increasing effective volume of the particles, which rotate losing the alignment imposed by the squeezing flow experienced when loading the sample [17] An additional contribution arises at higher Φ because of particle flocculation, which causes polymer confinement and more intensive hydrodynamic effects. Moreover, above the percolation threshold, Φ_c, a space-spanning filler network eventually forms/restores, further increasing the overall elasticity. Each of the previous phenomena presume some mobility of the nanoparticles. For homogeneous suspending mediums, if the viscosity of the liquid phase is too high or the particles/ aggregates are too big, the filler mobility is frustrated, and the viscoelastic moduli remain stable during time [18]. For the PS/PMMA/clay samples, where the organo-clay is mostly trapped at the polymer–polymer interface, filler rearrangements, able to affect the macroscopic viscoelastic response, would imply energetically costly processes, such as a detachment of the particles from the interface or the dragging/deformation of the drops on which they are adsorbed. As a result, the particle mobility is frustrated and the viscoelastic moduli do not appreciably grow during time. Nonetheless, once the available interface is saturated

Figure 2.: Time evolution of G′ at ω=0.1 rad s^{-1} normalized over the initial value for: (a) neat PS (solid line) and PS/clay samples at Φ=0.07, 0.44, 0.60, 1.32 and 1.63% (from bottom to top); (b) unfilled PS/PMMA blend (solid line) and PS/PMMA/clay samples at Φ=0.32, 0.75, 0.93, 1.32 and 2.05% (from bottom to top). The normalized G′ at the end of time scans are shown in the insets as a function of Φ; semitransparent symbols correspond to the samples shown in the main plots.

the exceeding particles are free to rearrange in the host medium irrespective of its biphasic nature. The sudden switch in the ageing curves of Figure 2b suggests that such a saturation occurs at Φ=1%. The comparison between the TEM micrographs of two samples around this threshold shown in Figure 3 supports this conclusion. Bare or partially covered PMMA droplets can be noticed at Φ=0.75%. The covering is instead nearly complete in the sample at Φ=1.32%, whose drops appear more distorted because of the bending stiffness of the lamellae which tile their surface.

Figure 3.: TEM micrographs of the PS/PMMA/clay samples at (a) Φ=0.75% and (b) Φ=1.32%.

As most of the interface is saturated, unconstrained tactoids suspended in the continuous PS phase can be also noticed. It is worth noting that some of such free particles connect clay-coated drops or drop clusters.
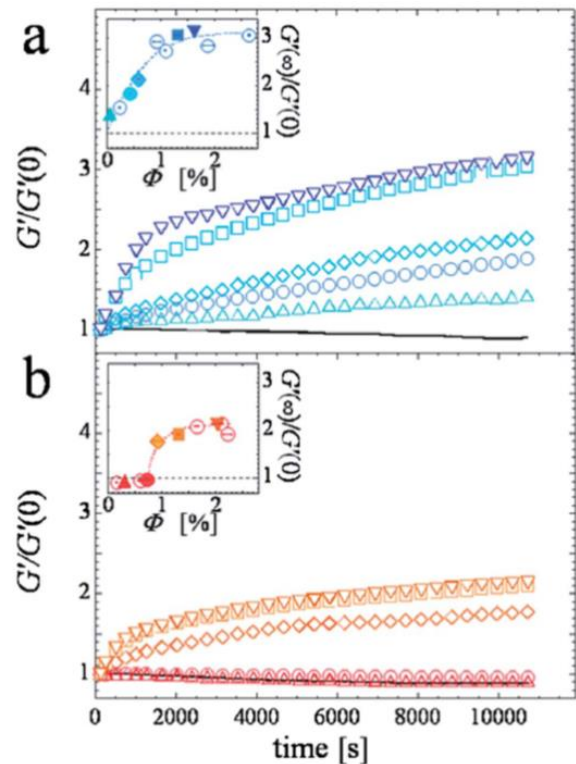
4.3.2. Co-continuous systems

With regard co-continuous systems, whole exhibit a co-continuous microstructure at the end of the preparation procedure. The morphology of a representative sample at $\Phi=0.22\%$ is shown in Figure 4. The characteristic size of the polymeric phases is of the order of few microns. The nanoclay is in the form of intercalated stacks lying at the PS-PMMA interface. The interfacial localization of the selected particles agrees with
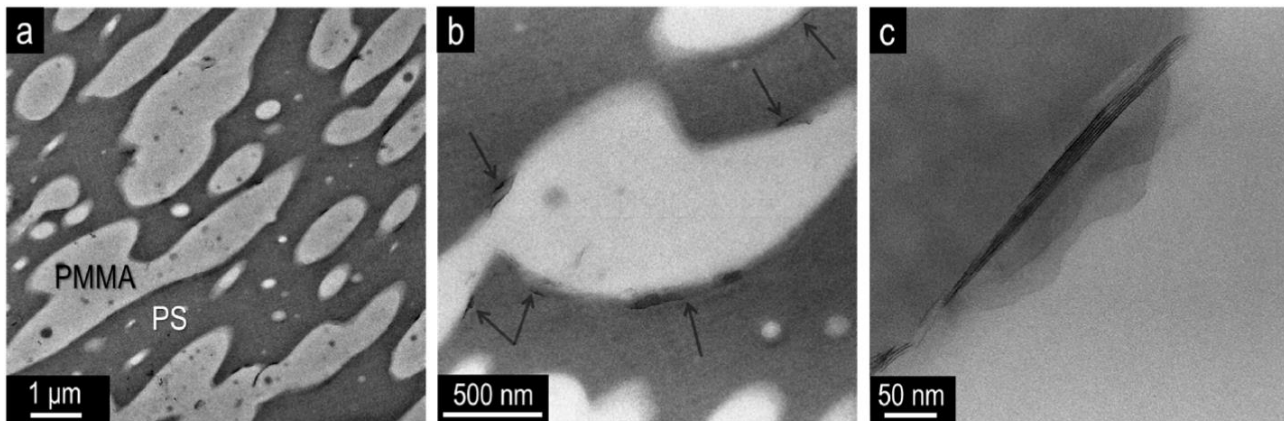

Figure 4.: TEM micrographs of the as-extruded blend at $\Phi=0.22\%$ at different magnifications. The bright and dark phases are PMMA and PS, respectively. The arrows in (b) indicate the clay lying at the polymer-polymer interface.

thermodynamic predictions based on wettability calculations (for details see Appendix B, Section B1). The presence of nanoplatelets accumulated at the polymer-polymer interface radically alters the coalescence (Figure 4), breakup and relaxation phenomena on the basis of the development of the microstructure in immiscible polymer blends [5].

The effect of the filler on the initial morphology of the blends is shown in Figure 5, where the average size of the PMMA domains in the as-prepared samples is reported as a function of filler content. The nanoparticles induce a drastic reduction of ξ, which falls to about one-seventh of its value in the unfilled blend by simply adding 0.22% of nanoclay to the initial polymer mixture. The effect rapidly decreases with Φ, and ξ approaches a limiting value <1 μm. Given that the lateral dimensions of montmorillonite-based nanoclays is of order of 0.5 μm, this value is in line with the prediction by Rafailovich and co-workers, who set that the minimum allowable domain size is of order of the lateral size of a nanoplatelet to avoid energetically unfavourable particle folding [19]. Nanoparticle-induced refinement is a well-known phenomenon in case of blends with drop-in-
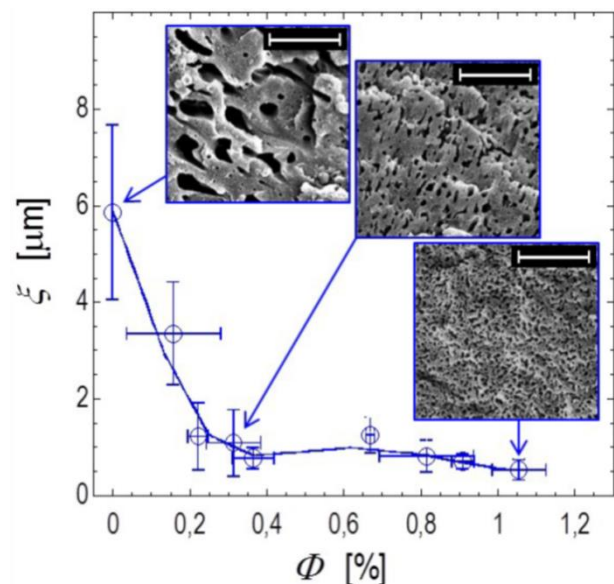

Figure 5.: Average size of the PMMA domains in samples at different filler contents before any thermal annealing treatment. The solid line is a guide for the eye. Representative SEM micrographs of selected as-prepared samples are shown as insets. The scale bars correspond 20 μm.

matrix morphology [5]. The most convincing arguments invoked to explain the phenomenon in case of interfacially-adsorbed plate-like nanoparticles are coalescence suppression and alteration of the interfacial rheology. The former mechanism assumes that nanoplatelets act as a physical barrier that prevents the direct contact between polymer domains during melt-mixing [20-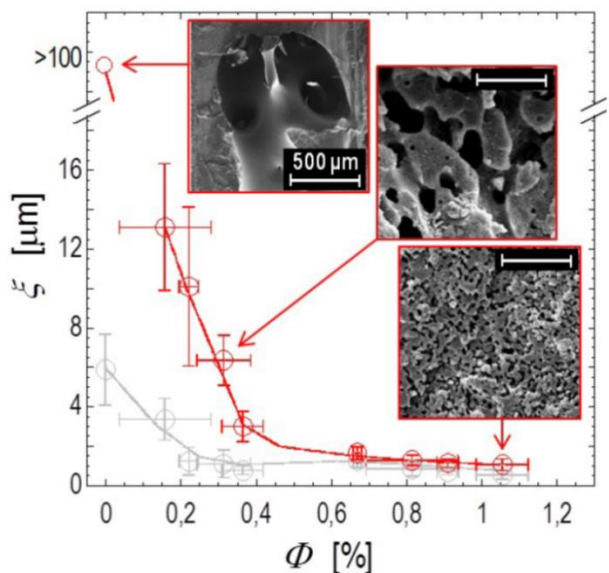21]. Regarding interfacial rheology effects, the nanoplatelets provide the interface with a marked viscous and elastic connotation, thus retarding the relaxation phenomena involved in the coarsening process in the melt state [22-23]. Despite the lack of focused studies, the previous mechanisms can be invoked also in case of melt-mixed co-continuous blends, whose microstructure stems from the same basic events occurring in blends with distributed morphology. Besides refining the initial morphology, interfacially-adsorbed nanoparticles are also known to stabilize the co-continuous microstructures against phase coarsening [7-9, 24-26]. The stabilizing action in the studied system is shown in Figure 6, where the average size of the PMMA domains in samples at different filler content is reported after a 3-hour annealing at T=215°C. Drastic phase coarsening occurs in the unfilled blend, whose polymer phases resulted completely segregated at the end of the annealing process. The presence of nanoparticles significantly stabilizes the morphology.

Figure 6.: Average size of the PMMA domains in samples at different filler contents after a 3-hour annealing at T=215°C. The data before annealing are also reported for comparison (semi-transparent symbols; same data as in Figure 5). Solid lines are guides for the eye. Representative SEM micrographs of selected samples are shown as insets. When not indicated, the scale bars correspond to 20 μm.

Two different behaviours can be recognized depending on the filler content. At Φ<0.67% the nanoparticles limit phase coarsening without arresting it, and their ability to do so is proportional to their content. The linear trend at 0.16≤Φ≤0.36% suggests a clever way to control the extent of interface, or equivalently the characteristic size of the polymer phases. The latter indeed can be finely tuned at the micron-scale by simply changing the particle loading and letting the blend to coarsen. Differently, at Φ≥0.67% full morphology stabilization is achieved irrespective of the filler content. Monitoring the viscoelastic moduli during annealing allows to shed light on the origin of morphology stabilization. We focus on G', which is strictly related to the extent and the elastic features of the polymer-polymer interface. The time dependence of G' is reported in Figure 7 for selected samples below and above the threshold that discriminates between partial (Φ<0.67%) and full (Φ≥0.67%) morphology stabilization. The G' of the unfilled blend decreases during time, eventually reaching a steady state value. The overall elasticity of polymer blends reflects the elasticity of constituents, which is stable in the investigated time window, plus an extra contribution stemming from the polymer-

polymer interface. The interfacial tension drives the system towards morphologies characterized by lower interfacial area. As the latter shrinks, the interfacial contribution decreases along with G'. We now consider the filled blends. At $\Phi \geq 0.67\%$, i.e. when the morphology is stable over time, a rapid growth of G' is observed in the early stages of the tests, then the modulus slowly approaches a steady value. Such a behaviour is well known in single-polymer nanocomposites, whose elasticity increases at rest due to space rearrangements of the filler [27]. Now consider the partially stabilized samples at $\Phi < 0.67\%$. At $\Phi = 0.16$ and 0.22%, G' decreases in the very early stages of the test, and then it starts

Figure 7.: Time dependence of the elastic modulus at $\omega=1$ rad s^{-1} for the unfilled blend (solid line) and filled blends at $\Phi=0.16$ (circles), 0.22 (diamonds), 0.67 (squares), and 0.91% (crosses).

growing. The higher the Φ, the lower the time required for the inversion of the sign of $\partial G'/\partial t$. The behaviour of these partially stabilized samples reminds that of polymer bijels based on spherical particles.16 Bijels are non-equilibrium structures which form due to the jamming of colloidal particles at the interface between two partially miscible low-viscosity fluids that undergo spinoda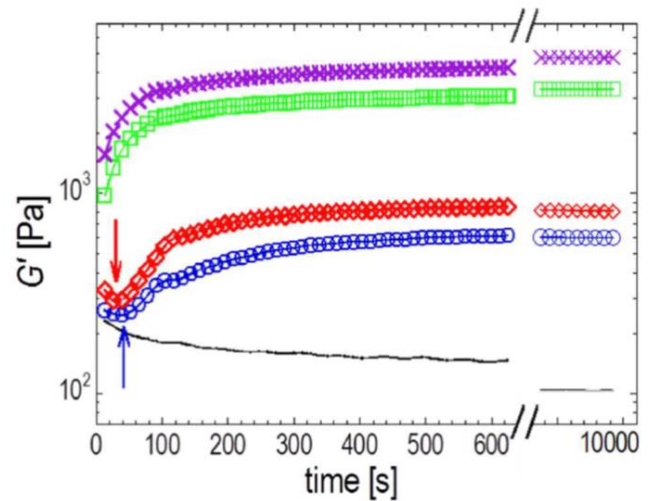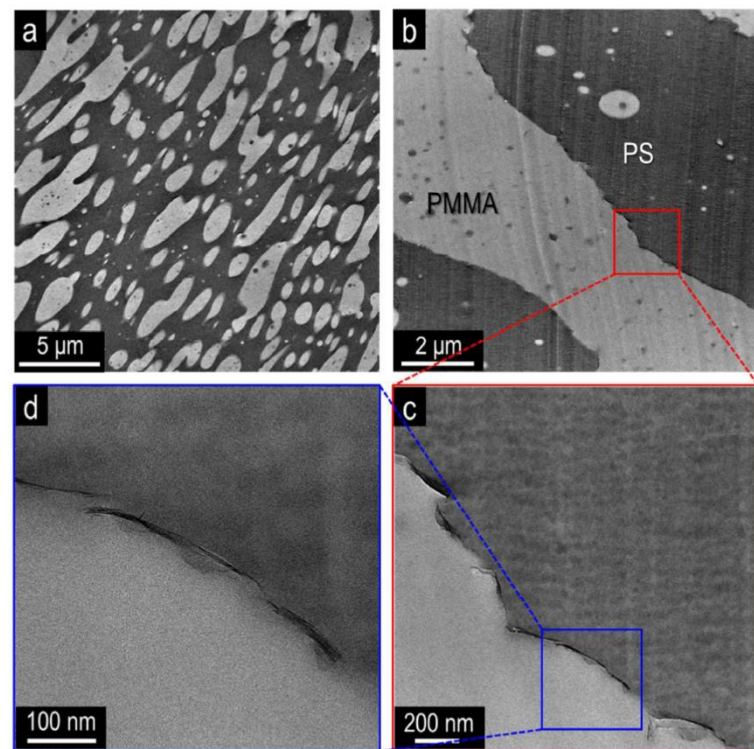l decomposition [28-29]. In such systems, the sequence of decrease and growth of G'(t) reflects the succession of interfacial shrinking and particle jamming at the liquid-liquid interface. Here, the liquids are inherently immiscible highly viscous polymers, and the particles are flexible plate-like nanoclays. Despite these substantial differences, the rheological analysis indicates that the mechanism of morphology stabilization is the same. The TEM micrographs of Figure 8 also support this conclusion. The morphologies of the sample at $\Phi=0.22\%$ before and after the thermal annealing are compared. The nanoclays, which initially lye on distinct points of the polymer-polymer interface (Figure 8.a; see also Figure 4.b), at the end of the annealing result well aligned along

Figure 8.: TEM micrographs showing the microstructure of the sample at $\Phi=0.22$ vol%: (a) as-prepared; (b-d) after 3-hours annealing at T=215°C. The bright and dark phases are PMMA and PS, respectively.

the contours of the residual interface (Figure 8.b-d). High magnification micrographs exclude significant

overlapping of the nanoplatelets, which rather seem to touch each other edge to edge. In this configuration, hydroxylated interactions establish between contiguous nanoplatelets [30], which form a superstructure that spans over the entire polymer-polymer interface. Further phase coarsening is hindered as it would imply energetically costly processes, such as detaching of the particles from the interface, bending of the clay stacks, or disruption of the network. The degree of morphology stabilization increases with the extent of coverage of the initial polymer-polymer interface. When the filler content is high enough, the particles saturate the initial interface and the morphology cannot evolve during time. According to Figure 6, this condition is achieved at some Φ between 0.36 and 0.67%. The morphology of the as-prepared sample at Φ=0.67% is shown in Figure 9. The particles indeed cover the entire initial interface, confirming that interfacial saturation is the requisite to achieve full morphology stabilization. Alternatively,
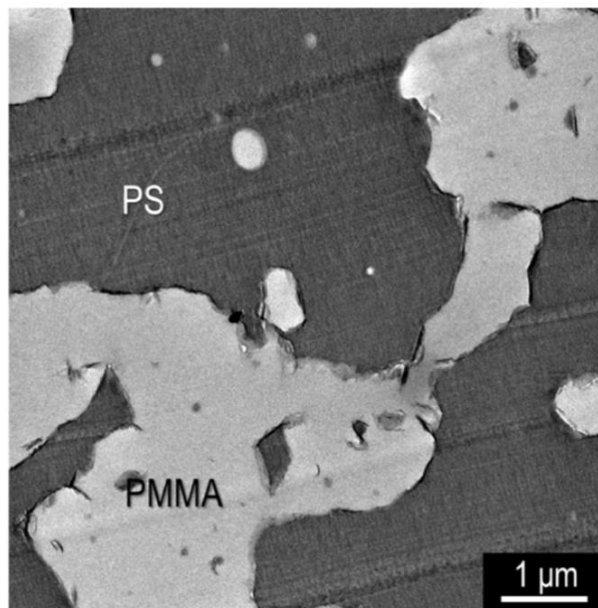

Figure 9.: Microstructure of the as-prepared sample at Φ=0.67%.

phase coarsening proceeds until the strength of the interfacial structure induced by the crowding of nanoclays offsets the interfacial tension. The stress-bearing ability of the interfacial network, ultimately responsible for the stability of the co-continuous structure, is studied in the next section through viscoelastic analysis.

4.4. Elasticity of the interfacial particle network

4.4.1. Drop-in-matrix systems

At the end of the time scans the linear viscoelastic moduli are stable enough to perform reproducible frequency scan experiments. The frequency dependence of the elastic moduli is shown in Figure 10 for the PS/clay and PS/PMMA/clay samples at different Φ. The neat PS is predominantly viscous throughout the investigated frequency range. The continuous PS phase governs the high-frequency behaviour of the unfilled PS/PMMA blend, whereas the enhanced elasticity at low frequency reflects the shape relaxation of the PMMA droplets. The clay radically affects the relaxation spectra of both systems. The effect is qualitatively the same: a slight increase of the moduli occurs at high frequency, the overall shape of the curves remaining essentially unaltered; over longer timescales the filler gradually slows down the relaxation dynamics. The flattening of G′ at low frequency reflects a gradual transition from liquid- (G″ >> G′) to solid-like behaviour (G′ > G″, weak ω-dependence). It is important to observe that the filler has a negligible effect in the PS/PMMA/clay samples up to Φ=0.61%. Only above this composition, which is close to the threshold above which the elasticity starts to
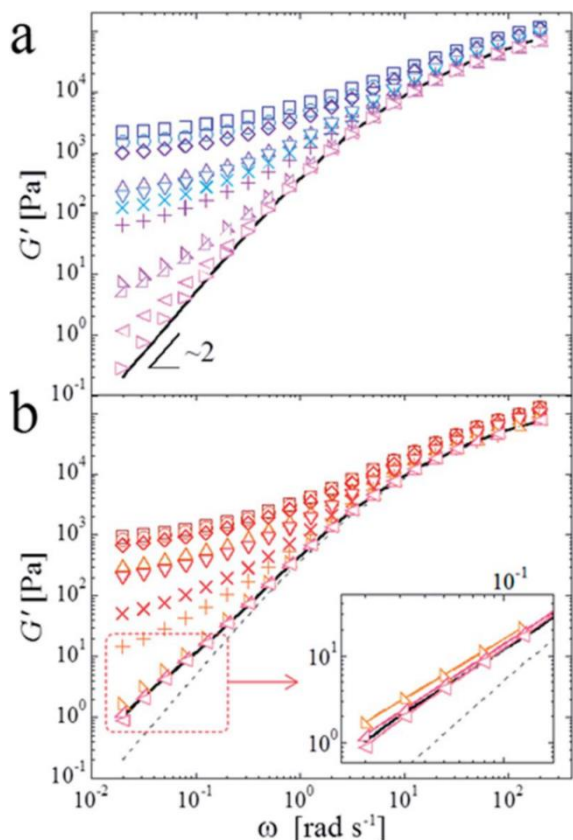
Figure 10.: Frequency dependence of the elastic moduli: (a) neat PS (solid line) and PS/clay samples at Φ=0.07%, 0.25%, 0.44%, 0.60%, 0.94%, 1.10%, 1.27%, 1.32%, 1.63%, 1.89% and 2.65% (bottom to top); (b) unfilled blend (solid line), neat PS (dotted line) and PS/PMMA/clay samples at Φ=0.18%, 0.32%, 0.61%, 0.75%, 0.93%, 1.32%, 1.66%, 2.05%, 2.12%, 2.24% (bottom to top).

increase over time (see Figure 10b), G′ begins to flatten out, reaching a low-frequency plateau at the highest filler contents. In other words, the particles trapped at the polymer–polymer interface and, hence, devoid of sufficient mobility in the melt are not able to appreciably alter the overall viscoelasticity imparting solid-like features to the matrix. On the other hand, after the constraint represented by the interface has been saturated, the particles can assemble into superstructures reminiscent of those that are formed in a homogeneous matrix. The TEM micrographs of two samples at Φ high enough to result in a comparable low-frequency plateau of the elastic modulus are compared in Figure 11. The tactoids are randomly suspended in the host matrix in the PS/clay sample. The considerable lateral dimension of such structures is due to hydroxylated edge–edge interactions between silicate layers [30]. The random assembly of the clay results in micron-sized flocs, which in turn assemble into a three-dimensional network that spans large sections of the sample. Larger portions of matrix are devoid of clay in the PS/PMMA/clay sample. Most of the particles either adhere at the surface of the drops, which hence assume highly irregular shapes, or are trapped within drop clusters. Nonetheless, looking at higher magnifications long-range connectivity of the particles can be noticed also in the PS/PMMA/clay sample. The main difference with the PS/clay system is that in this case the particle flocs embed the PMMA domains.

Aiming at isolating the contribution of the nanoparticles from that of the matrices, we refer to a simple two-phase model which has proved to satisfactorily describe the linear viscoelasticity of homopolymer-based nanocomposites above Φ_c [31]. The coexistence of two independent populations of dynamical species is assumed: (i) a fraction of free polymer, whose dynamics are not affected by the filler, and (ii) a three-dimensional network based on flocs of nanoparticles. The polymer phase accounts for the viscous feature of the nanocomposite, whereas the network-phase is the only responsible for the marked elasticity emerging at low frequency. When the suspending medium

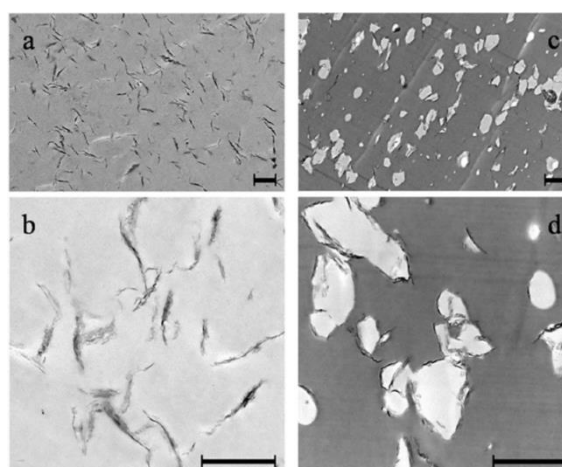**Figure 11.:** TEM micrographs of the samples at Φ=1.32%: (a and b) PS/clay and (c and d) PS/PMMA/clay. Scale bars are 1 μm.

is a biphasic fluid, an additional contribution arises at low frequency because of the interfacial elasticity. However, as inferable from Figure 10, the latter is not so important to invalidate the assumption that the network-phase encompasses the entire elasticity of the nanocomposite. Hence, the $G'(\omega)$ curves of blends at different $\Phi > \Phi_c$ can be scaled on a single master curve, and the elasticity of the filler networks can be precisely estimated and studied apart. The step-by-step procedure for scaling the G' curves is described in detail elsewhere [32] and it is reported here as Appendix B. The key steps for identifying the horizontal (a_Φ) and vertical (b_Φ) shift factors are summarized in the Appendix B. These shift factors have a precise physical meaning: a vertical shift factor, b_Φ, which represents the Φ-dependent network elasticity, and an horizontal shift factor, a_Φ, which is the frequency that separates the regime in which the behaviour is dominated by the particle network ($\omega < a_\Phi$) to that in which the polymer governs the macroscopic response ($\omega > a_\Phi$). The resulting master curves of the PS/clay and PS/PMMA/clay systems are shown in Figure 12. In both systems, the collapse of the moduli is satisfactory over about three decades of low scaled frequencies, which demonstrates the effectiveness of the two-phase model even in the case of biphasic polymer matrices. The non-superposing tails at high dimensionless frequency ω/a_Φ reflect the dynamics of the unfilled matrices, so their presence does not compromise the overall quality of the scaling. Surprisingly, the two systems approach the plateau at low ω/a_Φ following the same trend (see inset of Figure 12). At $\omega/a_\Phi \gg 1$ the behaviour is governed by the polymer-phase. Since the fastest relaxation modes of the
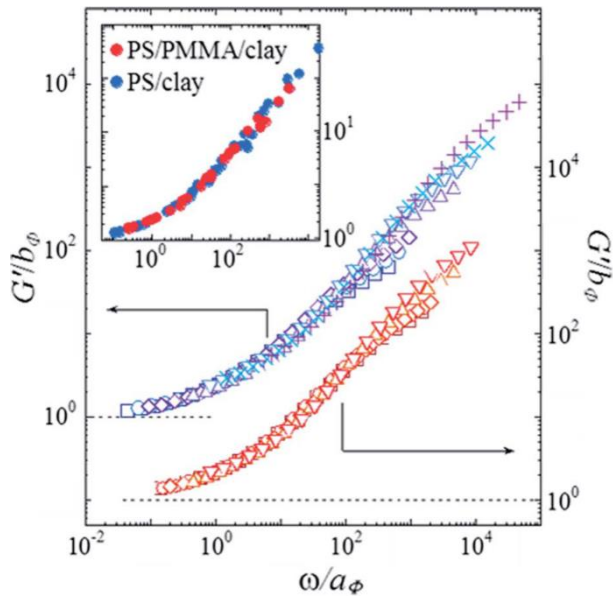

Figure 12.: Master curves of G' for the PS/clay (upper curve, left axis) and PS/PMMA/clay systems (lower curve, right axis). Symbols are the same as in Figure10. The inset shows a detail of the overlay of the two master curves; only one of three points is reported.

PS/PMMA blend are essentially those of its predominant PS phase, the overlay at high ω/a_Φ is not unexpected. The superposition at $\omega/a_\Phi \sim 1$ is more surprising. In this intermediate frequency range, the network and polymer-phase equally contribute to the system elasticity. Actually, the contributions of the two phases are not merely additional. Moreover, the polymer-phase of the PS/PMMA/clay system exhibits an additional elastic connotation due to the polymer–polymer interface. The complex interplay among the various sources of elasticity makes it difficult to discern the various contributions. Nonetheless, the main elastic features of the filler network prescind from the presence of PMMA drops embedded in it. As for the PS/clay system, the structure of the particle network in PS/PMMA/clay samples can be hence studied using the same approaches employed for particulate gels in homogeneous fluids.

4.4.2. Co-continuous systems

Rheological analysis, as in the previous case, provides valuable information on the elasticity and structure of percolating networks of nanoparticles embedded in host polymer matrices. Small amplitude frequency scans were performed at the end of time sweep experiments, i.e. when the interfacial network of nanoparticles was formed and the blend morphology was fully evolved. The dynamic moduli are shown in Figure 13. The unfilled blend exhibits the typical behaviour of co-continuous blends, characterized by a deviation from the terminal behaviour of single phase polymer melts ($G'(\omega \to 0) \sim \omega^2$ and $G''(\omega \to 0) \sim \omega^1$). In particular, the low-frequency elastic modulus scales with frequency as $G' \sim \omega^{0.7}$, while the effect on G'' is negligible. We now focus on the effect of the nanoparticles. Hereinafter we restrict our attention to G', which is much more sensitive than G'' to the presence of the filler. The nanoclays at the polymer-polymer interface cause a remarkable increase of G' at low frequency. The scaling law remains power law-like, but the exponent α decreases with filler content, becoming negligible at $\Phi \geq 0.67\%$ (see inset of Figure 13.a). This behaviour reminds that of nanocomposites based on single polymer matrix, whose relaxation dynamics arrest above the filler percolation threshold, Φ_c. In such conditions, the behaviour of the nanocomposite is dominated by the elastic particle network, and a descriptive two-phase model, as above mentioned, can be used to isolate its contribution and studying it separately [31]. The two-phase model, as we have seen, was already proved to be able to describe the viscoelasticity of a wide variety of polymer nanocomposite [31] including polymer blends with drop-in-matrix morphology [27]. Here we exploit it to isolate the contribution of the interfacial particle network from that of the host matrix. Such an approach is essential in the case of co-continuous blends, whose inherent elasticity could mask that of

Figure 13.: Elastic (a) e viscous (b) modulus as a function of frequency for the unfilled blend (solid line) and the filled samples at Φ=0.06 (plus), 0.16 (cross), 0.22 (right arrow), 0.31 (left arrow), 0.36 (reverse triangle), 0.67 (triangle), 0.81 (diamond), 0.91 (square), and 1.06% (circle). The inset in (a) shows the power-law exponents of the low-frequency dependence of the moduli.

the nanoparticles at low filler contents. To face this problem, first we build the master curve of G' starting from the samples at high filler contents, for which the network elasticity can be clearly identified (here the samples at $\Phi \geq 0.67\%$). Once the master curve is available, we scale on it the G' curves of the samples at lower Φ (for
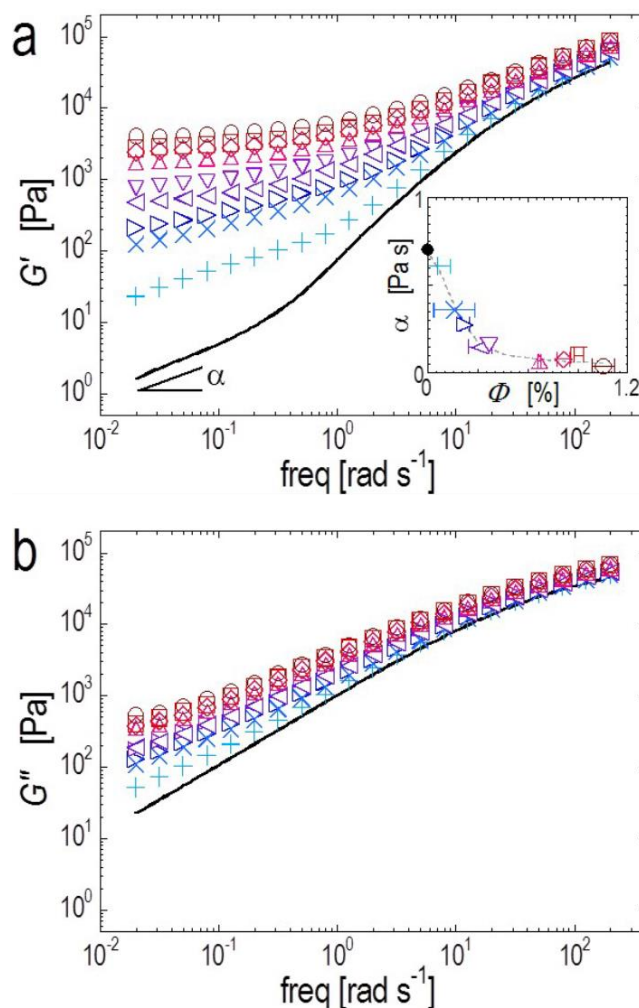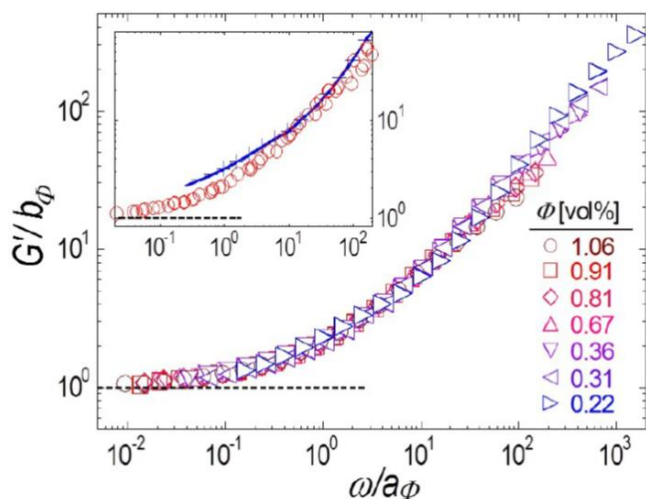
Figure 14.: Master curve of G' built by scaling the G' curves of samples at Φ≥0.22% (see Appendix B). Symbols and colours are the same as in Figure 13. The inset shows the non-scalability of the curve at Φ=0.16% (cross) on the master curve obtained from all the samples at Φ≥0.22% (circles).

details see Appendix B, Section B2). The resulting master curve is shown in Figure 14. The building of the master curve also allows to confidently identify all the samples above Φ_c. This can be done considering that the strict interrelationship between the horizontal and vertical shift factors implies the impossibility of scaling G' curves of samples below Φ_c unless violating the physical constraints of the two-phase model [34]. As a result, Φ_c can be sought in the Φ-range between the last non-scalable curve and the first scalable one. The overlay of the scaled G' curves of samples at Φ≥0.22% is excellent, while the G' curves of samples at Φ<0.22% are not scalable (see inset of Figure 14). Accordingly, the Φ_c of our system falls between 0.16 and 0.22%. The estimate

of Φ_c is carried out in the next Section. Here we limit the attention to the samples at Φ≥0.22%, whose scaled G' curves nicely overlap revealing the relaxation dynamics of the interfacial network of nanoparticles.

Remarkably, the master curve is perfectly superimposed to those obtained in a previous work [27] for systems based on the same polymers and nanoparticles as used here, but in which the matrix was either pure PS or a PS/PMMA blend with drop-in-matrix morphology (Figure 15). This means that the way in which the relaxation dynamics arrest because of the filler network does not depend on the microstructure of the host matrix. Nevertheless, in the next Section we show that the morphology of the matrix is crucial in determining the space arrangement of the nanoparticles within the network, substantially affecting its structure and elastic properties.

Figure 15.: Overlay of the master curve of G' of the co-continuous samples studied in this work (full circles) and those of samples based on pure PS (empty triangles) and on PS/PMMA blend (85/15 wt/wt) with drop-in-matrix morphology (empty diamonds) taken from ref. 27.

4.5. Percolation approach and structure of the interfacial particle network

4.5.1. Drop-in-matrix systems

In particular, a quantitative comparison between the structures of the networks which form in the mono- and biphasic matrices can be performed by referring to the percolation theory. The latter predicts the network

Figure 16.: Power-law dependence of the network elasticity on the reduced filler content for the PS/clay (blue) and PS/PMMA/clay system (red). Symbols are the same as in Figure 10.

Table 1.: Percolation thresholds and fitting parameters of the percolation law $G_0{'} \sim (\Phi - \Phi_c)^\nu$

	Φ_c [%]	k [Pa]	ν
PS/clay	0.76	656±26	2.34±0.36
PS/PMMA/clay	0.95	457±5	1.73±0.17

elasticity to grow with Φ as $G_0{'} \sim (\Phi - \Phi_c)^\nu$, the exponent n being related to the stress bearing mechanism [35]. To precisely identify the percolation threshold, the previous equation is fitted to the experimental data of $G_0{'}$ for different possible values of 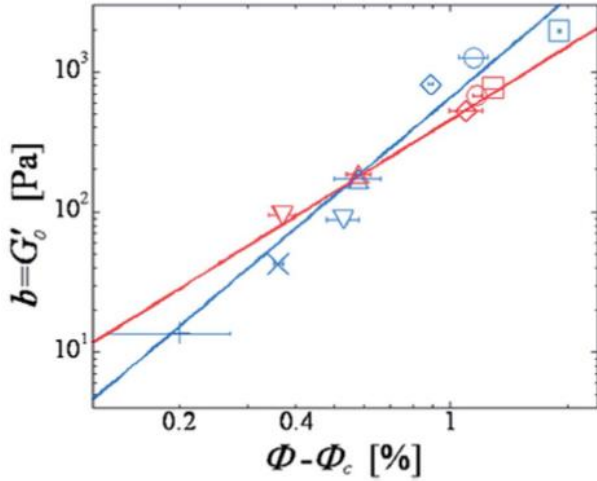Φ_c. The percolation threshold is thus taken as the one that returns the highest regression coefficient R^2. The advantage of using the two-phase model is double: first, the Φ_c can be sought in a restricted composition range, whose inferior limit is the highest Φ of the non-scalable G′ curves; second, the values of $G_0{'}$ to be fitted can be accurately estimated even for samples whose network is too weak to cause the actual arrest of the relaxation dynamics. In similar cases $G_0{'}$ is usually conjectured presuming a plateau value of G′ at frequencies much lower than those actually investigated. Such an extrapolation procedure, however, may result in non-trivial errors in the estimation of both Φ_c and ν. Any conjecture can be avoided by referring to the master curve, whose vertical shift factors b_Φ exactly correspond to the network elasticity $G_0{'}$ [34]. The results of the fitting procedure are shown in Figure 16, and the corresponding parameters are summarized in Table 1. The higher value of Φ_c found for the PS/PMMA/clay system is ascribed to the PMMA drops, which gather the tactoids and restrict their allowed space configurations. It is worth noting that the percolation threshold of the blend approximately coincides with the critical filler content above which the elasticity of the samples begins to increase over time (see Figure 2b). Such a finding upgrades the picture emerged from the analysis of the time sweep experiments: after the polymer–polymer interface has been saturated, the added particles possess sufficient mobility to rearrange in the reduced volume outside the coated drops, easily connecting them to form a spaces-panning filler network that embeds the PMMA phase. Concerning the critical exponents, both systems exhibit values of ν consistent with a number of previously characterized polymer nanocomposites [31] the filler network. Valuable information about this matter can be gathered considering that the stress transfer takes place across an elastic backbone of particle aggregates.

4.5.2. Co-continuous systems

The elasticity of particle networks just above Φ_c scales with filler content as $G'_0 = k(\Phi - \Phi_c)^\nu$, as above mentioned, where k is a measure of the strength of the network (k=G'_0 at $\Phi - \Phi_c = 1$), and ν is a constant related to the stress

bearing mechanism [31]. The low-frequency plateau of the G′ curves provides a rough estimate of the network elasticity, since G′$_0$=G′(ω→0). Rather than using extrapolation procedures, here we refer to the vertical shift factors used to build the master curve of Figure 14, which represents the network elasticity. Plotting b$_\Phi$ versus the reduced filler content, Φ-Φ$_c$, and fitting a power-law to the data provides a reliable estimate of Φ$_c$ as the value that returns the highest regression coefficient [32]. The result of this procedure is shown in Figure 17. The best power-law fitting to the experimental data (full circles) was obtained by setting Φ$_c$=0.17%, which leads to k=3779 ± 660 and ν=1.09 ± 0.29. Datasets and fitting lines are shown in Figure 17 for comparison with PS and a drop-in-matrix PS/PMMA blend (85/15 w/w). The fitting parameters of the three systems are summarized in Table 2. The comparison enables us to elucidate the role of the matrix in dictating the space arrangement of the nanoparticles. The value of Φ$_c$ found in case of co-continuous matrix is considerably lower than that obtained when the
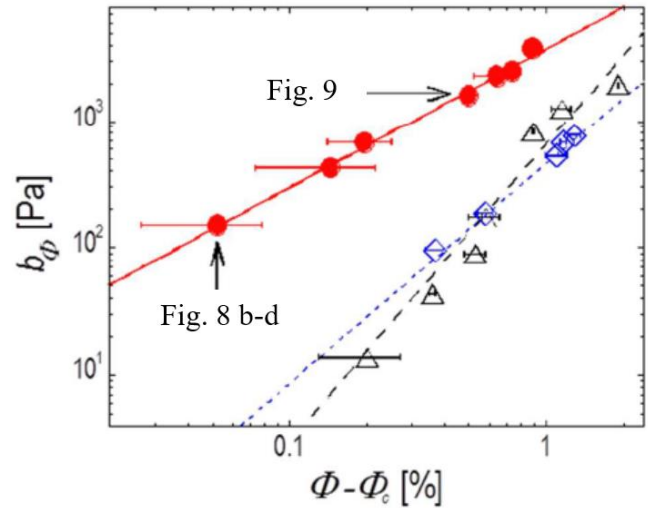

Figure 17.: Network elasticity as a function of reduced filler content (full circles) and power-law fitting to the experimental data (solid line). The data and corresponding fitting lines for systems based on pure PS (empty triangles) and a PS/PMMA blend (85/15 wt/wt) with drop-in-matrix morphology (empty diamonds) are reported for comparison (data from ref. 27).

Table 2.: Percolation thresholds and fitting parameters.

Matrix	Φ$_c$ [%]	k [Pa]	ν
Co-continuous blend (this work)	0.17	3779 ± 660	1.09 ± 0.29
Single polymer (pure PS)	0.76	656 ± 26	2.34 ± 0.36
Drop-in-matrix blend (PS/PMMA 85/15 w/w)	0.95	457 ± 5	1.73 ± 0.17

particles are dispersed in pure PS, which in turn is lower than that in the PS-PMMA blend with drop-in-matrix morphology. The previous ranking can be easily explained by accounting for the inclination of the nanoplatelets to gather at the polymer-polymer interface: when the blend exhibits co-continuous morphology, the particles are forced to align along a continuous path, thus percolating at low contents; in contrast, when drop-in-matrix blends are considered, the nanoplatelets accumulate in the proximity of isolated domains, and higher amount of particles are required to generate a continuous path [27]. Now we consider the elastic features of the interfacial network of nanoparticles which forms in the co-continuous blend. The data in Figure 17 and Table 2 reveal that the strength of the network in the co-continuous matrix is significantly higher than that of the networks that the same nanoparticles form in pure PS or in the blend with drop-in-matrix morphology. The difference is particularly pronounced at low reduced filler content. This experimental evidence can be explained in the light of the different structures of the networks in the three systems. Schematics inspired by the TEM analyses carried out here and in ref. 27 are shown in Figure 18.a. In the co-continuous blend, large volumes of sample are precluded to the particles, which are forced to lie on the

polymer-polymer interface. Such a configuration minimizes the probability of isolated nanoparticles and agglomerates, which are not effective in bearing the stress. In addition, strong edge-to-edge interactions are

predominant respect to the case of homogeneous PS matrix or in blends with drop-in-matrix morphology (Figure 18.a vs. Figure 18.b or c). On the other hand, the comparison between the critical exponents ν reveals that an incremental addition of nanoparticles above Φ_c has a minor effect in case of co-continuous matrix. To investigate the strengthening mechanism of the interfacial network with the increase in filler content, we refer to the expression of the elastic modulus of a nanoplatelet-coated polymer-polymer interface of a co-continuous blend, $G'_{int,}$ derived by Macosko and co-worker [36]:

$$G'_{int} = \frac{C \cdot K_{int}}{t^m} \cdot \frac{t^w}{\xi} \tag{4.1}$$

where C is a constant, K_{int} is the compressive modulus of the particle monolayer from interfacial rheology, t^w, is the average thickness of the walls of the filler network, and t^m is the thickness of the particle monolayer. According to Eq. 4.1, the strengthening of the interfacial network arises from the increase of the ratio t^w/ξ. Since in the studied systems ξ rapidly approaches a limiting lower value (see Figure 6), we conclude that the network strengthens with Φ mostly because of a thickening of the network branches. To test this hypothesis, the distributions of the thicknesses of the network walls were estimated for two samples at low and high filler content, and the calculated values of t^w were used to derive the theoretical values of the network
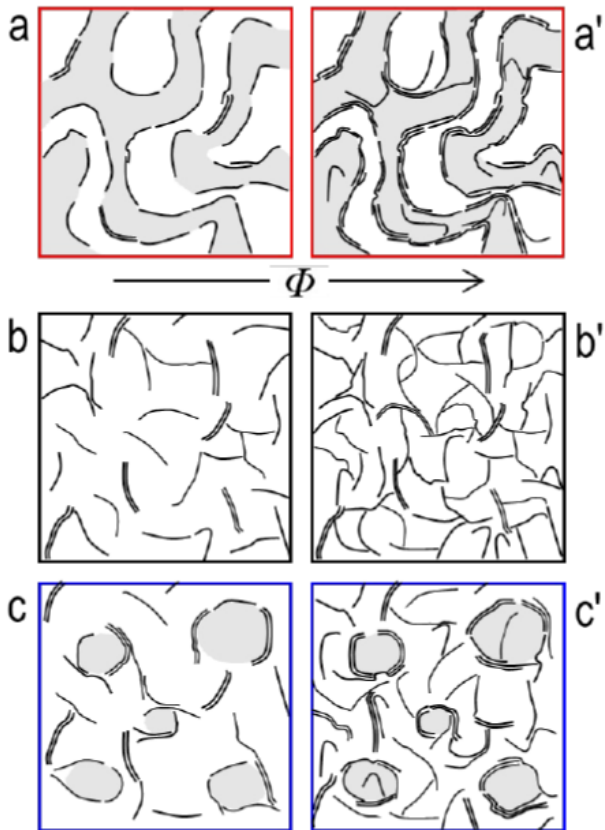

Figure 18.: Sketches showing the space arrangement of the filler in the co-continuous blend (a, a'), homogeneous matrix (b, b') and drop-in-matrix blend (c, c').

strength by means of Eq. 1 (calculations are provided as Appendix B, Section B3). The results summarized in Figure 19 confirm that the average thickness of the interfacial structure increases from $t^w \sim 9$ nm ($\Phi=0.22\%$) to $t^w \sim 14$ nm ($\Phi=0.67\%$); and the excellent quantitative agreement between calculated and experimental values of G'int (inset of Figure 19) corroborates the robustness of our analysis. If the interfacial network in the co-continuous matrix
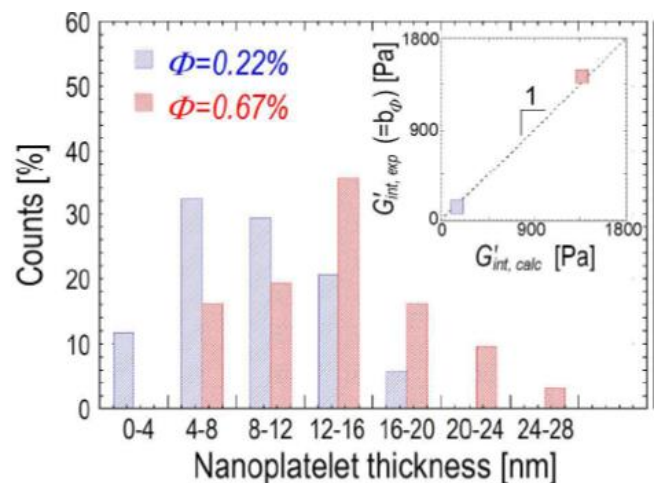

Figure 19.: Size distribution of the wall thickness of the nanoplatelet network in the co-continuous blends filled at $\Phi=0.22\%$ and 0.67%. The experimental value of the elasticity of the interfacial network ($G'_{int, exp}$) is reported in the inset as a function of the value calculated via Eq. 4.1 ($G'_{int, calc}$).

mainly strengthens due to the thickening of its branches (Figure 18.a vs. 18.a'), the reinforcing mechanisms is different when the host matrix is a single polymer phase. In this case, the added particles are free to randomly insert themselves into the preexisting network due to the absence of a preferred polymer-polymer interface. As a result, each incremental addition of particles potentially generates new effective particle-particle contacts (Figure 18.b vs. 18.b'). This increases the stress bearing ability of the network, reflecting in a high value of ν. It is not surprising to find out that the blend with drop-in-matrix morphology, in which a fraction of ineffective particles accumulates in the proximity of isolated droplets, places between the two extremes of single matrix and co-continuous blend (Figure 18.c vs. 18.c').

4.6. Conclusions

The assembly of clay nanoparticles in a PS/PMMA immiscible blend has been studied combining morphological investigations and rheological analyses. The use of a reference system based on pure PS allowed to highlight the effect of a polymer–polymer interface on the dynamics and structures of the filler in the melt. In particular:

- *Drop-in-matrix systems,* in this case particles adhere on the surface of the PMMA drops. As a result, flocculation phenomena are hindered and the viscoelastic behaviour of the blends at low filler content is not affected by the particles. Once the available polymer–polymer interface has been saturated, any further addition of particles causes an increase of elasticity during time, which reflects the rearrangement of the lamellae in the melt and their eventual assembly in a space-spanning network. The marked elastic connotation of such a superstructure exceeds the interfacial contribution of the drops, and the viscoelasticity of the filled blend can be described irrespective of the presence of the dispersed polymer phase. In particular, a simple viscoelastic model recently proposed for homopolymer-based nanocomposites has been successfully employed to study the Φ-dependent elasticity of the particle network. The filler percolation threshold in the polymer blend, assessed through the percolation theory as in the case of monophasic matrices, was slightly higher than in the neat PS. More exactly, the Φ_c coincides with the filler content above which the sample elasticity starts to increase over time, confirming the absence of flocculation of the particles trapped at the drop surface. The particle network in the blend exhibits a peculiar structure, which embeds and connects single and clustered clay-coated PMMA drops.

- *Co-continuous systems,* in this case the effect of small amounts ($\Phi \leq 1.06$ vol%) of nanoclay was studied. The filler selectively locates at the polymer-polymer interface, thus promoting a drastic decrease of the characteristic size of the polymer phases in the as-prepared samples. The extent of refinement is proportional to the filler content at low filler amount ($\Phi \leq 0.36\%$), while further additions of particles have a negligible effect on the size of the polymer phases. On the other hand, the refinement induced at $\Phi \leq 0.36\%$ is not permanent, and these samples experience noticeable phase coarsening during annealing at high temperature (T=215°C). In contrast, full morphology stabilization was found at $\Phi \geq 0.67\%$. A combination of rheological and morphological analyses proves that phase coarsening

takes place in the very early stages of the annealing, eventually causing the interfacial crowding of the nanoparticles. The resulting interfacial structure prevents from further evolution of the polymeric domains. The full morphological stability achieved in the samples at higher filler contents ($\Phi \geq 0.67\%$) originates from the saturation of the entire polymer-polymer interface in the as prepared samples. The structure and elasticity of the interfacial network of nanoparticles were investigated by means of linear viscoelastic analysis. The contribution of the filler network was isolated by exploiting a descriptive two-phase model. The relaxation dynamics of the interfacial network of nanoparticles were found to be very similar to those of reference systems based on pure PS and a PS/PMMA blend with drop-in-matrix morphology. On the other hand, the structure and elasticity of the particle network in the co-continuous blend are noticeably different from those of the reference systems. In particular, the selective accumulation of the particles at the polymer-polymer interface results in lower filler percolation threshold ($\Phi_c = 0.17\%$) and higher overall elasticity. Both results are a direct consequence of the peculiar space arrangement of the filler, whose alignment along the continuous polymer-polymer interface minimizes the probability of isolated particles and promotes strong edge-to-edge interactions. At the same time, the confinement of the nanoparticles brings about a low sensitivity of the network elasticity to the filler content. Indeed, once the interface is saturated there is no way to accommodate additional particles, which accumulate and form thicker branches without effectively contributing in strengthening the pre-existing network.

Appendix B

B.1. Predictions for filler localization: wetting and spreading coefficients

Considering all the lamellar fillers, organo-modified montmorillonites (Cloisite® 15A) has been selected through thermodynamic considerations based on the comparison among the interfacial tensions, γ_{ij}, between the constituents of the nanocomposites based on the biphasic matrix. The wettability parameter, ω_{12}, which represents the ability of the filler phase "*F*" to be wetted by components "*1*" and "*2*", is defined as:

$$\omega_{12} = \frac{(\gamma_{F2} - \gamma_{F1})}{\gamma_{12}} \tag{B.1}$$

In particular, γ_{F2} is the interfacial energy between organoclay and polymer "*2*", γ_{F1} is the interfacial energy between the filler and polymer "*1*", respectively. The interfacial energy between polymer "*1*" and polymer "*2*" is designated as γ_{12}. If the wetting coefficient is higher than 1 ($\omega_{12} > 1$) the filler will distribute in the phase "*1*", whereas with values lower than -1 ($\omega_{12} < -1$). On the other hand, an intermediate value of the wettability parameter, that is $|\omega_{12}| < 1$, means that the nanoparticles are inclined to accumulate at the interface between the two polymeric phases.

Here, we have considered a modified version of Harkins theory [1], that was first reported by Torza et al. [2]. Then Hobbs et al. [3] followed and developed a modified Harkins equation and calculated three spreading coefficients of ternary polymer systems to predict the possible morphological structures as shown in the following equation:

$$\lambda_{ij} = \gamma_{jk} - \gamma_{ik} - \gamma_{ij} \tag{B.2}$$

where λ_{ij} is defined as the spreading coefficient defining the tendency of component (*i*) to encapsulate or spread onto component (*j*) in the matrix of component (*k*). The interfacial tensions of the various polymer pairs are represented as γ_{ij}, γ_{ik}, and γ_{jk} [4]. A system with incomplete wetting is characterized by negative spreading coefficient and one with complete wetting is reflected by a zero (or positive) spreading coefficient. In this way, these results can support those obtained by the wettability parameter.

Deriving either ω_{Si} or λ_{Si} requires the knowledge of the interfacial tensions among the phases. The latter can be obtained from the surface tensions of the components, γ_i. The following two equations can be used for this purpose:

$$\gamma_{ij} = \gamma_i + \gamma_j - 4\frac{\gamma_i^d \gamma_j^d}{\gamma_i^d + \gamma_j^d} - 4\frac{\gamma_i^p \gamma_j^p}{\gamma_i^p + \gamma_j^p} \tag{B.3}$$

$$\gamma_{ij} = \gamma_i + \gamma_j - 2\sqrt{\gamma_i^d \gamma_j^d} - 2\sqrt{\gamma_i^p \gamma_j^p} \tag{B.4}$$

in which the apices "d" and "p" indicate the dispersive and polar component of γi, respectively. Eq. B3 is based on the harmonic mean, and it is customary used in case of materials with comparable surface tensions; Eq. B4 refers to the geometric mean and it is recommended for materials with very different surface tensions. The literature values of the surface tension at room temperature and the corresponding dispersive and polar components for the polymers and clay nanoparticles are reported in Table 1. To estimate the values of surface tension at 190°C (i.e. the temperature at which the mixing was performed), we assumed a linear dependence of γ_i on T and we used literature data for the temperature coefficients, $\partial\gamma_i/\partial T$. Then, we split the surface tension at high temperature in its polar and dispersive parts keeping the same ratio between the two as that at room temperature. The obtained values of γ_i are reported in Table 1.

Table 1.: Dispersive and polar components of the surface tensions of the pure materials at room temperature (T=20°C or 25°C) and at T=190°C as obtained by linear extrapolation using the reported temperature coefficients.

| Material | Surface tension at room temperature [mN/m] | | | | Surface tension at T=150°C [mN/m] | | |
	Total (γ_i)	Dispersive (γ_i^d)	Polar (γ_i^p)	$\partial\gamma_i/\partial T$ [mN/m °C]	Total (γ_i)	Dispersive (γ_i^d)	Polar (γ_i^p)
PS	40.7[a]	34.5[a]	6.1[a]	-0.072[a]	28.5	24.2	4.3
PMMA	41.1[a]	29.6[a]	11.5[a]	-0.076[a]	28.2	20.3	7.9
Clay 15A	45.3[b]	33.4[b]	11.8[b]	-0.136[c]	22.9	16.9	6.0

[a] Values at T=20°C, from ref. [5].
[b] Values at T=25°C, from ref. [6].
[c] Estimated from data in ref. [7].

The values of interfacial tension for the polymer-polymer and polymer-nanoparticles pair are summarized in Table 2. Eq. B3 was used to estimate $\gamma_{PS-PMMA}$, while Eq. B4 was employed to derive $\gamma_{PS-Clay15A}$ and $\gamma_{PMMA-Clay15A}$.

Table 2.: Interfacial tensions at

Pair	γ_{ij} [mN/m]
PS-PMMA	1.48
PS-Clay15A	0.91
PMMA-Clay15A	0.34

Finally, the values of interfacial tension at 190°C reported in Table 2 have been used to compute the wetting and spreading coefficients by using Eq. B1 and B2, respectively. The obtained parameters are reported in Table 3.

Table 3.: Wetting and spreading coefficients at T=190°C.

Parameter	
$\lvert \omega_{PS\text{-}Clay15A}\rvert$	0.39
$\lambda_{PS\text{-}Clay15A}$	-2.05
$\lambda_{PMMA\text{-}Clay15A}$	-0.91

The value of the wetting coefficient ($\lvert \omega_{Fl}\rvert <1$) suggests that the clay nanoplatelets should locate at the polymer/polymer interface at thermodynamic equilibrium. This conclusion is also supported by the spreading coefficients. The negative value of both $\lambda_{PS\text{-}Clay15A}$ and $\lambda_{PMMA\text{-}Clay15A}$ indicates that neither the PS nor the PMMA phase should encapsulate the nanoclays. As a result, the filler is expected to be located at the interface, in agreement with the considerations based on the wetting coefficient.

B.2. Procedure for the building of the master curve of *G′* and resulting shift factors[1]

The key steps for identifying the horizontal, a_Φ, and vertical, b_Φ, shift factors for the building of the master curve of the elastic modulus, G', are summarized in the following. Specifically, it is here provided a step-by-step guide for the scaling of each of the G' curve at different filler content, Φ:

I. account for hydrodynamic effects related to the presence of the filler by introducing an amplification factor B(Φ). It represents the ratio between the complex modulus G*(Φ) of the filled sample and that of the neat matrix (here the PS/PMMA blend) in the high-frequency range (Figure 1). See also reference [8] for further details on the topic.
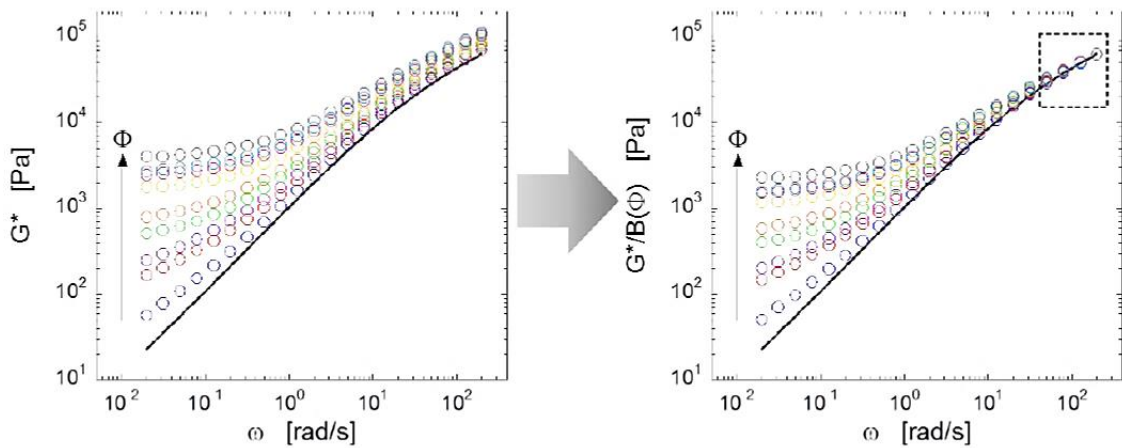
Figure 1.: (a) Frequency dependence of the complex modulus of the neat PS/PMMA blend (solid line) and blends at different filler content (symbols). (b) Frequency dependence of the complex modulus blends at different filler content (symbols) divided by the amplification factor B(Φ).1

---

[1] Here we have reported the procedure using values and results deriving from co-continuous systems. However, the procedure, changing the values properly, is the same even in the case of drop-in- matrix systems.

II. amplify the viscous modulus of the pure matrix by the obtained amplification factor: $G''(\omega) \times B(\Phi)$;

III. find a_Φ and b_Φ as the coordinates of the point at which the network elasticity, identified as the low-frequency plateau of the elastic modulus, equals the amplified viscous modulus of the pure PS/PMMA matrix (Figure 2).
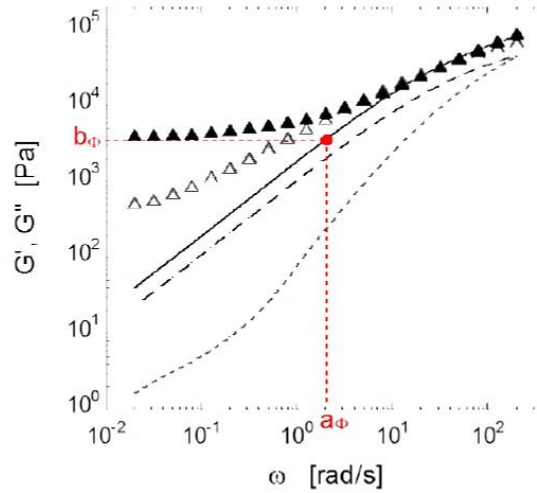

Figure 2.: Example of evaluation of the scaling factors to build the master curve of G′. Full triangles represent the elastic modulus of the sample at $\Phi = 1.06$ vol%, the dashed line is the viscous modulus of the unfilled blend, the solid line is the viscous modulus of the blend amplified to account for hydrodynamic effects. The horizontal and vertical shift factors to build the master curve of G′ are pointed out. The elastic modulus of the unfilled blend (dotted gray line) and the viscous modulus of the filled sample (empty gray triangles) are shown as well.

The amplification and scaling factors obtained according to the procedure previously described are resumed in Table A4 for all the PS/PMMA/clay samples at $\Phi > \Phi c$.

Table 4.: Amplification factors B(Φ), and shift factors, (a$_\Phi$; b$_\Phi$) of each scaled G′ curve of Figure 12 and Figure 14 of the main text.

System	Percentage volume fraction of filler [vol%]	B(Φ) [-]	a$_\Phi$ [rad s-1]	b$_\Phi$ [Pa]
PS/clay	0.94 ± 0.07	1.126	0.004	13.6
	1.10 ± 0.01	1.153	0.012	42.7
	1.27 ± 0.05	1.185	0.025	88.3
	1.32 ± 0.08	1.194	0.051	171.5
	1.63 ± 0.01	1.256	0.223	812.7
	1.89 ± 0.10	1.313	0.332	1256.3
	2.65 ± 0.01	1.500	0.454	1942.2
PS/PMMA/clay *drop-in-matrix*	1.32 ± 0.03	1.227	0.024	94.8
	1.66 ± 0.04	1.321	0.044	185.0

	2.05 ± 0.11	1.448	0.113	525.7
	2.12 ± 0.03	1.472	0.143	674.3
	2.24 ± 0.08	1.518	0.157	763.3
PS/PMMA/clay *co-continuous*	0.22 ± 0.026	1.23	0.114	150.1
	0.31 ± 0.071	1.28	0.313	420.9
	0.36 ± 0.055	1.35	0.477	669.1
	0.67 ± 0.011	1.48	1.051	1589.9
	0.81 ± 0.120	1.62	1.386	2268.3
	0.91 ± 0.028	1.73	1.496	2488.7
	1.06 ± 0.070	1.78	2.130	3758.4

The previous procedure only applies to samples above the percolation threshold, Φ_c. Actually, the physical constraints of the two-phase model allow to reliably identify the samples which exceed Φ_c. As a result, once the master curve has been built by referring to samples with a clear low-frequency plateau, the correct scaling of the G' curves of samples at lower Φ (yet at $\Phi > \Phi_c$) is ensured by the constraints imposed by the two-phase model in the identification of the shift factors. The positioning of each G' curve on the master curve is not obtained by looking for their partial superposition, being instead unambiguously dictated by the interrelationship between the shift factors. The latter establishes a precise track in the plane $G'/b_\Phi - \omega/a_\Phi$ on which the curve to be scaled can move [9-10] (Figure 3). This allows the accurate evaluation of the network elasticity (equal to b_Φ) for each sample above Φ_c, irrespective from the inherent elasticity of the polymer blend matrix.
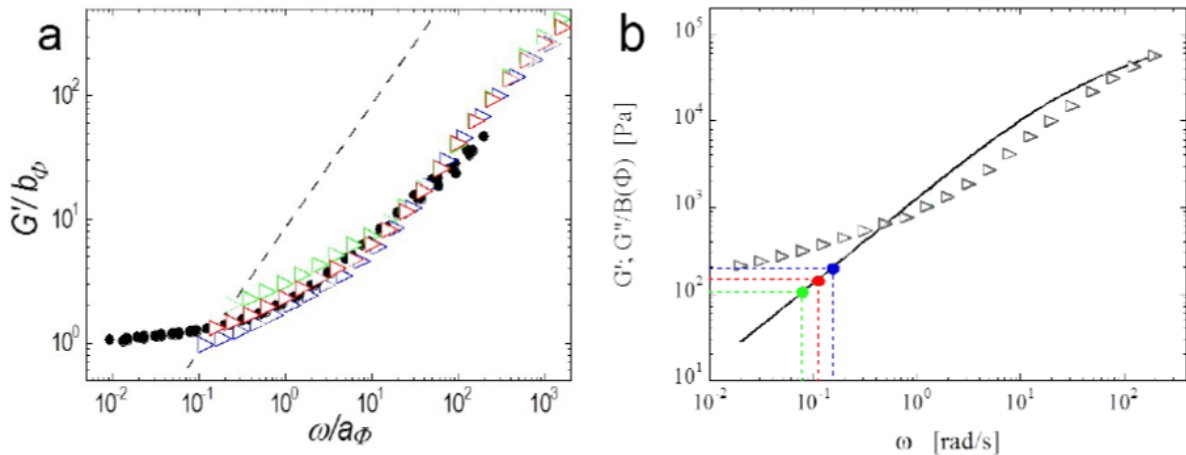

Figure 3.: Possible scaled curves of G' in accordance to the two-phase model for samples at $\Phi = 0.22$ vol%. The data are superimposed on the master curve derived from samples at higher filler contents (black symbols). The pairs of scaling factors (a_Φ; b_Φ) are shown in part (b) (coordinates of the symbols) together with the amplified G'' of the neat blend (solid and dashed line). Dashed line in part (a) represents the track on which the point at the lowest frequency of the curve to be scaled must move with changing the pair (a_Φ; b_Φ).

B.3. Correlation between interfacial elasticity and wall thickness of the interfacial filler network

The Yu's model for the interfacial elastic modulus of a co-continuous blend, G'_{int}, in the presence of an interfacial network of nanoparticles can be re-written as [R9]:

$$G' = C \cdot S_{int} \cdot (\gamma_{12} + G_S + K_{int})$$ (B.5)

where S_{int} is the interfacial area per unit volume, γ_{12} is the interfacial tension between the polymeric constituents of the blend, G_S and K_{int} are the surface shear modulus and surface compression modulus, respectively, of the nanoparticles at the polymer-polymer interface, and C is a constant given by [R10]:

$$C = \frac{1}{6}(k + \frac{3}{4}\frac{f_2\omega^2\tau^2}{f_1^2 + \omega^2\tau^2})$$ (B.6)

where k is a correction index to account for the random orientation and possible distortion of the co-continuous structure, $\tau = \eta_0\xi/\gamma_{12}$ is a characteristic time that depends on the ratio of the viscous stress to the interfacial tension, with η_0 and ξ being the zero-shear rate viscosity and characteristic domain size of the as-prepared neat blend, respectively. The parameters f_1 and f_2 depend on the viscosity ratio p of the two polymeric phases as:

$$f_1 = \frac{40(p+1)}{(2p+3)(19p+16)}, f_2 = \frac{5}{2p+3}$$ (B.7)

Since for many kinds of nanosheets $K_{int} \sim 101$ mPa m and $G_s \sim 10$-2 mPa m, Eq. B5 can be simplified by considering that $K_{int} \gg G_s$ [11]. The same consideration can be extended to γ_{12} which is of the order of 100 mPa m ($\gamma_{PS/PMMA} \approx 1.5$ mPa m). In the light of these considerations, we get:

$$G'_{int} \approx C \cdot S_{int} \cdot K_{int}$$ (B.8)

Looking at Eq. A8, the first observation is that the only variable is Sint, which is inversely proportional to the characteristic size of the polymeric domains, ξ. Accordingly, in principle one should find that:

$$G'_{int} \propto S_{int} \propto \xi^{-1}$$ (B.9)

Our experimental data of G'int for the samples at $\Phi > \Phi_c$ (i.e. the values of b$_\Phi$ in Figure 17 of the main text) are in reasonable agreement with this scaling law ($G'_{int} \propto \xi^{-1.16}$), in line with recent findings by Macosko's groups. Eq. B8 can be thus rewritten as:

$$G'_{int} \approx \frac{C \cdot K_{int}}{\xi}$$ (B.10)

Finally, the dependence of G'_{int} on the wall thickness of the particle network, t^w, emerges when considering that K_{int} refers to the surface compression modulus of a monolayer of nanoplatelets. As a result, it has to be

"corrected" in to take into account the variability of the wall thickness within K_{int}^w the co-continuous PS/PMMA blend filled with different amount of nanoclays:

$$K_{int}^w = K_{int} \cdot \frac{t^w}{t^m} \qquad \text{(B.11)}$$

where tm is the thickness of the particle monolayer and depends on the type of particles which is considered. By considering in Eq. B10, an explicit relationship between the strength of the network and the K_{int}^w thickness of its building blocks is finally obtained:

$$G_{int}' \approx \frac{C \cdot K_{int} \cdot (t^w/t^m)}{\zeta} \qquad \text{(B.12)}$$

Overall, this means that the following scaling law holds true:

$$G_{int}' \propto \frac{t^w}{\xi} \qquad \text{(B.13)}$$

In particular, for systems having the same characteristic size:

$$G_{int}' \propto t^w \qquad \text{(B.14)}$$

To appreciate the correctness of Eq. A12, the calculated values of G'_{int} have been compared to the experimental ones (see inset of Figure 19 in the main text). For the calculation of G'_{int}, the following values have been used. For the estimation of the prefactor C, the value of k was taken equal to 0.12, which is suitable for samples obtained by compression molding and tested in the parallel plate rheometer in the molten state, the value of k can be taken equal to 0.12 [11-12]. Then, we used $p = \eta_{PMMA}/\eta_{PS} \approx 10$, $\eta_0 \approx 1500$ Pa·s, $\xi = 5.86$ μm, $\gamma_{PS-PMMA} \approx 1.5$ mPa·m and $p \approx 4.36$, to get a value of $C \approx 0.037$ from Eq. A6-A7. A literature value obtained for Na–montmorillonite particles of $K_{int} \approx 20$ mPa·m [13] was considered and the ratio was estimated according to the data in Figure 19 of the t^w/t^m main text.

BIBLIOGRAPHY

1. Ramsden, W. (1903). Separation of solids in the surface-layers of solutions and 'suspensions' (observations on surface-membranes, bubbles, emulsions, and mechanical coagulation). --preliminary account. Proceedings of the royal Society of London, 72, 156-164.

2. Pickering, S. U. (1907). Cxcvi.—emulsions. Journal of the Chemical Society, Transactions, 91, 2001-2021.

3. Clegg, P. S. (2008). Fluid-bicontinuous gels stabilized by interfacial colloids: low and high molecular weight fluids. Journal of Physics: Condensed Matter, 20(11), 113101.

4. Taguet, A., Cassagnau, P., & Lopez-Cuesta, J. M. (2014). Structuration, selective dispersion and compatibilizing effect of (nano) fillers in polymer blends. Progress in Polymer Science, 39(8), 1526-1563.

5. de Luna, M. S., & Filippone, G. (2016). Effects of nanoparticles on the morphology of immiscible polymer blends–challenges and opportunities. European Polymer Journal, 79, 198-218.

6. Macosko, C. W. (2000, January). Morphology development and control in immiscible polymer blends. In Macromolecular Symposia (Vol. 149, No. 1, pp. 171-184). WILEY-VCH Verlag.

7. Liu, X. Q., Li, R. H., Bao, R. Y., Jiang, W. R., Yang, W., Xie, B. H., & Yang, M. B. (2014). Suppression of phase coarsening in immiscible, co-continuous polymer blends under high temperature quiescent annealing. Soft matter, 10(20), 3587-3596.

8. Feng, J. M., Liu, X. Q., Bao, R. Y., Yang, W., Xie, B. H., & Yang, M. B. (2015). Suppressing phase coarsening in immiscible polymer blends using nano-silica particles located at the interface. RSC Advances, 5(91), 74295-74303.

9. Dil, E. J., Virgilio, N., & Favis, B. D. (2016). The effect of the interfacial assembly of nano-silica in poly (lactic acid)/poly (butylene adipate-co-terephthalate) blends on morphology, rheology and mechanical properties. European Polymer Journal, 85, 635-646.

10. Cohen, E., Zonder, L., Ophir, A., Kenig, S., McCarthy, S., Barry, C., & Mead, J. (2013). Hierarchical structures composed of confined carbon nanotubes in cocontinuous ternary polymer blends. Macromolecules, 46(5), 1851-1859.

11. Nuzzo, A., Coiai, S., Carroccio, S. C., Dintcheva, N. T., Gambarotti, C., & Filippone, G. (2014). Heat-Resistant Fully Bio-Based Nanocomposite Blends Based on Poly (lactic acid). Macromolecular materials and engineering, 299(1), 31-40.

12. Zhang, Z., Wang, S., Zhang, J., Zhu, W., Zhao, X., Tian, T., & Chen, T. (2016). Self-formation of elastomer network assisted by nano-silicon dioxide particles: A simple and efficient route toward polymer nanocomposites with simultaneous improved toughness and stiffness. Chemical Engineering Journal, 285, 439-448.

13. de Luna, M. S., Galizia, M., Wojnarowicz, J., Rosa, R., Lojkowski, W., Leonelli, C., ... & Filippone, G. (2014). Dispersing hydrophilic nanoparticles in hydrophobic polymers: HDPE/ZnO nanocomposites by a novel template-based approach. Lett, 8, 362-372.

14. Imperiali, L., Clasen, C., Fransaer, J., Macosko, C. W., & Vermant, J. (2014). A simple route towards graphene oxide frameworks. Materials Horizons, 1(1), 139-145.

15. Lee, M. N., & Mohraz, A. (2010). Bicontinuous macroporous materials from bijel templates. Advanced Materials, 22(43), 4836-4841.

16. Bai, L., Fruehwirth, J. W., Cheng, X., & Macosko, C. W. (2015). Dynamics and rheology of nonpolar bijels. Soft Matter, 11(26), 5282-5293.

17. Filippone, G., & Acierno, D. (2012). Clustering of coated droplets in clay-filled polymer blends. Macromolecular Materials and Engineering, 297(9), 923-928.

18. Kim, H., & Macosko, C. W. (2009). Processing-property relationships of polycarbonate/graphene composites. Polymer, 50(15), 3797-3809.

19. Romeo, G., Filippone, G., Russo, P., & Acierno, D. (2009). Effects of particle dimension and matrix viscosity on the colloidal aggregation in weakly interacting polymer-nanoparticle composites: a linear viscoelastic analysis. Polymer bulletin, 63(6), 883.

20. Si, M., Araki, T., Ade, H., Kilcoyne, A. L. D., Fisher, R., Sokolov, J. C., & Rafailovich, M. H. (2006). Compatibilizing bulk polymer blends by using organoclays. Macromolecules, 39(14), 4793-4801.

21. Hong, J. S., Namkung, H., Ahn, K. H., Lee, S. J., & Kim, C. (2006). The role of organically modified layered silicate in the breakup and coalescence of droplets in PBT/PE blends. Polymer, 47(11), 3967-3975.

22. Huitric, J., Ville, J., Médéric, P., Moan, M., & Aubry, T. (2009). Rheological, morphological and structural properties of PE/PA/nanoclay ternary blends: Effect of clay weight fraction. Journal of rheology, 53(5), 1101-1119.

23. Vandebril, S., Vermant, J., & Moldenaers, P. (2010). Efficiently suppressing coalescence in polymer blends using nanoparticles: role of interfacial rheology. Soft Matter, 6(14), 3353-3362.

24. Labaume, I., Médéric, P., Huitric, J., & Aubry, T. (2013). Comparative study of interphase viscoelastic properties in polyethylene/polyamide blends compatibilized with clay nanoparticles or with a graft copolymer. Journal of rheology, 57(2), 377-392.

25. Trifkovic, M., Hedegaard, A. T., Sheikhzadeh, M., Huang, S., & Macosko, C. W. (2015). Stabilization of PE/PEO cocontinuous blends by interfacial nanoclays. Macromolecules, 48(13), 4631-4644.

26. Huang, S., Bai, L., Trifkovic, M., Cheng, X., & Macosko, C. W. (2016). Controlling the morphology of immiscible cocontinuous polymer blends via silica nanoparticles jammed at the interface. Macromolecules, 49(10), 3911-3918.

27. Filippone, G., Causa, A., de Luna, M. S., Sanguigno, L., & Acierno, D. (2014). Assembly of plate-like nanoparticles in immiscible polymer blends–effect of the presence of a preferred liquid–liquid interface. Soft Matter, 10(18), 3183-3191.

28. Herzig, E. M., White, K. A., Schofield, A. B., Poon, W. C. K., & Clegg, P. S. (2007). Bicontinuous emulsions stabilized solely by colloidal particles. arXiv preprint arXiv:0712.2213.

29. Cates, M. E., & Clegg, P. S. (2008). Bijels: a new class of soft materials. Soft Matter, 4(11), 2132-2138.

30. Sinha Ray, S., Okamoto, K., & Okamoto, M. (2003). Structure− property relationship in biodegradable poly (butylene succinate)/layered silicate nanocomposites. Macromolecules, 36(7), 2355-2367.

31. Filippone, G., & Salzano de Luna, M. (2012). A unifying approach for the linear viscoelasticity of polymer nanocomposites. Macromolecules, 45(21), 8853-8860.

32. Filippone, G., Romeo, G., & Acierno, D. (2009). Viscoelasticity and structure of polystyrene/fumed silica nanocomposites: filler network and hydrodynamic contributions. Langmuir, 26(4), 2714-2720.

33. Wu, H., & Morbidelli, M. (2001). A model relating structure of colloidal gels to their elastic properties. Langmuir, 17(4), 1030-1036.

34. Filippone, G., de Luna, M. S., Acierno, D., & Russo, P. (2012). Elasticity and structure of weak graphite nanoplatelet (GNP) networks in polymer matrices through viscoelastic analyses. Polymer, 53(13), 2699-2704.

35. Stauffer, D., & Aharony, A. (1992). Introduction to Percolation Theory.. 2nd EdTaylor and Francis. London 181pp.

36. Bai, L., He, S., Fruehwirth, J. W., Stein, A., Macosko, C. W., & Cheng, X. (2017). Localizing graphene at the interface of cocontinuous polymer blends: Morphology, rheology, and conductivity of cocontinuous conductive polymer composites. Journal of Rheology, 61(4), 575-587.

BIBLIOGRAPHY Appendix B

1. Harkins, W. D., & Feldman, A. (1922). Films. The spreading of liquids and the spreading coefficient. Journal of the American Chemical Society, 44(12), 2665-2685.

2. Torza, S., & Mason, S. G. (1970). Three-phase interactions in shear and electrical fields. Journal of Colloid and Interface Science, 33(1), 67-83.

3. Hobbs, S. Y., Dekkers, M. E. J., & Watkins, V. H. (1988). Effect of interfacial forces on polymer blend morphologies. Polymer, 29(9), 1598-1602.

4. Ravati, S., & Favis, B. D. (2010). Morphological states for a ternary polymer blend demonstrating complete wetting. Polymer, 51(20), 4547-4561.

5. http://www.surfacetension.de/solidsurface-energy.htm (accessed January, 2017): Solid surface energy data (SFE) for common polymers.

6. Kamal, M. R., Calderon, J. U., & Lennox, B. R. (2009). Surface energy of modified nanoclays and its effect on polymer/clay nanocomposites. Journal of Adhesion Science and Technology, 23(5), 663-688.

7. Picard, E., Gauthier, H., Gérard, J. F., & Espuche, E. (2007). Influence of the intercalated cations on the surface energy of montmorillonites: consequences for the morphology and gas barrier properties of polyethylene/montmorillonites nanocomposites. Journal of colloid and interface science, 307(2), 364-376.

8. Filippone, G., Romeo, G., & Acierno, D. (2009). Viscoelasticity and structure of polystyrene/fumed silica nanocomposites: filler network and hydrodynamic contributions. Langmuir, 26(4), 2714-2720.

9. Filippone, G., de Luna, M. S., Acierno, D., & Russo, P. (2012). Elasticity and structure of weak graphite nanoplatelet (GNP) networks in polymer matrices through viscoelastic analyses. Polymer, 53(13), 2699-2704.

10. Filippone, G., & Salzano de Luna, M. (2012). A unifying approach for the linear viscoelasticity of polymer nanocomposites. Macromolecules, 45(21), 8853-8860.

11. Bai, L., He, S., Fruehwirth, J. W., Stein, A., Macosko, C. W., & Cheng, X. (2017). Localizing graphene at the interface of cocontinuous polymer blends: Morphology, rheology, and conductivity of cocontinuous conductive polymer composites. Journal of Rheology, 61(4), 575-587.

12. Yu, W., Zhou, W., & Zhou, C. (2010). Linear viscoelasticity of polymer blends with co-continuous morphology. Polymer, 51(9), 2091-2098.

13. Wang, Y., Lu, F., Li, Y., Wu, T., Sun, D., Zhang, G., ... & Wang, G. (2012). Effects of Na–montmorillonite particles on the emulsification stability of polymer flooding produced water. Colloids and Surfaces A: Physicochemical and Engineering Aspects, 410, 125-129.

Assembly, elasticity and structures of clay nanoparticles embedded in either of the phases of co-continuous blends*

5.1. Introduction

The final properties of a polymer blend are strongly influenced by its morphology which can be tuned by varying the composition, processing conditions, and the chemistry and rheology of the blended polymers [1]. Of all possible polymer blend morphologies, co-continuous blends are of particular interest due to their unique property of possessing two continuous phases. This property allows co-continuous blends to be used for novel applications [2-3]. However, co-continuous morphologies are not in thermodynamic equilibrium. They are kinetically trapped, and during annealing, their features will coarsen into larger sizes as coalescence occurs and may eventually break up into dispersed morphologies. Nanofillers have the potential to be used as a more generic, economical approach to reduce coarsening. A single nanofiller has the potential to behave as an effective compatibilizer for multiple polymer blends, if the polymer−particle interaction results in a lower interfacial energy than the two-phase polymer−polymer interaction. In our previous work on polymer blends with nanoparticles we have reported that selective localization at the interface is the desired mechanism so that stabilization and refinement can be achieved with significantly fewer particles. However, accomplishing this often poses significant challenges due to the complex and little understood interplay of particle compatibility, transport behaviour, and rheology. Kinetic and thermodynamic effects are both important in this respect. Often the morphology/structure of the polymer blend nanocomposite is far from the expected one, due in part to the role of rheology in particle localization during nonequilibrium processes like melt mixing [4].

When a filler is added to a polymer blend with the specific idea of reinforcement, refinement and/or stabilization it is the influence of important factors, such as the nature of the nanoparticles and the parameter of process on the structuring of them, to play a vital role on the behaviour of final systems. The final properties of nanocomposites are widely determined by the localization of the particles in one of the two polymer phase or at the interface. Several aspects of fillers govern their localization, their compatibilizing role and their dispersion/aggregation in a polymer blend. Among particle properties the chemistry can lead to different final properties. Moreover, the chemistry of organically modified clays can change mechanical properties (stiffness) either in polymer blends with different polarities or when dispersed in the same polymer [5]. As pointed out

---

* The results presented in this section have still not been published.

earlier, it is difficult to form a strong bond between the filler and the matrix due to poor wettability of the filler especially in nonpolar, high melt viscosity polymeric systems, and due to the presence of contaminants or multimolecular layers of water on the mostly hydrophilic surfaces of fillers, which prevents physical or chemisorption of the polymer molecules. The interfacial bond can be enhanced, and the mechanical performance of the composites improved by suitable surface treatment. These days, most of the fillers are pretreated before they are used as a further phase in composite materials [6].

The subject of compatibilizing incompatible polymer blends by adding relatively cheap organoclays is very appealing from the standpoint of practical applications. However, the existing studies13–15 mainly dealt with the systems prepared by solution-casting, where the exfoliated clay structure may be quite favourable. In the system prepared by melt-mixing, the resulting morphology and physical properties may be quite different and require additional investigation [7]. The primary goal of this study is to determine the effect of organoclays on the structure and properties of clay-based polymer nanocomposites containing incompatible polymer mixtures by melt-blending. We are particularly interested in the understanding of relationships among the clay chemistry (e.g., hydrophobic, hydrophilic) and morphology (e.g., the extend of exfoliation/intercalation of layered silicates), the blend morphology (e.g., the average size of phase domains in immiscible polymer blends), and rheological properties of the final composites. As we recognized that the surfactant used in organoclays may also play an important role in influencing the final composite properties, two types of structurally similar organoclays (Cloisite® 15A and Cloisite® 30B) with different surfactant contents were used to prepare polymer nanocomposites containing polystyrene (PS)/poly (methyl methacrylate) (PMMA) blends and both homopolymers (PS and PMMA) by melt-blending for direct comparison purpose.

5.2. Experimental section

The polystyrene (PS) used for this study was provided by Polimeri Europa (Edistir® 2982), poly (methyl methacrylate) (PMMA), by Plaskolite, Inc. (Optix® CA-51). PS has glass transition temperature $T_g=100°C$, density $\rho=1.04$ g cm-3 and PMMA has $T_g=110°C$, $\rho=1.18$ g cm-3, respectively. Two organically modified clays (Cloisite 30B and Cloisite 15A) were used in these blends and were provided by Southern Clay Products, Inc., USA. Table 1 shows the chemical structure of the intercalating cations and the structural information on the nanoclays, provided by the material supplier.

Table 1.: Structural Information of Nanoclays - Clays are listed in order of descending hydrophilicity and ascending d-spacing. T = tallow: linear alkyl chains (C18 (65%), C16 (30%), C14 (5%)); HT = hydrogenated tallow.

Nanoclay	Interlayer cation	Cationic exchange capacity (meq/100g clay)	Basal spacing d_{001} (nm)
Cloisite 30B	$CH_3 - N^+ - T$ with two CH_2CH_2OH groups	90	1.85
Cloisite 15A	$CH_3 - N^+ - HT$ with HT and CH_3 groups	125	3.15

The batch melt compounding was performed in a recirculating, conical twin screw, micro-compounder (Xplore MC 15 by DSM). Blends were mixed at a rotor speed of 150 rpm and temperature of 190 °C for 5 min under nitrogen purge. The weight ratio was set at 55/45 wt % PS/PMMA (*co-continuous system*) for both unfilled and filled blends. The extrudate was granulated, dried again, and finally compression-moulded in the form of disks (diameter 40 mm, thickness ~1.5 mm) for the subsequent rheological and morphological analyses. The unfilled PS and PS/PMMA blend used as reference materials were processed in the same conditions.

The particle loading was accurately estimated for each sample by means of thermogravimetric analyses (TGA, Q5000 by TA Instruments). Tests were carried out small pieces cut from the disks recovered at the end of rheological analyses. The samples were heated at 10°C min^{-1} in nitrogen atmosphere from room temperature up to T=700°C, and the residuals were recorded at T=600°C. The reported values of filler content, expressed in terms of percentage volume fraction of the inorganic fraction, Φ, are averages computed from three independent measurements.

The blend morphology was examined by scanning electron microscopy (Quanta 200 FEG-SEM by FEI) to study the morphology of the polymer phases, and transmission electron microscopy (TEM, Tecnai G2 Spirit Twin T-12 by FEI) in order to determine nanoparticle localization within the blends. The samples were ~100 nm-thick slices randomly cut at room temperature from the disks used for rheological analyses by using a Leica EM UC7 ultra-microtome equipped with a diamond knife. Before SEM observations, the PMMA phase was selectively extracted in formic acid, for 1 h at 60 °C under magnetic stirring, and the remaining PS matrix was sputter-coated with a 15 nm thick Au/Pd layer. As regards TEM images, PMMA phases tended to be brighter (white in the images), where PS phases tended to be darker (gray in the images). Clay was evident as thin black particles. The SEM micrographs were, in the case of co-continuous systems, analysed to get an

estimate of the characteristic size of the PMMA phase, which was defined as 1/Q, where Q is the interfacial length per unit area. For each sample, several images at different magnifications were analysed by manually detecting the interfacial perimeter.

Rheological tests were performed at T=215°C in dry nitrogen atmosphere using a stress-controlled rotational rheometer (ARG2 by TA Instruments) in parallel-plate configuration. The elastic (G') and viscous (G") shear moduli were collected by means of time and frequency scans. All the tests were performed at strain amplitudes low enough to be in the linear regime. The latter was evaluated for each sample through preliminary strain amplitude tests.

5.3. Effects of nanoparticles embedded in the bulk phase on the blend microstructure

5.3.1. Thermodynamic prediction of nanoparticle localization

At thermodynamic equilibrium, location of filler in a polymer blend can be predicted by minimization of the interfacial energy. According to Young's equation, it is possible to find the equilibrium position of the filler by evaluating the wetting coefficient $\omega_{PS\text{-}PMMA}$:

$$\omega_{PS-PMMA} = \frac{(\gamma_{organoclay-PMMA} - \gamma_{organoclay-PS})}{\gamma_{PS-PMMA}} \tag{5.1}$$

where each γ represents the interfacial energy for all potential interfaces within the blend: the clay−PS interface, the clay−PMMA interface, and the PS−PMMA interface. If the wetting coefficient is >1, the clay is predicted to be in the PS phase, since the interfacial energy of the clay−PMMA interface is high and the interfacial energy of the clay−PS phase is very low. If ω has a value <−1, the clay will preferentially be located in PMMA. The value of wetting coefficient between −1 and 1 indicates that the difference between the clay−PS and clay−PMMA interfacial energy is less than the PS−PMMA interfacial energy, which causes the clay to localize at the PS−PMMA interface to minimize the energy. Because of the experimental difficulty in accurately evaluating interfacial energy between nanoparticle and a molten polymer, it was estimated from known surface energies of the components. The surface energy of a single blend component is characterized by the sum of the dispersive and polar contribution. The interfacial energy between two blend components can then be evaluated based on the surface energies of the components and through different approaches. The first is Owens-Wendt's geometric mean of the dispersive and polar contributions [8], as follows:

$$\gamma_{12} = \gamma_1 + \gamma_2 - 2\sqrt{\gamma_1^d \gamma_2^d} - 2\sqrt{\gamma_1^p \gamma_2^p} \tag{5.2}$$

The second is Wu's harmonic mean equation:

$$\gamma_{12} = \gamma_1 + \gamma_2 - 4\left(\frac{\gamma_1^d \gamma_2^d}{\gamma_1^d + \gamma_2^d} + \frac{\gamma_1^p \gamma_2^p}{\gamma_1^p + \gamma_2^p}\right) \tag{5.3}$$

In these equations, subscripts 1 and 2 reveal polymeric components, and c is the surface tension. Superscripts p and d denote the dispersive and polar parts of the surface tension [9]. The values of the surface energy of polymers and clays at the processing temperature have been extrapolated from values reported in the literature a [4, 10-11] and are summarized in Table 2:

Table 2.: Surface tension of polymers and clays.

	Surface tension at room temp. (mJ/m^2)				Surface tension at 190 °C (mJ/m2)		
Material	Total	Dispersive part	Polar part	Temperature coefficient – $d\gamma/dT$ (mJ/m^2)	Total	Dispersive part	Polar part
PS	40,7[a]	34,5[a]	6,1[a]	-0,072[a]	28,5	24,2	4,3
PMMA	41,1[a]	29,6[a]	11,5[a]	-0,076[a]	28,2	20,3	7,9
Cloisite 30B	48,35[b]	34,6[b]	14,75[b]	-0,1[c]	31,85	22,8	9,1
Cloisite 15A	42,54[b]	31,47[b]	11,06[b]	-0,1[c]	26,04	19,3	6,8

[a] From ref. [10].
[b] From ref. [11]
[c] From ref. [4]

The calculated values for the interfacial energy between each pair of blend components as well as the wetting parameter and the predicted location of the clays in the studied polymer blends are reported in Table 3.

Table 3.: Clay localization predictions based on wetting coefficients.

	Interfacial tension [mN/m]		Wetting coefficient, $\omega_{PS-PMMA}$		
Material	Geometric mean equation (Owens-Wendt)	Harmonic mean equation (Wu)	Geometric mean equation (Owens-Wendt)	Harmonic mean equation (Wu)	Location prediction
PS-PMMA-Cloisite 30B	$\gamma_{PS-PMMA} = 0.69$ $\gamma_{PS-30B} = 0.88$ $\gamma_{PMMA-30B} = 0.11$	$\gamma_{PS-PMMA} = 1.36$ $\gamma_{PS-30B} = 1.70$ $\gamma_{PMMA-30B} = 0.22$	-1,10	-1,08	PMMA

PS-PMMA-Cloisite 15A	$\gamma_{PS-PMMA} = 0.69$ $\gamma_{PS-15A} = 0.55$ $\gamma_{PMMA-15A} = 0.06$	$\gamma_{PS-PMMA} = 1,36$ $\gamma_{PS-15A} = 1,09$ $\gamma_{PMMA-15A} = 0.11$	-0,71	-0,71	Interface

In general, these predictions suggest that for the more hydrophilic clays (Cloisite 30B), the clay is predicted to be randomly dispersed within the PMMA phase, while the interfacial localization will be achieved with the most hydrophobic clays (Cloisite 15A).

5.3.2. Comparison with interfacial nanoparticles

The effect of incorporating organically modified Cloisite 30B and Cloisite 15A on the morphology of PS/PMMA blend is shown in Figure 1. SEM micrographs show the PS/PMMA 55/45 wt % blend with no clay (Figure 2a) and with several amounts of Cloisite 30B and Cloisite 15A (Figure 2b-g), respectively.
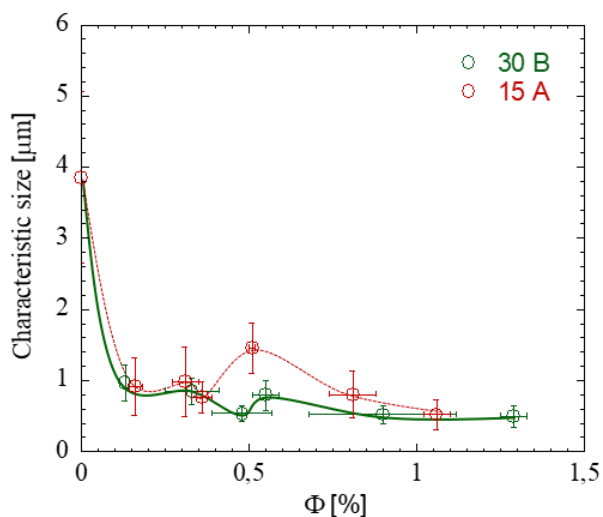

Figure 1.: Characteristic phase size with varying amounts of filler, before the annealing treatment. Solid and dashed lines are guides for the eye.

It can be also observed that phase domains appear less elongated and the blend morphology looks more uniform (Figure 2b, 2d, 2f)). However, Cloisite 30B depicts a clear compatibilization effect with characteristic size changes from 3.8 µm, in reference to the unfilled samples, to 0.49 µm for the sample with the higher filler content (Figure 1).

TEM micrographs show that Cloisite 30B (Figure 3) is primarily located in the PMMA phase with a little interfacial localization, while, as we have seen in the previous results (Chapter 4), Cloisite 15A is located at the interface between PS and PMMA domains.
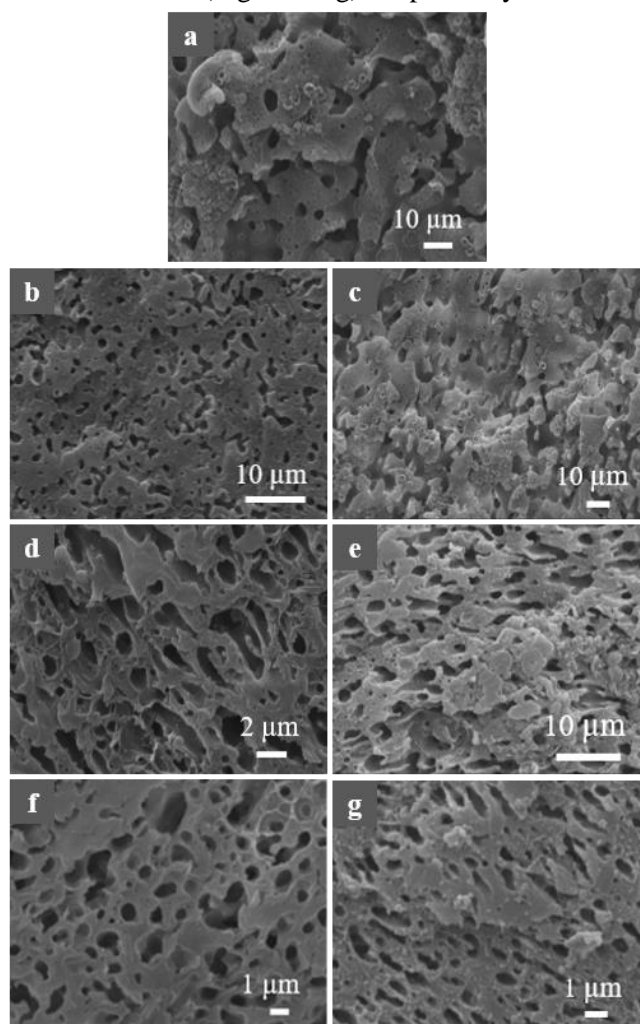

Figure 2.: SEM micrographs of PS/PMMA: (a) unfilled PS/PMMA; (b) PS/PMMA with Cloisite 30B at Φ=0.13 %; (c) PS/PMMA with Cloisite 15A at Φ=0.16 %; (d) PS/PMMA with Cloisite 30B at Φ=0.55 %; (e) PS/PMMA with Cloisite 15A at Φ=0.51 %; (f) PS/PMMA with Cloisite 30B at Φ=1.29 %; (g) PS/PMMA with Cloisite 15A at Φ=1.06 %.

This is consistent with predictions based on the interfacial wetting coefficient. The wetting coefficient for Cloisite 30B are close to -1 (-1.10 evaluated with geometric mean, and -1.08 evaluated with harmonic mean) thus, some interfacial localization is expected.

In the absence of significant interfacial localization of Cloisite 30B, the slight decrease in characteristic size is
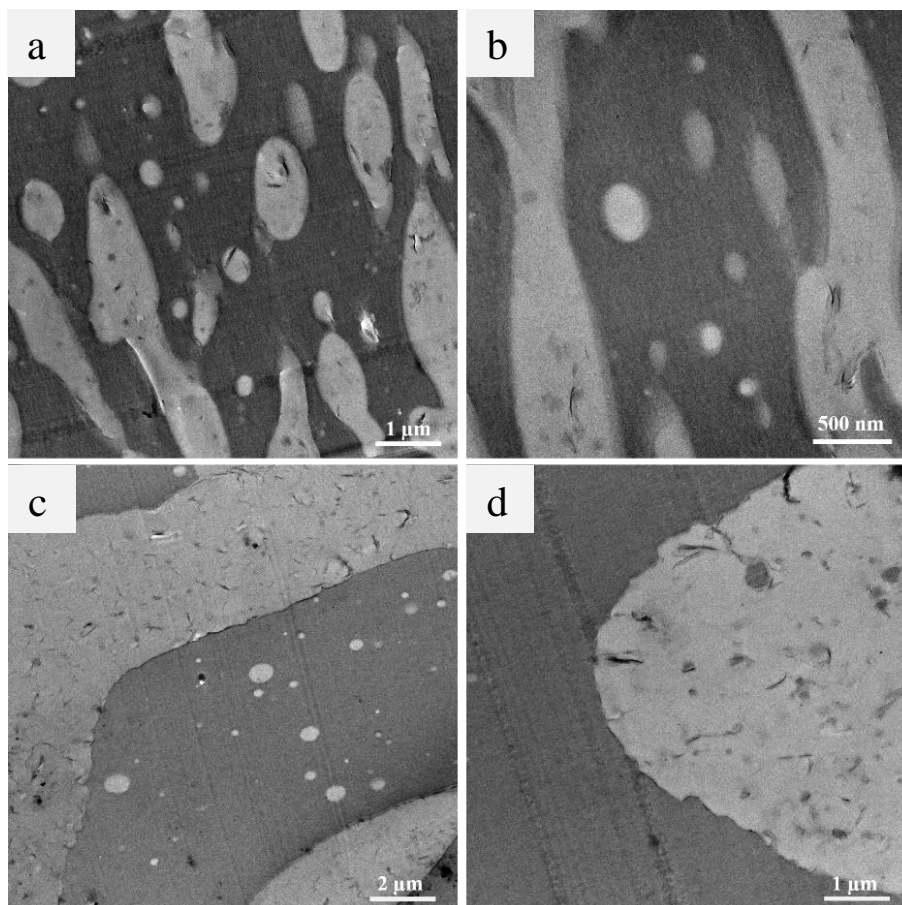

Figure 3.: TEM micrograph at different magnifications: (a, b) as-prepared; (c, d) after 3-hours of annealing at 215 °C. The bright and dark phases are PMMA and PS, respectively.

most likely due to the increase in viscosity of the PMMA phase (Figures 4). With two bulky tallow groups, the ammonium cations present in the Cloisite 15A are very hydrophobic and consequently has a relatively larger affinity for the interface.

Coarsening experiments were performed to examine the effect of clay on morphological stability. The characteristic pore size as a function of filler amount is shown in Figure 5. As expected, PS/PMMA with no clay coarsened, showing a dramatic increase in characteristic size after the annealing. In contrast, the blend containing interfacially localized Cloisite 15A showed a better suppression of coarsening during annealing than the blend filled with Cloisite 30B. In the former case, the clay is expected to be thermodynamically confined to the interface, as removing clay from the interface and dispersing it randomly into either phase would incur an energetic penalty due to the creation of new energetically unfavorable PS/PMMA interface.
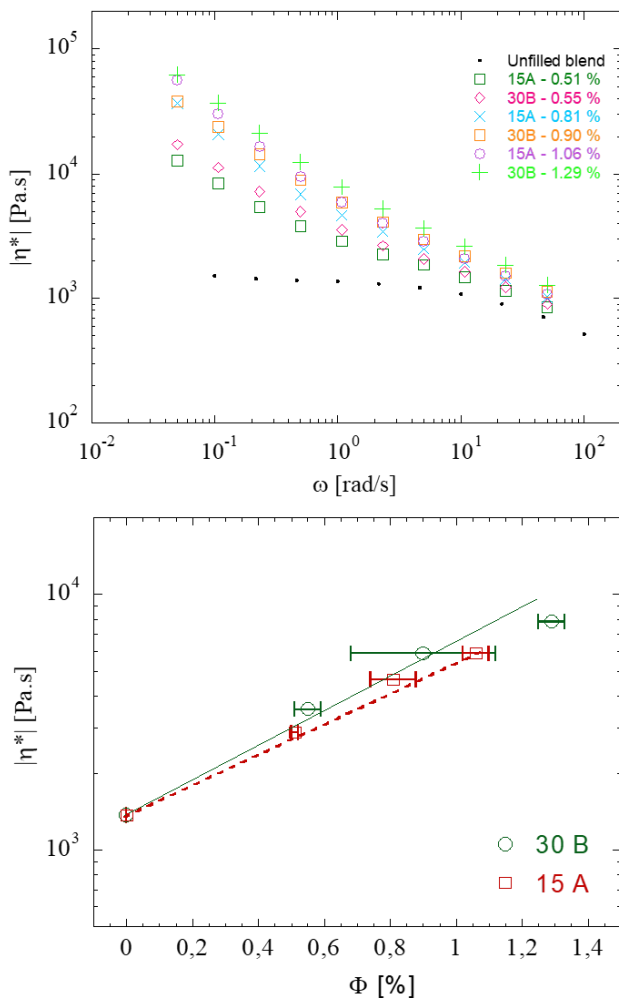
Figure 4.: Dependence of the complex viscosity on angular frequency (a), and on filler content at $\omega = 10^0$ rad s^{-1} (b).

Because the particles are confined, any reduction in the interfacial area due to coarsening would quickly cause the particles to crowd into each other, preventing further reduction in the interfacial area. These results show that simple presence of clay randomly dispersed through the blend, as in the case of 30B, is not sufficient for arresting coarsening, and that the clay must be localized at the interface in order to reap the stabilizing effects. More in general, clays with large d-spacing and a wetting coefficient nearest to zero gave the smallest size. This could make intuitive sense: large d-spacing encourages exfoliation, creating more clay surface area with which to stabilize the blend, and a wetting coefficient of zero would have the strongest preference for interfacial localization. Cloisite 30B, with wetting coefficient furthest from zero and the smallest d-spacing, resulted in the largest phase size domains. This could be attributed both to the wetting parameter, which predicts an increased propensity to localize in the PMMA phase rather than the interface, or to greater difficulty in achieving exfoliation due to

the smaller d-spacing. On the other hand, Cloisite 15A resulted in the smallest phase size. The large interlayer spacing allows polymer chains to more easily intercalate the layers, ultimately improving exfoliation and increasing the clay's surface area per volume, allowing it to more readily cover an interface. The end result was highly exfoliated particles with strong interfacial localization.
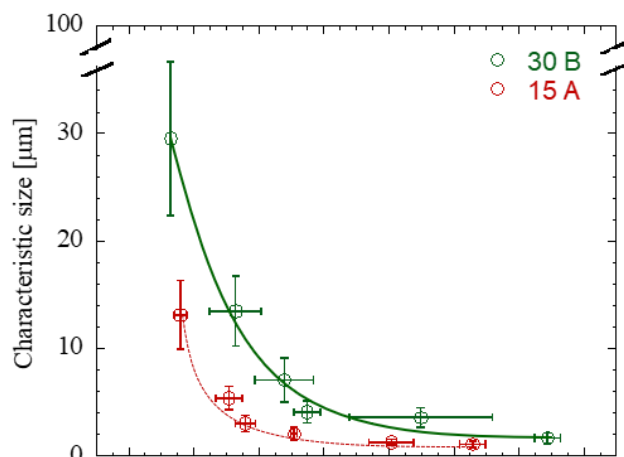

Figure 5.: Characteristic size as a function of filler percentage after a 3-hour annealing at 215 °C. Solid lines are guides for the eye.

5.4. Elasticity and structure of the nanoparticle network

While the dynamics of structural variation during annealing can be studied with scanning and transmission electron microscopy, the role of particles on the rheology of 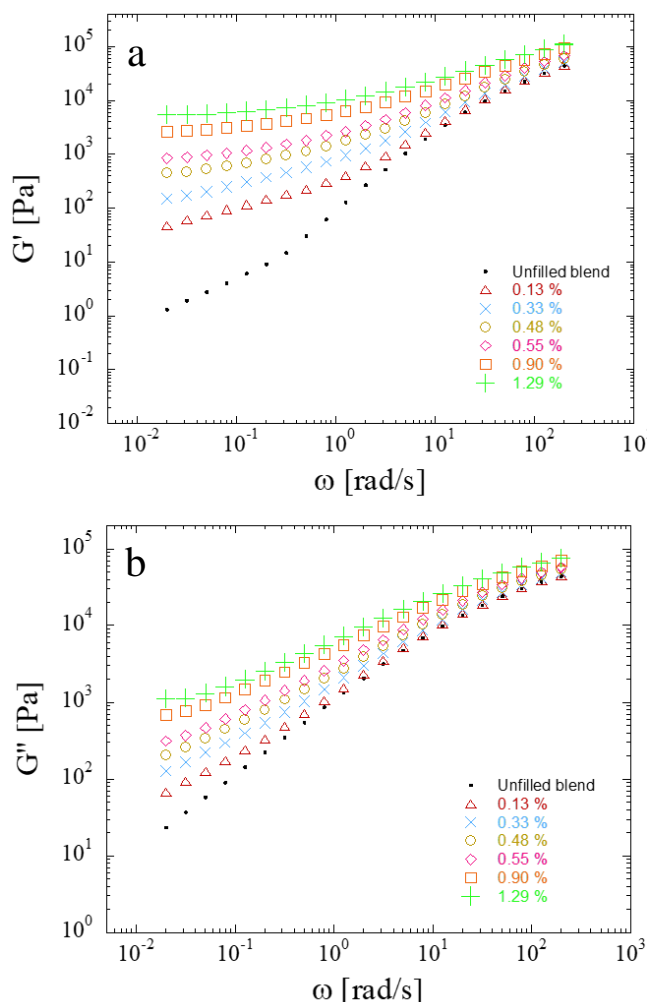polymer blends is still unknown. Storage modulus was measured as a function of frequency to explore the change of rheological properties. The frequency change of the storage modulus of the blends is shown in Figure 6. At low frequency region, a terminal behaviour is observed for the neat blends, indicating the morphology coarsening after 3-hours of annealing. However, the filled blends show power-law dependences with smaller terminal slopes in the same region, which is characteristic for co-continuous structures, while the effect on G'' is negligible. Hereinafter we restrict our attention to G', which is much more sensitive than G'' to the presence of the filler. This terminal behaviour gradually becomes more prominent, whereas the slopes of the elastic moduli decrease with increasing organoclay loading. For high organoclay loadings, a plateau is reached, which is a strong indication of a highly elastic response (solid-like behaviour). Enhancement of solid-like behaviour has been attributed to the emergence of filler networks [12-13] and compatibilization effects [12, 14-15] in polymer nanocomposites and immiscible blends, respectively,

Figure 6.: G' (a) and G'' (b) of the unfilled blend and filled samples at different compositions.

where both are associated with the relaxation process of the polymer chains and the relaxation process form (shape) of the dispersed phase [12].

Figures 7 shows the viscoelastic behaviour of samples, filled with Cloisite 30 B and Cloisite 15 A respectively, measured at 215 °C. In this plot is reported a comparison between their storage moduli at low frequencies, corresponding to long-time relaxation processes. The former (Cloisite 30 B) exhibits a significant increase in the elasticity for the blends containing up to 1.29 % of particles. The latter
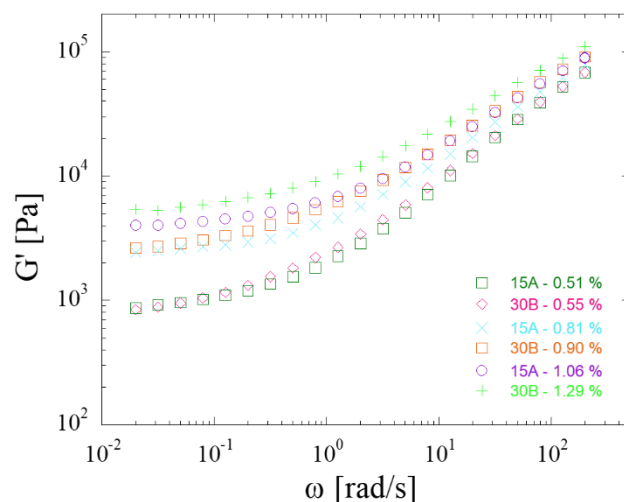

Figure 7.: A comparison between the storage moduli of samples filled with Cloisite 30 B and Cloisite 15 A.

behaviour can be attributed to interfacial interaction and the size of dispersed phase, the larger the droplets, the higher the elasticity [16]. The incorporation of clay and their peculiar localization affect the nanocomposites rheological properties significantly. Thus, the addition of Cloisite 30 B results in an increase in the storage modulus at the lowest frequency. In this concentration range, above Φ_c, the transition from the insulated to gathered behaviour occurs in nanocomposites, i.e. particle structures percolate and reinforce the whole volume of the specimens. Therefore, particle-particle interactions start to contribute to elastic properties of the material considerably.

A descriptive two-phase model can be used, also in this case, to isolate contribution of the particle network and to study it separately [17]. We deal with the generalization of our previous approach, showing that it can be easily used to capture the linear viscoelasticity of co-continuous systems in which particles are gathered in either of the two polymer phases, it once again occurs the arrest of the relaxation dynamics above a critical filler content Φ_c (Figure 6a). In the case of co-continuous blends, where inherent elasticity could mask that of the nanoparticles at low filler contents, the aforementioned approach is crucial. We tested the validity of our procedure by scaling the G′ curves of the samples at $\Phi=0.41$ %, in which the existence of the particle network can be suggested by the presence

Figure 8.: Master curve of G′ of the samples at $\Phi>0.41$%, built using a_Φ and b_Φ as shift factors. The inset shows a detail of the overlay of the two master curves: PS/PMMA/clay 30 B (green empty diamonds) and PS/PMMA/clay 15 A (red full circles).

of a clear low-frequency plateau of the elastic modulus. [17]. The G′(ω) curves of blends at different $\Phi>\Phi_c$ scaled on a single master curve, and the elasticity of the filler networks can be precisely estimated and studied apart. The procedure to build the master curve of G′ is described in detail in the previous chapter. The key steps for identifying the horizontal (a_Φ) and vertical (b_Φ) shift factors are the same as those summarized in the Appendix A (Chapter 4). The resulting master curves of PS/PMMA filled with Cloisite 30 B are shown in Figure 8. The inset reported in the Figure 8 shows a perfect overlapping between the master curves of systems filled with Cloisite 30 B and those filled with Cloisite 15 A. Even in this case is demonstrated the effectiveness of the two-phase model. In particular, we have shown that our analysis works irrespective of the nature of filler.
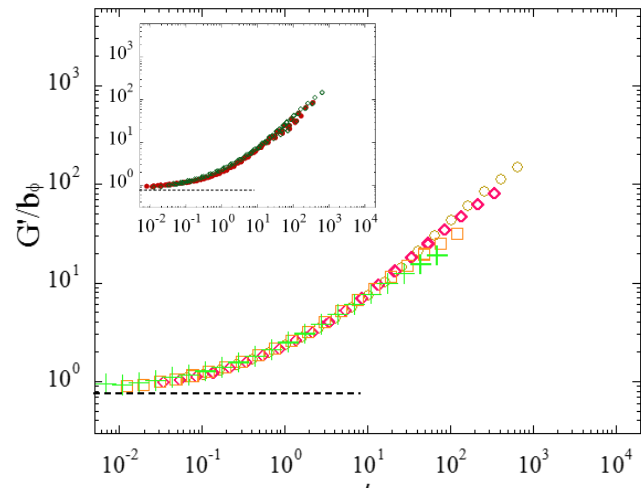
In addition, we show that our approach leads to a confident identification of the filler percolation threshold. The threshold represents the minimum particle volume fraction necessary for the formation of a space-spanning network, which can be either formed by bare clusters or mediated by a fraction of adsorbed polymer. Its identification allows us to compare the stress bearing mechanisms of the two kinds of elastic networks which form in the considered systems, looking for possible common trends. [17]. According to the percolation theory, the network is expected to exhibit a critical behaviour just above Φ_c, its elasticity growing with Φ as $G'_0 = k (\Phi - \Phi_c)^\nu$. We estimate the values of Φ_c by fitting the previous law to the vertical shift factors for the building of the master curves setting k and ν as fitting parameters while keeping Φ_c constant. The procedure is repeated for different Φ_c in a range of composition inferiorly limited by the highest Φ of the G' curves which cannot be scaled on the corresponding master curve (see Figure 8). Hence the percolation threshold is identified as the value of Φ_c which returns the maximum regression coefficient R^2. The power-law dependences of the network elasticity are shown in Figure 9 for the investigated systems; the numerical values of the coefficients are summarized in Table 4 [17]. The best power-law fitting to the experimental data (full circles) was obtained by setting $\Phi_c=0.41\%$, which leads to k=6420.4 $\pm$ 49.7 and ν=1.03 $\pm$ 0.11. The same procedure was previously applied to systems filled with clay 15 A. The value of Φ_c found in case of co-continuous matrix with Cloisite 30 B is higher than that obtained when the particles are located at the interface (Cloisite 15 A). The previous behaviour can be easily explained by accounting for the different localization of the nanoplatelets: when the particles are largely gathered in the bulk phase and minimally at the interface, as the Cloisite 30 B,
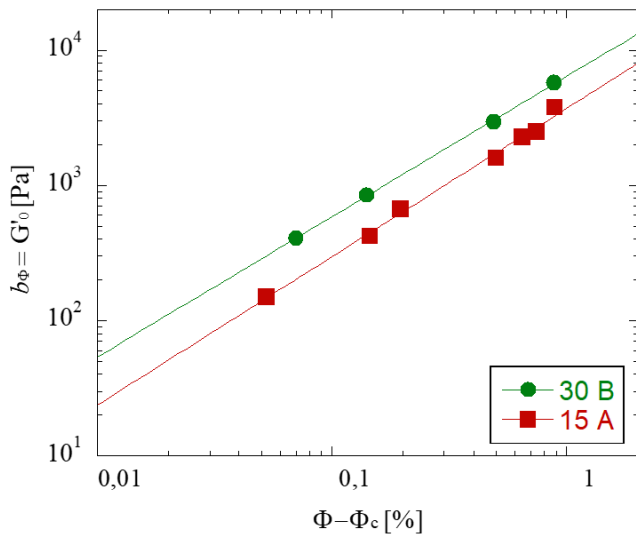

Figure 9.: Network elasticity as a function of reduced filler content (full circles) and power-law fitting to the experimental data (solid line). The data and corresponding fitting lines for systems based on PS/PMMA blend filled with Cloisite 15 A (full squares) are reported for comparison.

Table 4.: Percolation thresholds and fitting parameters.

System	Φ_c [%]	k [Pa]	ν
PS/PMMA/Cloisite® 30 B	0.41	6420.4 $\pm$ 49.7	1.03 $\pm$ 0.11
PS/PMMA/Cloisite® 15 A	0.17	3779 $\pm$ 660	1.09 $\pm$ 0.29

they percolate at higher contents; in contrast, for the inclination of the nanoplatelets to gather at the polymer-polymer interface, as Cloisite 15 A, they percolate at lower contents.

As regards the elastic features of the interfacial network of nanoparticles which forms in the co-continuous blend, the data in Figure 9 and Table 4 reveal that the strength of the network in the co-continuous matrix filled with Cloisite 30 B is higher than that of the networks that the Cloisite 15 A form in the same systems. These data can be seen considering the degree of polymer−filler interaction, and the declared or presumed good affinity expressed through the lower values of ν. On the other hand, in the immediate vicinity of Φ_c the elasticity of the networks which form in the absence of noticeable polymer−particle interactions is generally lower. The

strength of percolating networks reflects a complex interplay between energetic and structural features, but the mechanical strength ultimately depends on the way in which network elements are arranged in the space. A better dispersion of the clusters in case of good polymer–particle affinity may result in finer networks, which are more effective in bearing the stress than the noninteracting structures.

5.5. Conclusions

Blends of PS/PMMA containing different types of organoclay prepared by melt mixing technique and the organoclay distribution between two polymeric phases was studied. Two types of organoclay which have different polarities were investigated. Thermodynamic predictions based on wetting coefficients, calculated from the surface energies of the blend components, were largely successful in predicting the clay localization behaviour for the various organically modified clays. These calculations declared that the more hydrophilic organoclay (30B) would be located in PMMA, while the more hydrophobic would be founded at the interface. To confirm the predictions and determine the exact location of organoclays TEM experiments were performed and the morphology of nanocomposites was studied using SEM.

From the results and discussion above, it is evident that organically modified montmorillonite clays can serve as an effective compatibilizer for PS/PMMA blends. TEM results indicated that the addition of Cloisite® organoclays to the incompatible PS/PMMA blend resulted in a reduction of the microdomain size. The most hydrophilic clays (30B), those with high affinity for PMMA and wetting coefficients approaching 1, were the ones that performed the best for the morphology refinement. It is evident that although the surfactant present in organoclays behaves as a compatibilizing agent for PS/PMMA blends, the effect of organoclays on the morphology of PS/PMMA cannot be explained by presenting organosilicates as merely a vehicle for the surfactant delivery to the polymer matrix. The domain size reduction observed in incompatible PS/PMMA blends should be related to both thermodynamic (i.e., partial compatibilization by surfactant in organoclays) and kinetic (increased local viscosity in the interfacial region) factors. Instead, organically modified clays localized at the interface provided a suppression of coarsening. The effectiveness of the nanoclay increased as the wetting coefficient of the blend system approached zero and as the *d*-spacing of the clay increased, confirming that clays with a higher interfacial affinity and a higher likelihood to exfoliate performed best. In this sense, nanoparticles can be considered a "generic compatibilizer", so long as the clay can sufficiently exfoliate and is selected to produce an appropriate wetting coefficient.

The effect of nanoparticles located in the bulk phase on the viscoelastic behaviour of co-continuous blends during coarsening was investigated. The results were compared to the results of nanoparticles located at the interface. The incorporation of clay and their peculiar localization affect the nanocomposites rheological properties significantly. Thus, the addition of Cloisite 30 B results in an increase in the storage modulus and an increase in the complex viscosity at the lowest frequency. Even in this study is demonstrated the effectiveness of a descriptive two-phase model used to isolate contribution of the particle network and to study it separately. In particular, we have shown that this approach works irrespective of the nature of filler. Furthermore, the structure and elasticity of the considered systems are noticeably different. In particular,

systems with the selective accumulation of the particles in the bulk phase results in higher filler percolation threshold and higher overall elasticity. These behaviours are a direct consequence of the peculiar space arrangement of the filler, and of the polymer-filler interactions.

BIBLIOGRAPHY

1. Robeson, L. M. (2007). Polymer blends. Hanser, Munich, 24-149.

2. Lu, Q., D. A. Meltzer, and Y. Eckstein, "Electrostatic dissipative TPU and compositions thereof," U.S. patent 20110092648 A1 (2010).

3. RTP Company Permastat® Compounds Providing Permanent Antistatic Protection - Conductive and Antistatic Plastic Compounds. http://www.rtpcompany.com/products/conductive/permastat.htm (accessed Dec 17, 2014).

4. Trifkovic, M., Hedegaard, A. T., Sheikhzadeh, M., Huang, S., & Macosko, C. W. (2015). Stabilization of PE/PEO cocontinuous blends by interfacial nanoclays. Macromolecules, 48(13), 4631-4644.

5. Taguet, A., Cassagnau, P., & Lopez-Cuesta, J. M. (2014). Structuration, selective dispersion and compatibilizing effect of (nano) fillers in polymer blends. Progress in Polymer Science, 39(8), 1526-1563.

6. Shenoy, A. V. (2013). Rheology of filled polymer systems. Springer Science & Business Media.

7. Gelfer, M. Y., Song, H. H., Liu, L., Hsiao, B. S., Chu, B., Rafailovich, M., ... & Zaitsev, V. (2003). Effects of organoclays on morphology and thermal and rheological properties of polystyrene and poly (methyl methacrylate) blends. Journal of Polymer Science Part B: Polymer Physics, 41(1), 44-54.

8. Owens, D. K., & Wendt, R. C. (1969). Estimation of the surface free energy of polymers. Journal of applied polymer science, 13(8), 1741-1747

9. Wu, S. (1982). Polymer interface and adhesion. M. Dekker.

10. Van Krevelen, D. W., & Te Nijenhuis, K. (2009). Properties of polymers: their correlation with chemical structure; their numerical estimation and prediction from additive group contributions. Elsevier.

11. Taguet, A., Cassagnau, P., & Lopez-Cuesta, J. M. (2014). Structuration, selective dispersion and compatibilizing effect of (nano) fillers in polymer blends. Progress in Polymer Science, 39(8), 1526-1563.

12. Salehiyan, R., Ray, S. S., Bandyopadhyay, J., & Ojijo, V. (2017). The distribution of nanoclay particles at the interface and their influence on the microstructure development and rheological properties of reactively processed biodegradable polylactide/poly (butylene succinate) blend nanocomposites. Polymers, 9(8), 350.

13. Sangroniz, L., Palacios, J. K., Fernández, M., Eguiazabal, J. I., Santamaria, A., & Müller, A. J. (2016). Linear and non-linear rheological behavior of polypropylene/polyamide blends modified with a compatibilizer agent and nanosilica and its relationship with the morphology. European Polymer Journal, 83, 10-21.

14. Maani, A., Heuzey, M. C., & Carreau, P. J. (2011). Coalescence in thermoplastic olefin (TPO) blends under shear flow. Rheologica acta, 50(11-12), 881-895.

15. Maani, A., Blais, B., Heuzey, M. C., & Carreau, P. J. (2012). Rheological and morphological properties of reactively compatibilized thermoplastic olefin (TPO) blends a. Journal of Rheology, 56(3), 625-647.

16. Graebling, D., & Muller, R. (1990). Rheological behavior of polydimethylsiloxane/polyoxyethylene blends in the melt. Emulsion model of two viscoelastic liquids. Journal of Rheology, 34(2), 193-205.

17. Filippone, G., & Salzano de Luna, M. (2012). A unifying approach for the linear viscoelasticity of polymer nanocomposites. Macromolecules, 45(21), 8853-8860.

Future perspectives and concluding remarks[*]

6.1. Influence of surface modification of halloysite nanotubes on immiscible polymer blends

6.1.1. Introduction

It is well acknowledged that the discrepancy of polarity between the polymer matrices and the fillers is a major obstacle to the improvements in properties of the filled composites. [1-3] For example, so far, few of the layered clay reinforced polymer composites has been commercialized due to the unsatisfactory dispersion of the clay such as montmorillonite although numerous studies had been conducted on the polymer/clay composites [1,4-5]. For the nonpolar polymers, the dispersion of the inorganics seems more challengeable. Consequently, easily dispersed inorganics in polymer matrix are still highly desirable. Generally, inorganics with high aspect ratio have preferable reinforcing effects than particulate inorganics [9, 10]. For this reason, glass fibres have been widely used as a reinforcing material for many polymers. The incorporation of glass fibres in polymer matrix will, however, reduce the melt flow rate sharply and consequently gives rise to processing problems [1, 6-7]. Recently, CNTs with high respect ratio and specific high strength and modulus have been introduced into polymers for reinforcing, flame retardancy and other purposes [1, 8-9]. Although composites incorporated with CNTs, as reported, exhibit excellent mechanical properties, flame retardant effects and thermal stability, the high cost of such composites is not acceptable in many applications [1].

Halloysite is a natural nanomaterial consisting of multilayer aluminosilicate nanotubes [14-17] (NTs). In the literature, halloysite nanoparticles having thread-like, spherical, flat, disk-shaped, and other shapes have been also reported [14, 17]. Halloysite is contained in kaolinite clay, which is formed in the Earth's crust by the weathering of geological materials formed under high pressure in the layers of silicon dioxide and aluminium oxide. The cost of obtaining of halloysite nanotubes (HNTs) is lower than that of carbon nanotubes because of the high prevalence of kaolinite deposits. The morphology of the halloysite nanotube can be seen as a kaolin layer (having a thickness of about 0.7 nm) folded to a ''roll'', see Figure1 [14]. The two main polymorphs of halloysite are the hydrated form, $Al_2Si_2O_5(OH)_4 \cdot 2H_2O$, with a basal distance of approximately

---

[*]The results presented in this section have still not been published.

10 Å and the dehydrated form, $Al_2Si_2O_5(OH)_4$, which is identical to kaolinite. The hydrated form is irreversibly converted to the dehydrated form upon drying below 100°C. Water loss sharpens the basal reflections and reduces the basal d-spacings to approximately 7.2 Å, although this value is never so small as that of typical kaolinite (7.14 Å) [18.19]. The HNTs length is ranging from 0.5 µm to 1.2 µm and diameter is <100 nm. HNTs can be used as ''ready-made'' nanocontainers [14, 16]. When added in polymer matrices, HNTs may serve a dual function: to increase the strength of the material due to bonding with the polymer matrix and to
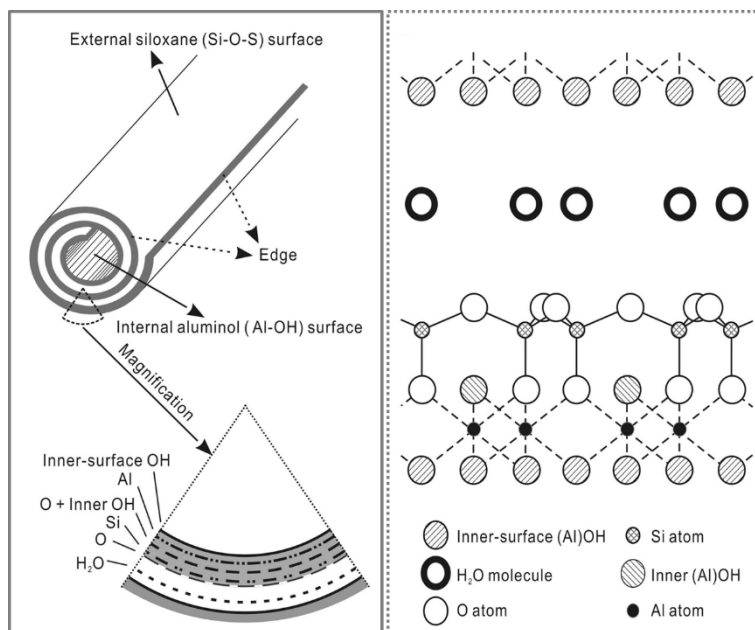

Figure 1.: Schematic representation of (a) the crystalline structure of halloysite-(10 Å), and (b) the structure of a halloysite nanotube. Reproduced from [14].

provide a variety of additives contained in their inner cavity, this leading to many varieties of applications [14, 20]. Recently, more and more studies have been focused on the application of HNTs in polymer area. [1]. There are many benefits associated with HNTs used as filler in polymer based composites: i) HNTs have low surface charges so there will be no intercalation and exfoliation needed compare to other two-dimensional nanoclays fillers such as Montmorillonites (MMTs). So, they provide ease in processing when mixed with other polymers to give homogeneous particle dispersion. ii) Modifications at the surfaces of HNTs provide an opportunity to expand the basal spacing of HNTs by the intercalation of inorganic and organic compounds in their inter layers, which further enhance the possibility of producing a homogeneous mixture of HNTs with polymers during blending. iii) Surface modification of HNTs enhances their wet ability and bond formation with different polymers. iv) Expansion of base layers provides HNTs exfoliation. v) HNTs are comprised of siloxane and hydroxyl groups, which gives HNTs potential for the formation of hydrogen bonds and hence improve dispersion. vi) Larger luminal diameter of halloysite nanotubes can accommodate different polymer molecules which further offer polymeric composites [21].

The surface properties of halloysite nanotubes have a significant impact on physical properties of polymer nanocomposites. Due to the high surface energy HNTs readily form aggregates, and this decreases the mechanical strength of nanocomposites. To increase the degree of dispersion, HNT surface is preliminarily subjected to an appropriate modification, e.g. covalent functionalization using cationic surfactants, polycations [14,16] (due to the negative charge of HNT surface), organosilanes [14, 22-25], other modifiers [14, 26-27], or non-covalent functionalization [14, 24]. The modifier's role is to prevent the aggregation of nanoparticles. To increase the degree of HNT dispersion, it is highly desirable to use modifiers possessing a high degree of

compatibility with monomers of the matrix, otherwise the incompatibility of the modifier and the polymer matrix may induce a phase separation in the system [14, 28]. Organo-functional silanes are unique hybrid materials that contain both hydrophilic and hydrophobic structures, thus they can be used as compatibilizer between organic and inorganic structures. Figure 2 shows gener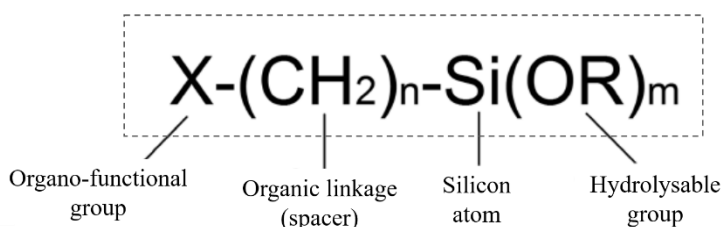al structure of silanes, where "X" is the nonhydrolyzing organofunctional group connecting to the organic matrix and depending on the polymer type it could be amino-, epoxy, vinyl, or other groups. "‒(CH$_2$)$_n$" is the linkage group connecting the Si atom to the organo-functional group, here "n" indicates length of this group

Figure 2.: General formula for a silane coupling agent.

influencing the stability of silane structure. "(‒OR)$_m$" is a hydrolysable group, usually an alkoxy, which condenses onto the inorganic reinforcement surfaces. Silanization reactions are complex and generally carried out in two steps. First, silicon functional groups hydrolyse to silanol groups with the presence of water very quickly (Reaction 1). Then, these silanol groups condense with M−OH groups present on the reinforcement surfaces (Reaction 2) [29].

In the present preliminary work, pristine HNTs and silane treated HNTs were utilized to prepare co-continuous polystyrene (PS)/poly (methyl methacrylate) (PMMA)/HNTs systems. It is expected that the dispersion property and high aspect ratio are advantageous compared with other widely used silicates. We made a first attempt to investigate the particle distribution in the polymer nanocomposites through preliminary analyses.

6.1.2. Experimental section

HNTs as powder, sodium hydroxide (NaOH, ≥98%), hydrogen peroxide (H$_2$O$_2$, 33%, v/v), ethanol (95%), 3-aminopropyl-trimethoxysilane (APTMS, 97%), 3-mercaptopropyl-trimethoxysilane (MPTMS, 95%), methanol (>99%), and acetic acid (>99%) were purchased from Sigma–Aldrich. The polystyrene (PS) used for this study was provided by Polimeri Europa (Edistir® 2982), poly (methyl methacrylate) (PMMA), by Plaskolite, Inc. (Optix® CA-51).

Since the organic contamination has a negative effect on the compatibility of the HNTs with the polymer matrix, the as received HNTs were treated by H$_2$O$_2$ to remove organic impurities. Typically, 30.0 g of the as-received HNTs was added into 200 mL 30% H$_2$O$_2$ aqueous solution and magnetically stirred for 1 h. The HNTs dispersion was then ultrasonicated for 10 min prior to the centrifugation treatment to separate HNTs from the liquid phase. The resultant purified HNTs were first dried at 110 °C for 12 h in an oven and then dried at 60 °C in a vacuum oven for 12 h. To enhance hydroxyl groups, the purified HNTs were then treated by NaOH. Typically, 2.00 g of purified HNTs was dispersed in 100 mL deionized water. Subsequently, 0.058 g of NaOH was added and the mixture was magnetically stirred for 24 h at room temperature. The resultant hydroxylated HNTs solid phase was then separated by centrifugation and rinsed several times with water until the pH reached

7. The prepared hydroxylated HNTs were first dried at 110 °C for 12 h in an oven and then dried at 60 °C in a vacuum oven for 12 h [30]. The increase in the hydroxyl groups is usually recommended before performing silane reactions on the reinforcement surfaces. This process enhances the density of available silanol (Si OH) sites for silane reaction, improving the efficiency and repeatability of the surface modification process [31].

The surface modification procedure with two organosilane (Figure 3), with different chemical functionality (X): thiol (X_1: SH) and amino (X_2: NH$_2$), was performed using the sol-gel deposition process from aqueous/alcohol solution (75% distilled water:25% methanol, pH = 4.5±0.2 with acetic acid). The specific organosilane reagent was added to yield a 2% (v/v) final concentration, allowing 10 min for the hydrolysis of alkoxide and silanol formation. Next, 5 g of the hydroxylated HNTs were immersed in this solution for 30 min and then rinsed with ethanol to remove unbound silane from the surface and cured at temperature of 110±10 °C for 30 min for condensation reactions. This procedure is important because it assures that the excess of organosilanes precursors and also
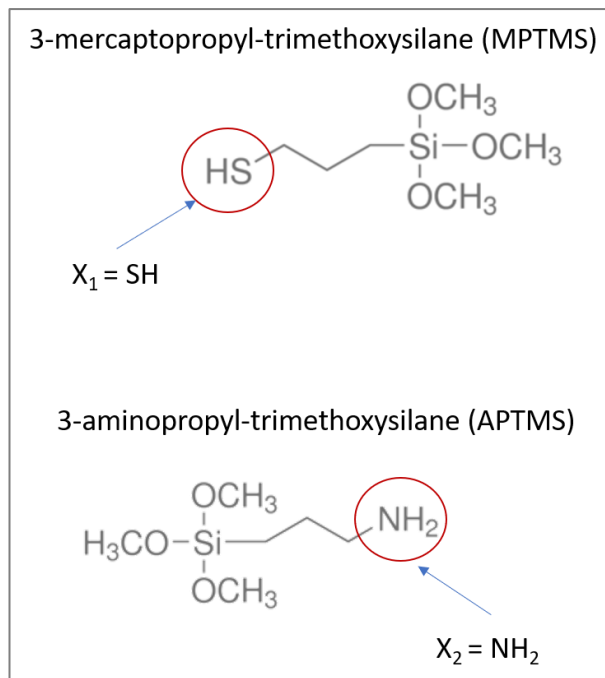

Figure 3.: General formula for MPTMS and APTMS.

unreacted species were fully removed before proceeding to the next step of glutaraldehyde linking [31]. The resultant untreated and treated HNTs will be named in the text as HNTs (unmodified), AHNTs (treated with APTMS) and MHNTs (treated with MPHNTs). Unfilled and filled PS/PMMA blends at 55/45 (*co-continuous systems*) weight ratio were prepared by melt compounding the constituents using a recirculating, conical twin screw micro-compounder (Xplore MC 15 by DSM). The polymers and all types of HNTs (99:1 and 95:5 w/w) in powder form, first dried overnight under vacuum at T=90°C, were loaded simultaneously in the mixing apparatus. The extrusions were performed at T=190°C in nitrogen atmosphere at a screw speed of 150 rpm. The residence time was about 5 minutes. The extrudate was granulated, dried again, and finally compression-moulded in the form of disks (diameter 40 mm, thickness ~1.5 mm) for the subsequent analyses. Preliminary thermogravimetric analyses (TGA, Q5000 by TA Instruments) were carried out. The samples were heated at 10°C min^{-1} in nitrogen atmosphere from room temperature up to T=700°C, and the residuals were recorded at T=600°C. The morphology of the samples was investigated by means of electron microscopy. TEM analyses (Tecnai G2 Spirit Twin T-12 by FEI) were carried out to identify the space arrangement of the nanoparticles. The samples were ~100 nm-thick slices randomly cut at room temperature from the disks used for rheological analyses by using a Leica EM UC7 ultra-microtome equipped with a diamond knife.

6.1.3. Preliminary results

TEM analysis

The morphology of the PS/PMMA filled with HNTs, AHNTs, and MHNTs is shown in Figure 4. As can be seen, some agglomerates were found. TEM images show the effects of HNTs loading and surface modification on the dispersion of HNTs in co-continuous PS/PMMA systems, both untreated and treated HNTs are badly dispersed in the polymer matrix. This behaviour could suggest that surface modification of HNTs didn't work as we expected. Modification of the HNTs didn't reduce the aggregation of the HNTs in our systems, probably because the surface modification procedure should be improved, and/or because it is necessary to change the mixing procedure, and/or because system parameters should be tuned (i.e.: filler content, initial silane concentration, and pH of reaction solution). However, further analyses are required to evaluate and improve these aspects.
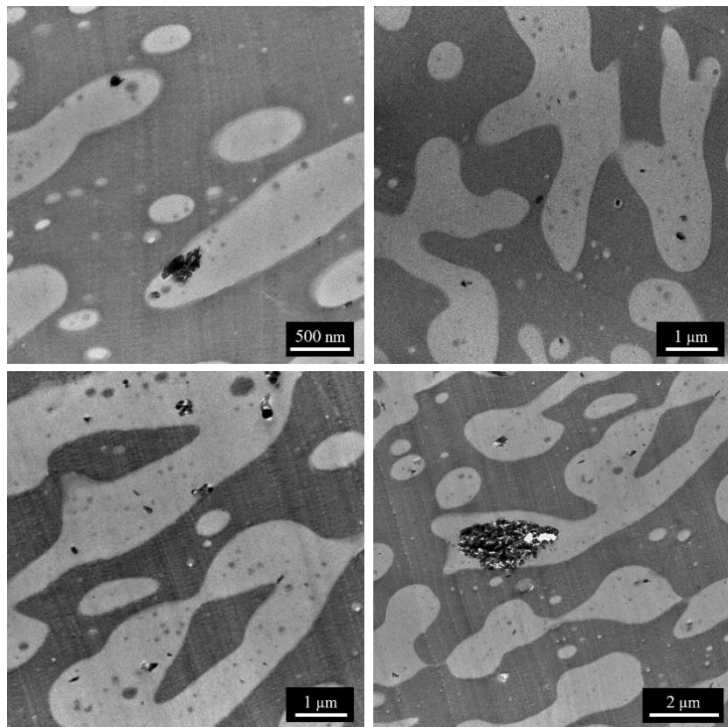
Figure 4.: TEM micrograph at different magnifications: (a) PS/PMMA/AHNTs 1%, (b) PS/PMMA/HNTs 1%, (c, d) PS/PMMA/MHNTs 1%. The bright and dark phases are PMMA and PS, respectively.

Thermal Analysis

Thermal stability was investigated with thermogravimetric analysis. The TGA curves for the filled and unfilled systems are shown in Figure 5 and the characteristic weight loss temperatures are summarized in Table 1. The data reveals that the loading of HNTs and the surface modification of HNTs have important effects on the thermal stability of the nanocomposites. As shown in Table 1, the temperature at 5% weight loss for unfilled PS/PMMA is 354 °C. However, this temperature for the nanocomposite filled with 1% of modified HNTs is decreased to 336 °C and 337 °C for AHNTs and MHNTs, respectively, which is 18 °C and 17 °C lower than that of unfilled PS/PMMA. This temperature for the nanocomposite filled with 5% of modified HNTs and that at maximum weight loss rate show a similar trend. The modification of the HNTs decreased the thermal resistance of our systems, this behaviour could be due to the rigid phase reinforcement, and devastation of the polymer network topology. Some literature studies suggested that the barrier properties of the nanoscale fillers
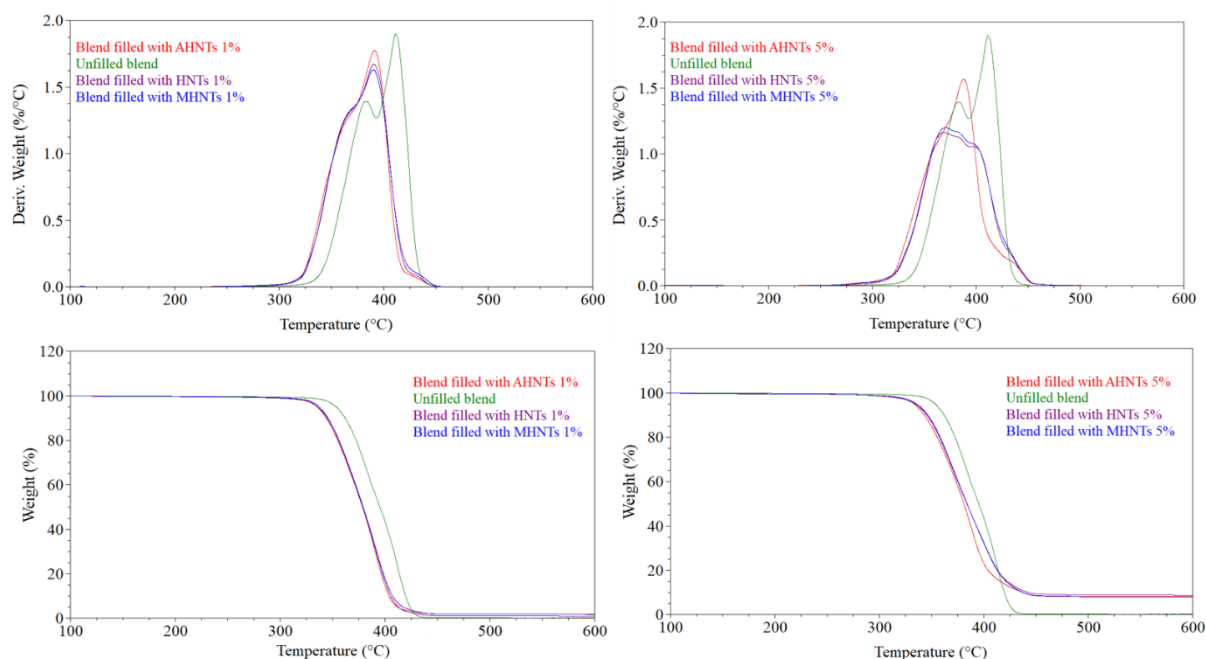
Figure 5.: TGA curves of unfilled blend PS/PMMA, blend filled with HNTs 1%, blend filled with AHNTs 1%, blend filled with MHNTs 1%, blend filled with HNTs 5%, blend filled with AHNTs 5%, blend filled with MHNTs 5%

Table 1.: TGA data of unfilled and filled samples.

System	Filler content (%)	Temperature at 5% weight loss/°C	Temperature at maximum weight loss rate/°C
Unfilled blend	0	354	412
Blend filled with HNTs	1	336	391
Blend filled with AHNTs	1	336	391
Blend filled with MHNTs	1	337	390
Blend filled with HNTs	5	334	369
Blend filled with AHNTs	5	334	388
Blend filled with MHNTs	5	336	371

were responsible for the enhancement of thermal stability of nancomposites. Gilman believes that the barrier properties could include both the thermal barrier [32-34], which protects the polymer from contacting with fire, and the mass transport barrier, which slows down the escape of the volatile products during the process of degradation, and the investigations also showed that the intercalated layered silicate nanofiller had much better effects on thermal stability of polymer matrix than exfoliated layered silicate nanofiller [32-33]. It is reasonable to postulate that the barrier effects of HNTs with tubular structure may somewhat be inferior to

those of layered silicate nanofillers, especially the intercalated layered silicate nanofillers. Du et al. show that the lumen of the HNTs plays the leading role in improving the thermal stability of the nanocomposites. During the initial degradation stage of polymer nanocomposites, the degradation products may considerably be entrapped into the lumens of HNTs, resulting in an effective delay in mass transport and a remarkably increased thermal stability. The modified HNTs should be dispersed more evenly in the polymer matrix, resulting in higher randomness of lumen ends, in this way the latter can entrap the degradation products more effectively. Therefore, nanocomposites with modified HNTs loading has better thermal stability than that of unmodified ones [32]. However, as we have seen above, in our system both untreated and treated HNTs are badly dispersed, this could be reasonable related to the insufficient thermal stability of final samples. A deeper examination of these aspects could be very interesting.

6.2. Concluding remarks

The ultimate goal of the research activity reported in the present dissertation was the investigation of the physical mechanisms governing the nanoparticle dynamics and connectivity in polymer melts. A systematic study related to the mechanisms by which the filler affects the blend microstructure and how the fluids in turn affect the nanoparticle assembly is carried out, from both a theoretical and practical point of view. The first part of this work treated in greater detail, through an overview of the state-of-the-art, changes in the polymer blend microstructure, which result from phase deformation generated during blending, and the impact of the filler addiction on the viscoelastic performance. Instead, the aim of the second part of this research was to study the origin of the uneven distribution of the filler in a multiphase host matrix, if this distribution is merely dictated by thermodynamic arguments, and if it is possible to drive the systems towards desired non-equilibrium configurations.

To do so, was explored a first approach studying the time evolution of the linear viscoelastic response for a nanocomposite system based on a biphasic polymer matrix with a co-continuous morphology, in which the filler phase is inclined to gather at the polymer-polymer interface. The investigation was directed to the rheological implications of the network formed by the nanoparticles, once the filler percolation threshold is exceeded. The structure and elasticity of the particle network in the co-continuous blend were found to be noticeably different from those of the reference systems based on pure polymer and a blend with drop-in-matrix morphology. Results are a direct consequence of the peculiar space arrangement of the filler, whose alignment along the continuous polymer-polymer interface minimizes the probability of isolated particles and promotes strong edge-to-edge interactions. A further approach was to explore to what extent fillers with a different chemistry, and gained in either of the polymer phases, could influence the size reduction of the polymer phases, the mechanisms by which these nanoclays stabilize against coalescence and their effect on the rheological behaviour. As a result of a comparative analysis it was found that the refinement ability of the filler was slightly better in the case of bulk localization, but interfacial nanoplatelets were more effective in stabilizing co-continuous morphologies against phase coarsening in the melt state.

In the end, the gained fundamental knowledge on polymer nanocomposites is exploited to verify the effect of the filler morphology on co-continuous polymer systems. In detail, a case study particularly relevant in the field of polymer nanocomposite science was considered, or rather the difficulties related to the de-agglomeration and dispersion of hydrophilic halloysite nanotubes (HNTs) during the mixing with the hydrophobic polymer. The aim was to couple the good filler dispersion with the feasibility of conventional melt mixing. Specifically, to increase the degree of dispersion and consequently their hydrophobicity, HNTs surface was preliminarily subjected to an appropriate modification with organosilanes. Nevertheless, to demonstrate the effectiveness of the proposed approach further analyses are still needed.

BIBLIOGRAPHY

1. Du, M., Guo, B., Cai, X., Jia, Z., Liu, M., &Jia, D. (2008). Morphology and properties of halloysite nanotubes reinforced polypropylene nanocomposites. e-Polymers, 8(1), 1490-1503.

2. Kornmann, X., Lindberg, H., & Berglund, L. A. (2001). Synthesis of epoxy–clay nanocomposites: influence of the nature of the clay on structure. Polymer, 42(4), 1303-1310.

3. Fekete, E., Molnar, S. Z., Kim, G. M., Michler, G. H., &Pukanszky, B. (1999). Aggregation, fracture initiation, and strength of PP/CaCO3 composites. Journal of Macromolecular Science—Physics, 38(5-6), 885-899.

4. Ranade, A., D'Souza, N. A., & Gnade, B. (2002). Exfoliated and intercalated polyamide-imide nanocomposites with montmorillonite. Polymer, 43(13), 3759-3766.

5. Varghese, S., Karger-Kocsis, J., & Gatos, K. G. (2003). Melt compounded epoxidized natural rubber/layered silicate nanocomposites: structure-properties relationships. Polymer, 44(14), 3977-3983.

6. Tibbetts, G. G., & McHugh, J. J. (1999). Mechanical properties of vapor-grown carbon fiber composites with thermoplastic matrices. Journal of Materials Research, 14(7), 2871-2880.

7. Sinnott, S. B., Shenderova, O. A., White, C. T., & Brenner, D. W. (1998). Mechanical properties of nanotubule fibers and composites determined from theoretical calculations and simulations. Carbon, 36(1-2), 1-9.

8. Ozkoc, G., Bayram, G., & Bayramli, E. (2005). Short glass fiber reinforced ABS and ABS/PA6 composites: processing and characterization. Polymer composites, 26(6), 745-755.

9. Tjong, S. C., Xu, S. A., & Mai, Y. W. (2003). Process–structure–property relationship in ternary short-glass-fiber/elastomer/polypropylene composites. Journal of applied polymer science, 88(5), 1384-1392.

10. Qian, D., Dickey, E. C., Andrews, R., & Rantell, T. (2000). Load transfer and deformation mechanisms in carbon nanotube-polystyrene composites. Applied physics letters, 76(20), 2868-2870.

11. Ajayan, P. M., Schadler, L. S., Giannaris, C., & Rubio, A. (2000). Single-walled carbon nanotube–polymer composites: strength and weakness. Advanced materials, 12(10), 750-753.

12. Coleman, J. N., Khan, U., & Gun'ko, Y. K. (2006). Mechanical reinforcement of polymers using carbon nanotubes. Advanced materials, 18(6), 689-706.

13. Du, F., Fischer, J. E., & Winey, K. I. (2003). Coagulation method for preparing single-walled carbon nanotube/poly (methyl methacrylate) composites and their modulus, electrical conductivity, and thermal stability. Journal of Polymer Science Part B: Polymer Physics, 41(24), 3333-3338.

14. Komarov, P., Markina, A., & Ivanov, V. (2016). Influence of surface modification of halloysite nanotubes on their dispersion in epoxy matrix: Mesoscopic DPD simulation. Chemical Physics Letters, 653, 24-29

15. Kamble, R., Ghag, M., Gaikawad, S., & Panda, B. K. (2012). Halloysite Nanotubes and Applications: A Review. Journal of advanced scientific research, 3(2).

16. Lvov, Y., & Abdullayev, E. (2013). Functional polymer–clay nanotube composites with sustained release of chemical agents. Progress in Polymer Science, 38(10), 1690-1719.

17. Joussein, E., Petit, S., Churchman, J., Theng, B., Righi, D., & Delvaux, B. (2005). Halloysite clay minerals–a review. Clay minerals, 40(4), 383-426.

18. Khunova, V., Kristof, J., Kelnar, I., & Dybal, J. (2013). The effect of halloysite modification combined with in situ matrix modifications on the structure and properties of polypropylene/halloysite nanocomposites. eXPRESS Polymer Letters, 7(5).

19. Brindley, G. W., & Robinson, K. (1946). Randomness in the structures of kaolinitic clay minerals. Transactions of the Faraday Society, 42, B198-B205.

20. Rawtani, D., & Agrawal, Y. K. (2012). Multifarious applications of halloysite nanotubes: a review. Rev. Adv. Mater. Sci, 30(3), 282-295.

21. Rawtani, D., & Agrawal, Y. K. (2012). Multifarious applications of halloysite nanotubes: a review. Rev. Adv. Mater. Sci, 30(3), 282-295.

22. Yuan, P., Southon, P. D., Liu, Z., Green, M. E., Hook, J. M., Antill, S. J., & Kepert, C. J. (2008). Functionalization of halloysite clay nanotubes by grafting with γ-aminopropyltriethoxysilane. The Journal of Physical Chemistry C, 112(40), 15742-15751.

23. Joo, Y., Jeon, Y., Lee, S. U., Sim, J. H., Ryu, J., Lee, S., ... & Sohn, D. (2012). Aggregation and stabilization of carboxylic acid functionalized halloysite nanotubes (HNT-COOH). The Journal of Physical Chemistry C, 116(34), 18230-18235.

24. Szpilska, K., Czaja, K., & Kudła, S. (2015). Halloysite nanotubes as polyolefin fillers. Polimery, 60(6), 359-371.

25. Pasbakhsh, P., Ismail, H., Fauzi, M. A., & Bakar, A. A. (2010). EPDM/modified halloysite nanocomposites. Applied Clay Science, 48(3), 405-413.

26. Xu, W., Luo, B., Wen, W., Xie, W., Wang, X., Liu, M., & Zhou, C. (2015). Surface modification of halloysite nanotubes with l-lactic acid: An effective route to high-performance poly (l-lactide) composites. Journal of Applied Polymer Science, 132(7).

27. Tang, Y., Deng, S., Ye, L., Yang, C., Yuan, Q., Zhang, J., & Zhao, C. (2011). Effects of unfolded and intercalated halloysites on mechanical properties of halloysite–epoxy nanocomposites. Composites Part A: Applied Science and Manufacturing, 42(4), 345-354.

28. Komarov, P. V., Mikhailov, I. V., Chiu, Y. T., Chen, S. M., & Khalatur, P. G. (2013). Molecular Dynamics Study of Interface Structure in Composites Comprising Surface-Modified SiO2 Nanoparticles and a Polyimide Matrix. Macromolecular Theory and Simulations, 22(3), 187-197.

29. Riza Erdogan, A., Kaygusuz, I., & Kaynak, C. (2014). Influences of aminosilanization of halloysite nanotubes on the mechanical properties of polyamide-6 nanocomposites. Polymer Composites, 35(7), 1350-1361

30. Zeng, S., Reyes, C., Liu, J., Rodgers, P. A., Wentworth, S. H., & Sun, L. (2014). Facile hydroxylation of halloysite nanotubes for epoxy nanocomposite applications. Polymer, 55(25), 6519-6528

31. Marques, M. E., Mansur, A. A., & Mansur, H. S. (2013). Chemical functionalization of surfaces for building three-dimensional engineered biosensors. Applied Surface Science, 275, 347-360

32. Du, M., Guo, B., & Jia, D. (2006). Thermal stability and flame retardant effects of halloysite nanotubes on poly (propylene). European Polymer Journal, 42(6), 1362-1369.

33. Gilman, J. W. (1999). Flammability and thermal stability studies of polymer layered-silicate (clay) nanocomposites. Applied Clay Science, 15(1), 31-49.

34. Gilman, J. W., Jackson, C. L., Morgan, A. B., Harris, R., Manias, E., Giannelis, E. P., ... & Phillips, S. H. (2000). Flammability properties of polymer− layered-silicate nanocomposites. Polypropylene and polystyrene nanocomposites. Chemistry of Materials, 12(7), 1866-1873.